

**STUDIES ON ENERGY EXCHANGE AND UPPER OCEAN THERMAL STRUCTURE IN
ARABIAN SEA AND HEAT TRANSPORT IN NORTHERN INDIAN OCEAN**

THESIS SUBMITTED TO
THE COCHIN UNIVERSITY OF SCIENCE AND TECHNOLOGY
FOR THE DEGREE OF
DOCTOR OF PHILOSOPHY

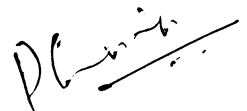
BY
KERALA VARMA K., M. Sc.

**PHYSICAL OCEANOGRAPHY AND METEOROLOGY DIVISION
SCHOOL OF MARINE SCIENCES
COCHIN UNIVERSITY OF SCIENCE AND TECHNOLOGY
COCHIN - 682 016**

APRIL 1989

CERTIFICATE

This is to certify that this Thesis is an authentic record of research work carried out by Sri Kerala Varma, K. under my supervision in the Physical Oceanography and Meteorology Division, School of Marine Sciences for Ph.D. Degree of Cochin University of Science and Technology and no part of it has been presented earlier for any degree in any university.



Dr. P.G. KURUP,
Professor,
School of Marine Sciences,
Cochin University of Science and Technology,
(Supervising Teacher)

DECLARATION

I hereby declare that this Thesis entitled "Studies on Energy Exchange and Upper Ocean Thermal Structure in Arabian Sea and Heat Transport in Northern Indian Ocean" is an authentic record of the research carried out by me, under the supervision and guidance of Dr. P.G. Kurup, Professor, School of Marine Sciences, in partial fulfilment of the requirements for Ph.D degree of Cochin University of Science and Technology and that no part thereof has been presented for any degree in any university.

College of Fisheries,
Panangad



Kerala Varma, K.
Associate Professor

ACKNOWLEDGEMENTS

I wish to express my deep sense of gratitude to Dr. P.G. Kurup, Professor of Physical Oceanography, School of Marine Sciences, Cochin University of Science and Technology, for valuable guidance, constant encouragement and critical scrutiny of the manuscript.

I am thankful to Dr. M. G. Joseph and Dr. P.G.K. Murthy, Scientists, Naval Physical and Oceanographic Laboratory, for going through the manuscript and for supplying some of the sorted temperature data respectively. I wish to thank many scientists, especially Sri C.K.B. Kurup, of Naval Physical and Oceanographic Laboratory who had been of help to me during the course of this work.

Several helps, in particular the assistance in computer programming, by Sri C.A. Babu, Research Scholar, School of Marine Sciences, are gratefully acknowledged.

I am thankful to Sri N.N. Raman, Junior Assistant Professor, College of Fisheries for helping in some analysis of MONEX-79 data and to Dr. K.S.N. Namboodiripad, Reader, School of Marine Sciences, for discussions.

Thanks are due to the authorities of Naval Physical and Oceanographic Laboratory for making available the subsurface temperature data and to the authorities of Kerala Agricultural University for giving me the necessary permission to carry out the work.

I am thankful to my wife, Usha Varma, for her patience and helpful attitude during this work.

C O N T E N T S

	Page
PREFACE	i
LIST OF SYMBOLS AND ABBREVIATIONS	iii
CHAPTER 1 PART 1 : INTRODUCTION	1
PART 2 : MATERIALS AND METHODS	17
CHAPTER 2 SHORT-TERM VARIATIONS	36
CHAPTER 3 UPPER OCEAN THERMAL STRUCTURE IN AREA I (NORTHERN PART OF SOMALI CURRENT AREA)	59
CHAPTER 4 UPPER OCEAN THERMAL STRUCTURE IN AREA II (CENTRAL EASTERN ARABIAN SEA)	83
CHAPTER 5 HEAT TRANSPORT IN THE NORTHERN INDIAN OCEAN	101
CHAPTER 6 SUMMARY AND CONCLUSIONS	115
REFERENCES	123

PREFACE

Annual reversal of winds due to changing monsoons is a spectacular phenomenon occurring over north Indian Ocean. The large amount of rainfall associated with southwest (summer) monsoon is very vital for the economy of the countries bordering Indian Ocean, especially the Indian Subcontinent. The change from one monsoon to the other is also associated with alterations of surface circulation in equatorial and north Indian Ocean.

During the southwest monsoon season, Somali current sets in along the east African coast as a swift northerly current. Recent studies have revealed that there are two eddies in the Somali Basin during this season. The 'turning offshore' regions of these eddies and the associated upwelling regions translate northwards with the advance of the southwest monsoon. During this period upwelling is noticed in the eastern Arabian Sea also.

Unlike other Oceanic Areas, SST in Arabian Sea decreases during summer. The summer cooling is a consequence of the southwest monsoon. Energy exchange parameters exhibit bimodal variations in the northern Indian Ocean under the influence of the monsoons.

The present thesis is an attempt to understand the upper ocean thermal characteristics at selected areas in the western and eastern Arabian Sea in relation to surface energy exchange and dynamics, on a climatological basis. It is also aimed to examine, the relative importance of different processes in the evolution of SST at the western and eastern Arabian Sea. Short-term variations of energy exchange and upper ocean thermal structure are also investigated. Heat transport cycle in the north

Indian Ocean is also studied with an aim to understand the seasonal variation of net transport across different latitude belts.

The thesis is divided into six chapters. Chapter 1 has two parts. Part 1 provides a brief review of earlier studies, description of area of study and the scope of the study. In Part 2, various data used in this study and the methods followed in the analysis of data are presented.

Second Chapter deals with short term variations of air-sea interaction and upper ocean thermal characteristics at selected stations in Arabian Sea, using data collected during MONEX-79.

Climatology of upper ocean thermal structure and related characteristics in a selected area in western Arabian Sea, in relation to dynamics and air-sea energy exchange are studied in Chapter 3.

In Chapter 4, climatological studies are extended to an area in eastern Arabian sea and the similarities and differences between the two areas are brought out.

Fifth Chapter deals with zonally averaged heat transport in the northern Indian Ocean, obtained as a residual of net surface heat gain and upper ocean heat storage.

The summary of the results of present investigation and the conclusions based on the study are presented in Chapter 6.

LIST OF SYMBOLS AND ABBREVIATIONS

A	α	coefficient of thermal expansion of sea water
a_1, a_2		constants
B		buoyancy flux
C_D, C_H, C_E		bulk aerodynamic coefficients
C		specific heat of seawater at constant pressure
C_p		specific heat of air at constant pressure
e		vapour pressure
g		acceleration due to gravity
HC		heat content
HP		cyclone heat potential
h		mixed layer depth
I_0		solar irradiance
k		von Karman constant
k_1, k_2		constants
L		latent heat of evaporation; Monin-Obukhov length
ML		mixed layer
MLD		mixed layer depth
MLT		mixed layer temperature
n		cloudiness
P		atmospheric pressure
Q, Q_0, Q_R, Q_b)	heat energy flux quantities
Q_e, Q_v, Q_s, Q_h, Q_t)	
q_0, q_a		specific humidities at sea surface and at deck height
SATD		sea minus air temperature difference
SST		sea surface temperature

T	temperature at different levels in the sea($^{\circ}\text{C}$);Temperature($^{\circ}\text{K}$)
t, t_0, t_1	time
U, U_a	wind velocity at deck height
U_*	surface layer friction velocity
u, v, w	velocity components
W_e	entrainment velocity
z	depth
α	albedo of sea surface
Υ	extinction coefficient for solar radiation
ϵ	emmissivity
σ	Stefan-Boltzmann constant; standard deviation; r.m.s. error
ρ_a	density of air
ρ_w	density of sea water
τ	wind stress
θ_a	air temperature($^{\circ}\text{C}$)
θ_0, θ	SST($^{\circ}\text{C}$)
θ_E	estimated SST($^{\circ}\text{C}$)
J	joules
kg	kilograms
m	metre
mb	millibar
N	newton
W	watt
$^{\circ}\text{C}$	degrees Celsius
$^{\circ}\text{K}$	degrees Kelvin

CHAPTER 1

PART 1 : INTRODUCTION

1.1.1. AIR - SEA ENERGY EXCHANGE

There are several components of energy exchange that occur at the sea-atmosphere interface. These exchanges take place in a wide spectrum of temporal and spatial scales. Turbulent exchanges between the two media are small scale processes. The quasi-stationary circulations in oceans and atmosphere are a result of macroscale processes. Different aspects of large scale interactions and the climatology of different heat budget components have been discussed in detail by Malkus (1962).

Energy exchanges, at sea surface, like momentum, heat and water vapour transfers play a role in the atmospheric and oceanic circulations. Ocean and atmosphere need be considered as a single system with oceanic processes being influenced by the atmospheric phenomena and at the same time feeding back to the atmosphere. Roll (1972) has opined that until recently, oceanographers and meteorologists paid more attention to their respective fields only.

Ocean-atmospheric exchange is an aspect of study which has several applications like commercial fishing, ocean engineering, climatology, wave forecasting, weather modification, marine resources etc. Studies on air-sea interaction are, however, difficult to be carried out as is clear from the observation by Stewart (1975): "Study of the boundary layer is not only very important but is also very hard. The difficulties are both observational and conceptual. The conceptual problem lies in the fact that with trivial exceptions, the boundary layer is turbulent". In

his monograph dealing with different aspects of marine meteorology, Roll (1965) has discussed the observational aspects. Development of the knowledge of ocean-atmosphere system from the times of the Greeks has been summarized by Perry and Walker (1977).

Various experiments like Joint Air-Sea Interaction Project (JASIN), Barbados Oceanographic and Meteorological Experiment (BOMEX), Frontal Air-Sea Interaction Experiment (FASINEX), Airmass Transformation Experiment (AMTEX) etc. have been carried out for studying different aspects of air-sea interaction. Several other projects had air-sea interaction as one of the components (eg: International Indian Ocean Expedition, IIOE; GARP Atlantic Tropical Experiment, GATE; Mid-Ocean Dynamics Experiment, MODE). Studies on these topics were given due importance in Indo-Soviet Monsoon Experiment (ISMEX), MONSOON-77 and Monsoon Experiment (MONEX-79).

Since the coupling of ocean with atmosphere is accomplished by the fluxes through sea surface, studies for improving the knowledge of exchange of physical properties and also for establishing the uncertainties in their estimation are of importance. These have been included as one of the specific projects in World Ocean Circulation Experiment (WOCE). The working group on air-sea energy exchange for WOCE has identified the sources of errors in these exchanges as measurement errors, errors due to lack of data and errors in the formulation of bulk transfer. The tolerance in air-sea fluxes depends on their application. For estimating global ocean transports, the error must be less than 10 W/m^2 . The accuracies of 20 W/m^2 and 30 to 40 W/m^2 are sufficient for modelling studies and for heat fluxes to drive thermocline models respectively (Anon, 1986).

1.1.2. UPPER OCEAN THERMAL STRUCTURE

Vertical distribution of temperature in the sea does not show linear decrease with depth. From surface to a depth of 50-150m a homogenous layer of nearly uniform temperature is seen. This is known as the mixed layer (ML). From the base of the mixed layer, to a depth of about 1000 m, temperature decreases rapidly. This region is termed as the thermocline. Thermocline will not be present in high latitudes, since here surface and deepwater temperatures will not be very different. In regions of pronounced annual cycles of heating, a shallow thermocline forms during summer. This, however, vanishes after summer to form a deeper ML.

There are several processes that determine the characteristics of upper ocean thermal structure. Heat exchange at surface is one of the factors. When sea loses heat, convective mixing due to buoyancy flux produces deep mixed layer. Entrainment of cold water from below the ML due to wind forcing and current shear is another contributing factor. Further, in areas of upwelling and sinking, thermal structure variations can be found. As upwelling brings cold subsurface water upwards, a temperature drop can be noticed. Isotherms rise upwards and the thermocline shoals. Reverse conditions prevail during sinking. As a response to the atmospheric disturbances like cyclones, the thermal structure of upper ocean is found to undergo changes (Camp and Elsberry, 1978; Elsberry and Camp, 1978; Elsberry and Garwood, 1980; Ramesh Babu and Sastry, 1984; Rao, 1986).

Depth of ML has been defined in different ways. Scott (1902) considers it to be a depth where a minimum gradient of $2^{\circ}\text{C}/25\text{m}$ is

encountered. Defant (1961) suggests this gradient to be 0.05 C/m for tropical ocean. In another method, mixed layer depth (MLD) is considered to be the depth where temperature drops by a fixed value from sea surface temperature (SST). Most widely used drop is 1°C (Sastry and D'Zouza, 1970; Wyrcki, 1971; Ramesh Babu et al, 1976; Ramam et al, 1979; Varma et al, 1980). Robinson et al (1979) consider a drop of 1.1°C while Camp and Elsberry (1978), Rao (1986) and several others consider a drop of 0.2°C.

Another criterion was also used by Wyrcki (1971). After locating the shallowest depth interval where temperature difference is 0.5°C, these points were joined by a straight line. The depth of intersection of this line with the vertical line drawn from SST is taken as MLD. Both methods have been employed by Colborn (1975) also.

Considerable interest has, of late, been generated in the studies of ML. The spatial and temporal variations of MLD and MLT (mixed layer temperature) have been studied extensively. Attempts have also been made to develop capabilities for predicting these parameters using numerical models. Upper ocean being the lower boundary of the atmosphere, the capability to predict this boundary condition turns out to be a necessary requirement for prediction of atmospheric phenomena, using ocean-atmosphere coupled models (Meehl, 1984; Washington and Meehl, 1984; Meehl and Washington, 1985).

Upper ocean has also a crucial role in the general circulation of oceans (Holland, 1977). About the far-reaching impact of upper oceans, Kraus (1977) noted "The state of sea surface and water below concern us for many reasons. Ship traffic, naval operations, fisheries, the well-being and the very existence of coastal settlements have all been affected

by it. Beyond its immediate influence on human affairs, the upper ocean modulates almost all processes which shape the terrestrial environment".

Knowledge of thermal structure and its variations has applications also in ocean thermal energy conversion (OTEC) and determination of optimum locations for disposal of pollutants.

1.1.3. HEAT BUDGET OF THE OCEANS

Sun is the ultimate source of energy for earth. Sun's energy is converted into various forms by nature, some of which are even conserved for distant future after transformations as fossil fuel. Solar radiation received on surface is the primary heat source for oceans. The sea, in turn, radiates energy back to atmosphere. Heat is lost from sea due to evaporation. The sea either gains or loses heat through conduction at sea surface.

Apart from the above mentioned major components of air-sea heat exchange, there are minor components which include conversion of mechanical energy and conduction of heat between the oceans and the ocean floor. The picture will be complete if the advection of the heat by ocean currents is added to the major components. Thus the heat budget equation can be written as

$$Q_o = Q_s - Q_b - Q_e - Q_h - Q_v \quad (1.1)$$

where Q_o is net heat gain, Q_s is short wave radiation, Q_b is back radiation, Q_e is latent heat of evaporation, Q_h is sensible heat conducted at sea surface and Q_v is heat advection. Because of high specific heat of sea water, sea can temporarily store more heat than atmosphere. This heat is then transported from surplus to deficit regions as well as released

later to atmosphere. This process, in a way, controls the climate of the earth. Sverdrup et al (1942) remarked that oceans exercised a "thermostatic control" over the climate. Anomalies in various processes of heat budget can influence the climate. Developments in air-sea interaction and upper ocean studies have been reviewed by Garwood (1979).

1.1.4. EARLIER INVESTIGATIONS

There have been a large number of studies on air-sea energy exchange and thermal structure in the world oceans. The present survey of literature is, therefore, mainly limited to investigations in Arabian Sea. Mean currents and temperatures in 2° quadrangles for the entire Indian Ocean have been presented by Galle (1924). Mean thermal characteristics on a monthly basis have appeared in various atlases. SST and surface currents as well as different oceanographic conditions in Indian Ocean by U.S. Navy (Anon, 1950, 1960), oceanographic and meteorological parameters by Netherlands Meteorological Institute (Anon, 1952) are some of the earlier atlases. Wooster et al (1967) present the oceanographic properties in Arabian Sea at different subsurface layers. Distribution of oceanographic properties including derived parameters in the Indian Ocean (Wyrcki, 1971), oceanographic and meteorological parameters of Atlantic and Indian Oceans (Gorskho, 1978), monthly mean thermal characteristics and mean salinities of surface layer in north Atlantic and Indian Oceans (Robinson et al, 1979), surface meteorological parameters for Indian Ocean (Hastenrath and Lamb, 1979a) are some of the recent atlases.

Some of the important works on solar radiation are the atlas of heat balance by Budyko (1956) and the world maps of global solar radiation by Black (1956), Ashbal (1961) and Landsberg et al (1963).

Early work over Indian Ocean on these lines provides charts for February and August (Alberecht, 1958). Monthly and annual maps of global solar radiation and net radiation over Indian Ocean have been presented by Mani et al (1965). Using the data for 1963-64, Portman and Ryznar (1971) have given the monthly net radiation.

Evaporation in the Indian Ocean has been computed using climatological data by Venkateswaran (1956) and Privett (1959). International Indian Ocean Expedition gave an opportunity to study the air-sea interaction processes with more reliable and extensive data. Mean monthly fluxes during individual years have been presented by Miller et al (1963). Ramage et al (1972) have presented an atlas of the surface climate for 1963 and 1964. Based on studies on evaporation and moisture balance over Arabian Sea during southwest monsoon season, Pisharoty (1965) concludes that considerable amount of water vapour is added from Arabian Sea to the monsoon flow. Suryanarayana and Sikka (1965) studied evaporation over Indian Ocean during 1963 and Saha (1970b) examined the mean monthly fluxes during 1964. Saha and Suryanarayana (1972) observe that during July-August, evaporation is higher in Arabian Sea, Bay of Bengal and south Indian Ocean compared to the equatorial region. They suggest also that higher evaporation in Bay of Bengal compared to Arabian Sea is due to higher SST in the Bay of Bengal. Bhumralkar (1978) studied evaporation over Arabian Sea and its relation to rainfall at west coast of India during southwest monsoon.

Annual variations of air-sea energy exchange components at six selected stations in Arabian Sea have been presented by Colon (1964). Considerable increase of heat flux from sea surface to atmosphere is noticed during southwest monsoon. Maximum evaporation during monsoon is

located away from Somali upwelling region. Minimum evaporation is observed in Somali upwelling region, despite the strong winds. Similar findings are reported by Hastenrath and Lamb (1979b, 1980). Colon (1964) points out that there is a vast reservoir of moisture near the surface. Convergence associated with synoptic systems is required for upward release of this moisture and for precipitation to occur. Rao et al (1978) have noticed that during normal monsoon condition, Bay of Bengal loses more heat than Arabian Sea and during break monsoon condition, Arabian Sea loses more heat.

Mean monthly temperatures off northwest coast of India indicated a fall in SST towards north (Gogate, 1960). A striking feature of annual variation of SST, off southwest coast of India obtained by Ramasastry and Myrland (1959) is the bimodal oscillation with a pronounced cooling during southwest monsoon season. Similar results, off north Canara (Noble, 1968) and in coastal waters off different parts of west coast of India have been reported (Sharma, 1968; Colborn, 1975; Anjaneyulu, 1980; Anon, 1980). Various aspects of Arabian Sea oceanography during southwest monsoon, including thermal structure, stratification and circulation, have been presented in a series of papers by Sastry and D'Zouza (1970, 1971, 1972, 1973). Colborn (1975) presented the thermal structure of upper 500m in Indian Ocean, after dividing the region into several subareas and discussed its general relationship to variation of climatic pattern and subsurface dynamic processes. Based on oceanographic characteristics observed off the west coast of India in early months of 1966, Elizarov (1973) indicates that the region can be divided into northern and southern parts with a transition zone around 18° - 21° N. Ramam et al (1979) find that during summer monsoon, together

with a fall in SST, there is an increase in MLD in the central Arabian Sea. The upward slope of ML towards coast of India indicates southerly flow which may cause upwelling.

During southwest monsoon season, SST increases from west to east in Arabian Sea. Very cold waters in the western part is due to intense upwelling. Ramesh Babu et al (1976) studied meridional and zonal sections of temperature in May and July and found a thick mixed layer at 15° - 16° N in central Arabian Sea and attributed this to the possible sinking of the water upwelled off the west coast of India.

Ramam et al (1979) and Anjaneyulu (1980) are of the opinion that the drop in SST in Arabian Sea during southwest monsoon is due to strong winds. Rao et al (1976) studied the summer cooling of Arabian Sea using data in a zonal belt. Krishnamurti (1981) suggested that cooling of surface waters in central and eastern Arabian Sea around 10° N latitude during June 1979 was governed by mid-oceanic upwelling due to positive wind stress curl associated with monsoon onset. Ramesh Babu and Sastry (1984) indicate that summer cooling in central Arabian Sea is due to the mixing at the base of warm surface layer caused by entrainment associated with increased current shear at the base. On examining the various heat budget components in Arabian Sea viz., surface heat flux, upwelling and advection, in relation to summer cooling, Düing and Leetmaa (1980) have concluded that upwelling is the major factor. Sastry and Ramesh Babu (1985) reviewed the various processes responsible for summer cooling of Arabian Sea. The thermal structure of upper 200 m in central Arabian Sea (Marsden square 066) has, recently, been studied using historic data (Rao, 1988). From estimates of monthly heat advection, he observes

that the semi-annual signal seen in upper layers does not penetrate beyond 50m.

During fair weather season, off west coast of India, SST is found to increase from north to south and the isotherms in the surface layers slope down towards south (Ramesh Babu et al, 1980). Thermohaline structure in northern Arabian Sea during February-April has been studied by Varma et al (1980). Numerical model studies of upper ocean thermal structure in a zonal section in central Arabian Sea indicate that except during southwest monsoon, surface heat and momentum fluxes dominate mixed layer processes (Shetye, 1986).

Studies on short-term variations from fixed locations in Arabian Sea are largely limited to southwest monsoon season, using data collected during ISMEX, MONSOON-77 and MONEX-79. Ramesh Babu et al (1976) found that in the latter part of May, over the continental shelf off west coast of India, temperature of upper 25 m increased slightly in 4 days while, further offshore, temperature decreased. Heat budget from fixed stations in the north Indian Ocean has been studied by Ramanadham et al (1981) and Rao et al (1981a). Using data mostly from Russian polygons during MONEX-79, Shajahan (1980) and Reddy et al (1984b) find sudden increase in fluxes with the formation of the monsoon onset vortex. Using data of Russian polygon positions during MONSOON-77, Rao et al (1981b) have found that cooling and deepening rates of mixed layer are higher in central part than in eastern part of Arabian Sea. Making use of these stations, Rao et al (1985) have observed that energy loss from sea surface during disturbed weather is nearly double than during fair weather and also that east central Arabian Sea acts as a heat source to monsoon atmosphere. Using data from fixed stations occupied by Indian and Russian ships during

MONSOON-77, Rao (1986) and Rao (1987b) have studied thermal response to monsoon in eastern and central Arabian Sea respectively. In eastern Arabian Sea, two layers of increased vertical temperature gradient are, in general, noticed in upper ocean during early monsoon which subsequently merge to form a single layer. The ML deepening has been penetrative and non-penetrative in central and eastern Arabian Sea respectively. Using same Russian polygon data, Rao (1987a) finds that surface cooling dominates both entrainment and advection in the mixed layer cooling in central Arabian Sea. Rao (1984), analysing data from two fixed stations, suggests that surface cooling in eastern Arabian Sea as a result of the onset vortex during MONEX-79 can be attributed to air-sea energy exchange and advection. Turbulent fluxes in the eastern Arabian Sea during MONEX have been studied by Varma and Raman (1987). Nansen data at one location were used by Rao (1987) for studying thermal characteristics.

Gopalakrishna et al (1987) have found that net surface heat exchange, which is mainly controlled by evaporation, have almost accounted for heat content variation in ML in east central Arabian Sea during weak spell of monsoon. Diurnal variability of surface layer hydrographic conditions (Murthy and Madhusoodanan, 1987) and fine structure of ML (Vijayarajan and Santha Devi, 1987) during February, off Calicut on the west coast of India, have been studied. Using satellite data, Simon (1987) has observed greater evaporation near the onset vortex in June 1979. Seetharamayya and Master (1984) point out that increase in air-sea temperature difference in eastern Arabian Sea may have provided turbulent exchange of heat and moisture, helping the development of this onset vortex.

Ellis (1952) has concluded that during flood year, SST is more

and during draught year, SST is less. Zonal anomaly of SST produced by intense upwelling off Somali area is found to have an effect on monsoon activity (Saha, 1970a). Shukla (1975) has found from numerical experiments that positive SST anomaly in western Arabian Sea increases monsoon rainfall while according to Shukla and Mishra (1977) positive anomaly in central Arabian Sea increases rainfall. However, using empirical orthogonal functions, Weare (1979) observes that higher SST is related to decrease in rainfall. Positive anomaly is found to be related to good monsoon by Jambunathan and Ramamurthy (1975). Pisharoty (1981a) has shown that monsoon onset can be forecast by warm SST anomaly and break monsoon by cold anomaly over central Arabian Sea.

Joseph and Pillai (1986) have studied selected areas of Arabian Sea and Bay of Bengal and have noticed that good monsoon produces negative and weak monsoon produces positive SST anomalies during post-monsoon months. These anomalies last till next monsoon. Pisharoty (1981b) put forth a theory that summer monsoon is a delayed response of ocean-atmospheric system to a poleward heat transport across $30^{\circ} - 40^{\circ} \text{N}$ during the preceding winter. Using a numerical model, Keshavamurthy (1981) has found that warm SST anomalies in equatorial and western Pacific Ocean may be one of the factors for the variation in summer monsoon. The monsoon activity appears to be related in a complex manner to El-Nino, which is the occurrence of unusually warm waters in eastern Pacific Ocean (Sikka, 1980).

Because of the diverse nature of the topics dealt with in this thesis, further literature are referred to under the relevant chapters.

1.1.5. SCOPE OF PRESENT STUDY

Short-term variations in energy exchange and upper ocean thermal structure at fixed stations in Arabian Sea are studied using time series data collected during pre-onset and after the onset of the southwest monsoon, in the wake of an onset vortex. Annual variation of upper ocean thermal structure is studied at two selected areas using long-term data. Areas I and II are located in the western and eastern parts of Arabian Sea. These areas come under the influence of monsoons and hence that of annually reversing current patterns. However, they differ in the subsurface dynamics. Oceanic heat storage in these areas are compared with net surface heat gain and heat advection is obtained as a residual of these two. Using a model presented by Mc Phaden (1982) the importance of different processes contributing to the evolution of SST is evaluated. The possible errors in the estimated SST have also been worked out.

Annual cycle of heat transport in north Indian Ocean is also studied. Zonally averaged oceanic heat transports are obtained as the difference between the zonally averaged surface heat gain and oceanic heat storage. Some studies on these lines were earlier initiated by the present author (Varma, 1988).

1.1.6. AREA OF STUDY

In the present study, short-term variations in energy exchange and upper ocean thermal structure at two fixed locations in Arabian Sea are investigated. The historic subsurface data are used to study upper ocean thermal structure climatology at two selected areas in Arabian Sea. Area I is located at the northern part of Somali current and is bounded by latitudes 5° and 10° N and longitude 55° E on east and 50° E and African coast

on the west. Area II is located off central west coast of India and is bounded by latitudes 14° and 18° N and longitude 70° E on west and the Indian coast on the east. Annual cycle of heat transport in the northern Indian Ocean is also studied. The regions of study are shown in Fig. 1.1.

Northern Indian Ocean comes under the influence of seasonal reversal of winds due to the monsoons. The two monsoons are termed as southwest or summer monsoon and northeast or winter monsoon. Of these two, the southwest monsoon lasts longer and is stronger and steadier. Generally, by the middle of May, wind turns southwesterly and by early June, there is a sudden strengthening of the wind or the 'burst' of monsoon along the southwest coast of India. Southwest monsoon brings copious rains to the Indian subcontinent. This summer monsoon weakens by the end of September and is followed by transition period during October-November. Northeasterly winds, generally, prevail in the months of December and January and the transition begins in February.

In response to the reversal of winds, the surface currents also change its direction during the course of the year. This reversal has been recorded as early as 8th or 9th century AD (Warren, 1966; Aleem, 1967, 1973). During northeast monsoon, current in the open ocean is westerly and coastal current flows counter clockwise in Arabian Sea and Bay of Bengal. Current direction reverses during southwest monsoon to flow eastwards in open ocean and clockwise along the coast in Arabian Sea and Bay of Bengal.

Circulation in north Indian Ocean as deduced from dynamic topography, indicates, apart from reversal in direction, very complex nature comprising of several eddies (Düing, 1970). Sastry and D'Zouza

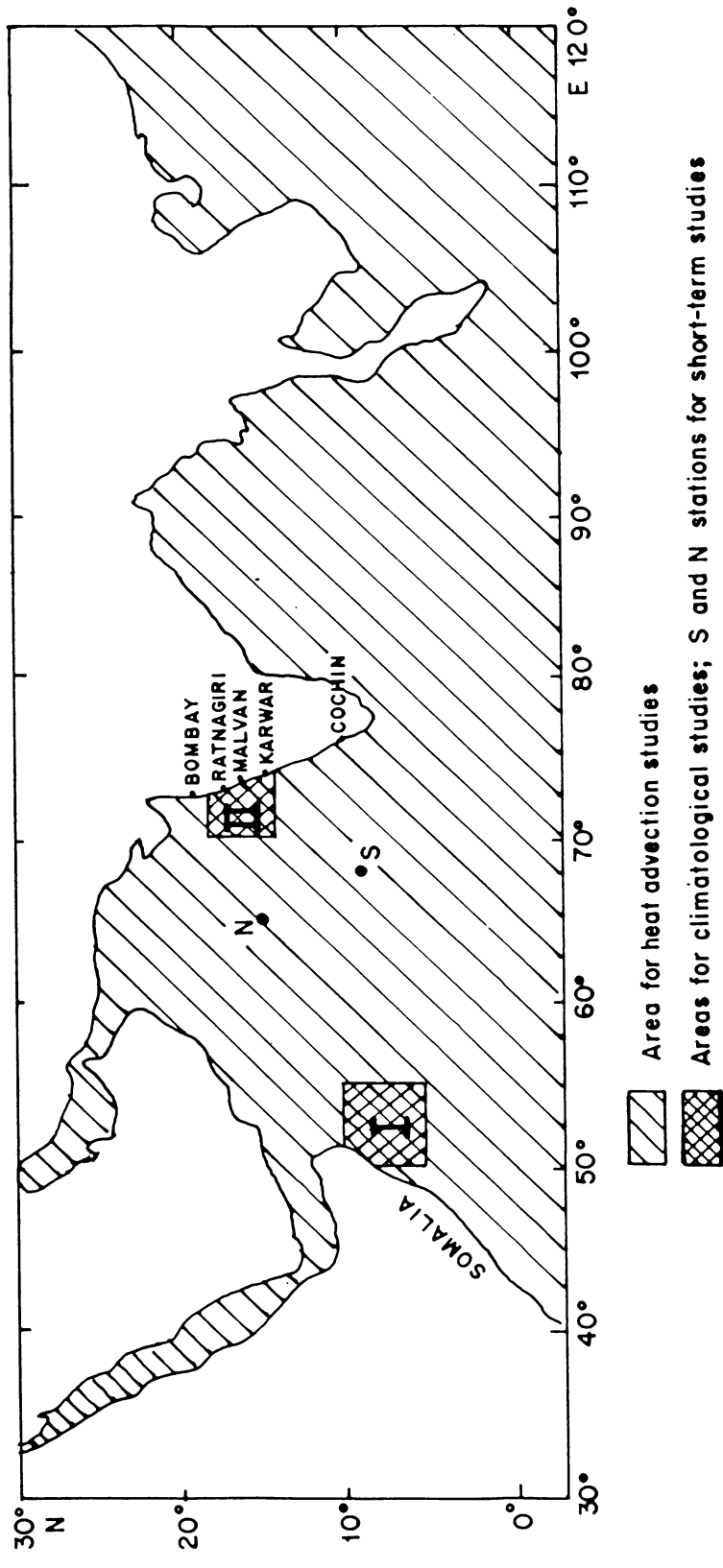


Fig.1.1 Map showing areas of study.

(1971) observed cyclonic and anticyclonic eddies in Arabian Sea during southwest monsoon and Das et al (1980) reported eddies in northern Arabian Sea during February-April. Along the east coast of Africa, during southwest monsoon season, a swift northeasterly current, known as Somali current, develops. More details about Somali current are presented in Chapter 3.

With the changing pattern of monsoon winds, the annual cycle of air-sea energy exchange parameters also undergoes changes in Arabian Sea and Bay of Bengal. Arabian Sea is a region where net annual heat gain is seen. Largest net radiation balance of more than $140 \text{ k cal/cm}^2/\text{year}$ is observed in the northern part of Arabian Sea (Budyko, 1974). Annual march of heat budget components at a representative location in the Arabian Sea (15° N , 70° E) presented by Budyko (1974) shows that the net radiation reaches a maximum in April-May and thereafter decreases due to the cloudiness associated with southwest monsoon. After this, net radiation slightly increases in September-October and decreases again to a winter minimum. Evaporation is high during southwest and northeast monsoon seasons. Sensible heat loss of very small magnitude is noticed throughout the year. In this region, during summer monsoon, slight net heat loss is noticed and in autumn and spring substantial heat gain is seen.

Similar to the pattern of energy exchange components, annual variation of SST is also bimodal. Low values of SST are noticed during summer and winter. Summer cooling in Arabian Sea is a combined effect of different factors like reduced insolation, increased evaporation, turbulent mixing resulting in the deepening of ML and the spreading of cold upwelled water. During southwest monsoon, in the central Arabian Sea, MLD increases from about 40 m to about 80 m.

Because of the strong winds for a period of about four months during southwest monsoon, Arabian Sea also provides a unique area for studying the processes and dynamics of upper ocean response to strong and sustained atmospheric forcing (de Zoeke and Paulson, 1987). Thus, Arabian Sea provides a possible site for such process oriented experiments.

PART 2 : MATERIALS AND METHODS

1.2.1. SHORT-TERM VARIATIONS

The short-term variations in air-sea interaction and upper ocean thermal structure at selected stations in Arabian Sea are studied using data collected during MONEX-79 and are discussed in Chapter 2. The two fixed locations, 15° N, 68° E and 9° N, 65° E, were occupied during different periods of May and June 1979 (Fig. 1.1). Surface meteorological data obtained from India Meteorological Department and subsurface bathythermograph data supplied by the Naval Physical and Oceanographic Laboratory are utilised for this study. Sources of different data utilised in the thesis are shown in Table 1.1.

Surface wind stress, radiation balance at sea surface and fluxes of latent and sensible heats are evaluated using surface meteorological data. Subsurface thermal characteristics like MLD, heat content and cyclone heat potential have been evaluated using BT data.

Radiation balance

Radiation balance is the difference between the incident and reflected solar radiation and the net long wave radiation.

$$Q_R = Q_S (1 - \alpha) - Q_b \quad (1.2)$$

where Q_S is the short wave radiation received from the sun and sky and α , the albedo of sea surface, is the ratio of the radiation reflected from sea surface to the incoming radiation. Q_b is the net long wave radiation i.e., the difference between long wave radiation emitted by sea and that radiated downwards from the atmosphere.

Table 1.1. Data utilized in the study

SERIAL NO.	DATA	SOURCE
1.	Short-term surface meteorological data during MONEX-79	College of Fisheries data base
2.	Short-term upper ocean B.T. data during MONEX-79	NPOL data base
3.	Long-term upper ocean B.T. data at selected areas in Arabian Sea	NPOL data base
4.	Heat budget components at selected areas in Arabian Sea	Hastenrath and Lamb (1979b)
5.	Zonally averaged net heat gain in northern Indian Ocean	Hastenrath and Lamb (1980)
6.	Zonally averaged upper ocean heat storage in northern Indian Ocean	Meehl (1984)

The short wave radiation, both direct and from sky, are affected by the presence of clouds. Kimball (1926) used the formula

$$Q_s = Q [0.29 + 0.71 (1-n)] \quad (1.3)$$

where Q_s and Q are the short wave radiation under actual and cloud free conditions respectively and n is the mean cloudiness in fractions of unity. Budyko (1956) has developed a formula

$$Q_s = Q (1 - \alpha) (1 - k_1 n) \quad (1.4)$$

where the albedo varies with latitude and month. Constant k_1 is a function of latitude. Budyko (1974) gave a quadratic formula after Berliand (1960) for short wave radiation

$$Q_s = Q (1 - \alpha) (1 - a_1 n - a_2 n^2) \quad (1.5)$$

This equation in a way accounts for cloud forms. With an increase in cloudiness, the amount of low clouds, which reduce solar radiation most, usually increases. Thus as cloudiness increases, the fall in radiation occurs slowly at first and then more rapidly. Budyko (1974) had, however, pointed out that both equations gave similar results in many monthly calculations.

Seckel and Beaudry (1973) used for daily average clear sky radiation, an empirical formula as a function of latitude and time of year. Reed (1977) found that this formula agreed only with the formula given by Lumb (1964) for obtaining hourly estimates of solar radiation. Reed (1977) has further given a quadratic equation for incident solar radiation relating it to cloudiness and noon altitude of sun.

Following Roden (1959), in the present study, equation (1.4) is

utilized for calculating short wave radiation. Average day time cloudiness are evaluated from 3 hourly observations. Values of Q , α and k_1 have been adapted from the tables by Budyko (1974). Albedo for present latitudes agree with average day time values for low latitudes given by Payne (1972). Hastenrath and Lamb (1979b) used a constant albedo of 6 percent while using climatological data for the preparation of atlas. Short wave radiation is presented in W/m^2 .

Effective back radiation from sea surface has been evaluated using the following equation which is used by several authors (Roden, 1959; Ramage et al, 1972; Budyko, 1974).

$$Q_b = \epsilon \sigma T_o^4 (0.39 - 0.05 \sqrt{e}) (1 - k_2 n^2) + 4 \sigma T_o^3 (T_o - T_a) \quad (1.6)$$

where T_o and T_a are SST and air temperature in degree Kelvin, ϵ is the emmissivity, σ is the Stefan-Boltzmann constant, e is the vapour pressure, n is the cloudiness and k_2 is an empirical constant for cloud correction. Hastenrath and Lamb (1979b) used a constant value of 0.53 as correction factor (k_2) for cloudiness in Indian Ocean. Reed (1976) and Simpson and Paulson (1979) gave slightly different constants for tropics and 30° latitudes respectively. Vapour pressure in millibars is calculated using

$$e = 6.11 \times 10^{(8.573 - \frac{2340}{T})} \quad (1.7)$$

Daily average meteorological parameters are used to get daily back radiation. k_2 was adapted from Budyko (1974). Emmissivity is 0.98 and Stefan-Boltzmann constant is $5.65 \times 10^{-8} W/m^2 / K^4$.

Turbulent fluxes of momentum, sensible heat and latent heat of evaporation

In the present study, the bulk aerodynamic method is followed. The most commonly used method for obtaining turbulent fluxes, using routine meteorological observations, is the bulk aerodynamic method in which

$$\tau = \rho_a C_D U_a^2 \quad (1.8)$$

$$Q_h = \rho_a C_P C_H (\theta_o - \theta_a) U_a \quad (1.9)$$

$$Q_e = \rho_a L C_E (q_o - q_a) U_a \quad (1.10)$$

Here U_a is wind speed in m/s at deck height, θ_a and q_a are the temperature and specific humidity respectively at this height, θ_o is SST and q_o is the specific humidity of saturated air at SST. C_D , C_H and C_E are non-dimensional exchange coefficients for momentum, heat and water vapour respectively. ρ_a (air density) is 1.2 kg/m^3 , C_P (specific heat at constant pressure of air) is $1005 \text{ J/kg/}^\circ\text{K}$ and L (latent heat of evaporation) is $24.5 \times 10^5 \text{ J/kg}$. After calculating vapour pressure (equation 1.7), specific humidity is estimated using

$$q = \frac{0.623e}{P} \quad (1.11)$$

where P is atmospheric pressure in mb. Heat fluxes are obtained in W/m^2 and the wind stress in N/m^2 .

Bulk aerodynamic coefficients

C_D is called drag coefficient, C_H is called Stanton number and C_E is called Dalton number. All unknown factors of turbulent exchange are assumed to be included in these coefficients. It has been noticed that these constants do not have universal values, but are dependent on wind

speed and atmospheric stability. As wind speed increases, turbulence is enhanced and larger exchange takes place. When the atmosphere is unstable, exchange increases due to convective mixing. Under stable conditions, turbulence is suppressed and transfer of properties is reduced.

Many investigations, both theoretical and observational, suggest increase in C_D with increasing wind speed (Charnock, 1955; Smith and Banke, 1975; Melville, 1977; Smith, 1980; Wu, 1980; Large and Pond, 1981). However, there is a large variation in the numerical values obtained. Launiainen (1979) has pointed out that such variations in neutral drag coefficients, especially at low wind speeds are possible due to different reasons.

Examining the various wind stress measurements Wilson (1960) concludes that C_D under light winds is 1.5×10^{-3} and increases asymptotically to 2.4×10^{-3} for very strong winds. Slight increase of C_D with wind speed has been noticed by Deacon (1962) and Deacon and Webb (1962). Different aspects of air-sea interaction including the drag coefficients have been discussed by Roll (1965) and Kraus (1972). Brocks and Krugermeyer (1972) have obtained $C_D = (1.3 \pm 0.18) \times 10^{-3}$ and do not find much dependence on wind upto speed of 13 m/s. Dunkel et al (1974) obtained $C_D = 1.39 \times 10^{-3}$ for Atlantic, following direct methods. Smith (1980) finds $C_D = (0.61 + 0.063U) \times 10^{-3}$ where U is wind speed in m/s and also indicates that drag coefficient appears to be nearly constant for winds below 10m/s but increases rapidly at higher wind speeds. Garratt (1977) shows that within range of wind speeds 4 to 21m/s, neutral drag coefficient is $0.51 U^{0.46} \times 10^{-3}$ or in the linear form $C_D = (0.75 + 0.067 U) \times 10^{-3}$. These relations are similar to those proposed by Deacon

and Webb (1962) and by Wu (1969) for wind speeds $< 15\text{m/s}$. This, however, does not support constant C_D above 15m/s suggested by Wu (1969). Smith and Banke (1975) also obtained a similar relationship $C_D = (0.63 + 0.66 U) \times 10^{-3}$. Garratt (1977) summarized the different investigations giving the respective values of C_D , its variability and the wind speeds under which the investigations were carried out. Wu (1980) suggests a relationship $C_D = (0.8 + 0.065 U) \times 10^{-3}$ which favourably agrees with that given by Garratt (1977).

According to Wu (1980), although C_D must increase with wind speed, at very high wind speeds ($> 20\text{m/s}$) C_D must be constant, because sea surface is disrupted by sea spray which plays a role in momentum transfer. However, these exchanges at high wind speeds are less understood because of difficulties in making observations (Roll, 1972). Examining the effect of wind fetch, Smith (1980) finds that C_D is not very much dependent on fetch. But at limited fetches, C_D can be higher as the growing waves may extract more energy from winds.

Since stability of atmosphere influences turbulence, the bulk transfer coefficients must be dependent on stability. Effect of stability is mainly caused by the effect of temperature gradient. The effect of moisture on stability is insignificant when conditions are not near-neutral (Launiainen, 1979). From profile studies, Launiainen (1979) has found that the relative effect of moisture is dependent on temperature gradient. This is because when temperature difference is very small, it is mainly the moisture that determines stability. Smith (1980) finds a dependence of C_D on stability though he has not obtained quantitative relationship. Fissel et al (1977), in their computation of surface fluxes

from climatological and synoptic data, indicate that the effect of stability may not be important over open ocean because of the low air-sea temperature difference. Kondo (1975) and Bunker (1976) have shown the variation of the coefficients with stability and wind speed.

C_D , C_E and C_H have been considered to be identical by various authors (Sverdrup, 1937; Jacobs, 1942; Budyko, 1956). Subsequent investigations, however, revealed that bulk exchange coefficients for latent and sensible heats are different from drag coefficient. There are fewer works on the bulk transfer coefficients for sensible and latent heats, mainly due to observational difficulties. Frieche and Schmitt (1976), using data during moderate wind speeds, find that C_H is 0.86×10^{-3} in stable and is 0.97×10^{-3} in unstable cases, over a range of $U(\theta_o - \theta_a) = -15$ to 20°C.m/s , where U is wind speed at 10m. If very high wind speed is also included in this data set, C_H becomes 1.4×10^{-3} . According to Smith (1980), heat flux coefficient does not depend strongly on wind speed but depends on stability. This coefficient is low under stable (0.83×10^{-3}) and high under unstable (1.10×10^{-3}) conditions. Kondo (1975) plotted the bulk coefficients as a function of wind speed and stability.

Several workers have suggested $C_H = C_E$. Hicks (1972) finds both coefficients to be 1.4×10^{-3} . Pond et al (1974) have obtained $C_H = C_E = 1.5 \times 10^{-3}$ under normal temperature conditions. Smith (1974) suggests a value of 1.2×10^{-3} for both C_H and C_E . Bunker (1976) points out that C_E can be used for estimating sensible heat transfer also. According to most experiments, the assumption that $C_H = C_E$ is still valid (Launiainen, 1979). He has also shown the increase of bulk transfer coefficients of moisture and sensible heat from stable to unstable

conditions. Smith (1980) indicates that since heat is not transported by form drag, wind dependence, may not be necessary. However, as the waves and spray increase the surface area, C_H may increase with wind speed.

From these studies on bulk transfer coefficients, it can be seen that their use involves some uncertainties. Mentioning the uncertainties and difficulties in their use, Launiainen (1979) observes "the exact values of universal bulk transfer coefficients, if they exist, remain, at least for the present, more or less an academic question". He further points out that comparisons of drag coefficients from different environments should be made with reservation since the character of turbulence depends not only on the external factors, mainly wind conditions, but also on local features.

Some of the workers have used constant values of bulk exchange coefficients for the Indian Ocean. (Venkateswaran, 1956; Privett, 1959; Ramanadham et al, 1968; Saha and Suryanarayana, 1972; Ramage et al, 1972; Hastenrath and Lamb, 1979b). Colon (1964) used two different coefficients, smaller one for low wind speed conditions and a larger one for high wind speed conditions. Similar method has been followed by Padmini (1981).

In the present study, C_D and $C_H = C_E$ have been adapted from the tables (Bunker, 1976) which give the coefficients for different wind speeds and air-sea temperature differences. These values of the coefficients are widely used. Weare (1983) and Hsiung (1985) used C_E presented by Bunker (1976) for latent and sensible heat computations. Hellerman and Rosenstein (1983) developed a polynomial using values of C_D given by Bunker. In analysing climatological data from Indian Ocean,

recent workers have utilized these coefficients (Rao et al, 1978; Reddy et al, 1984a; Subrahmanya and Rao, 1984). These coefficients have also been utilised for short-term studies using MONEX data by Anto et al (1982), Reddy et al (1984b) and Rao and Naidu (1987).

In the present study six hourly observations are used to compute the fluxes and average daily fluxes are obtained.

Upper ocean temperature data

B.T. data collected from fixed stations are used for studying the thermal structure. Six hourly profiles have been averaged to obtain daily profiles of temperature. Data are checked and obvious errors have been removed. Very high temperature, noticed in the surface layers on certain days, have been reconciled. MLD is taken as the depth at which temperature decreases by 1°C from SST.

Heat content in the different 50 m layers from surface to 200m are calculated using the equation.

$$HC = \int_{z_1}^{z_2} \rho_w C T dz \quad (1.12)$$

where z_1 and z_2 are the upper and lower depths. T is temperature and dz is 10m. Following Bathen (1971), $\rho_w C$ is taken to be 0.977 cal/cm³/K which works out to be 4.1 x 10⁶ J/m³/K.

Cyclone heat potential which gives the indication of energy available in the upper ocean in excess of a selected temperature, has been estimated using

$$HP_{28} = \int_0^{z_{28}} \rho_w C (T - 28) dz \quad (1.13)$$

where z_{28} is the depth at which 28°C is observed.

The relative importance of wind stress and buoyancy flux in driving the mixing in upper ocean can be evaluated using Monin-Obukhov length (L) given by

$$L = \frac{U_*^3}{kB} \quad (1.14)$$

where U_* is surface layer friction velocity ($(\tau/\rho_w)^{1/2}$), k is von Karman's constant (0.4) and B is the surface buoyancy flux. Although buoyancy flux is caused by surface heat and salt fluxes, buoyancy flux due to salinity change usually makes only a small contribution (Shay and Gregg, 1986). Hence, temperature change alone is considered in the present computations.

The buoyancy flux B is given by

$$B = \frac{-g A}{\rho_w c} Q_o \quad (1.15)$$

where g is acceleration due to gravity (9.80 m/s^2), A is coefficient of thermal expansion of water (2.5×10^{-4}) and other factors have the same values as given earlier. Heat loss from sea surface is considered as positive and hence B would be negative in that case.

L is negative for surface heat loss. L can be considered as the depth at which turbulence energy produced by wind and by buoyancy flux are equally important. h/L , where h is MLD, can be considered as a bulk stability parameter (Shay and Gregg, 1986). This ratio gives the relative importance of the two controlling factors, viz., mechanical and convective turbulence in the mixing (Niiler and Kraus, 1977).

The rate of supply of turbulent energy by wind action is given by the product of wind stress and wind velocity (Niiler and Kraus, 1977),

a fraction of which is available for mixing. Following Shay and Gregg (1986); the factor

$$E = \tau U_a \quad (1.16)$$

is also estimated for every day.

1.2.2. CLIMATOLOGICAL DATA

For studying the upper ocean thermal structure at two selected areas in Arabian Sea (Chapters 3 and 4) long-term data have been utilised (Table 1.1)

For Area I (Sec. 1.1.6), all bathythermograph data at 10m depth intervals till 1978, from NODC (National Oceanographic Data Centre) data files, are extracted. For those months with less than 5 profiles, temperature from hydrographic cast is also utilised. These are linearly interpolated to obtain data at 10m intervals. Levitus and Oort (1977) used linear interpolation of XBT profiles to get temperature data at standard depths. Lamb and Bunker (1982) used linear interpolation for generating temperature data at selected depths from XBT and nansen cast for Atlantic (see also Lamb, 1984).

Quality control is applied on the temperature profile data. First of all, obviously unusual values have been removed. Subsequently for every month, at each depth, the average and standard deviation are found out. Any observation that fell outside the limit, $\text{mean} \pm 2\sigma$ has been discarded. Final data at any depth is taken as the average of remaining observations. Levitus and Oort (1977) and Lamb and Bunker (1982) employed the limit $\pm 5\sigma$ for global and Atlantic data sets respectively.

An initial examination of present data has shown that this limit becomes too wide and hence the $\pm 2\sigma$ limit is employed in the present case.

For Area II (Sec. 1.1.6) slightly different procedure is employed. This area has been divided into four 2 degree squares. In cases where continental shelf region comes under any of the squares, further division into shelf and deep water regions is made. The average profiles for different subregions formed the subsets which are then pooled to get monthly average profiles. Unclassified data such as NODC data, data of PFP, Indo - Polish and OCEANAVEX expeditions available with Naval Physical and Oceanographic Laboratory (NPOL) data base have been utilised.

Because of the difference in data compilation, the quality control procedure used for area II is also slightly different. At any depth, the subset value that exceeded $\pm 2\sigma$ limit from the average has been rejected. The remaining values are averaged to get final profiles for every month.

Number of observations of final data at each depth for Areas I and II are presented in Tables 1.2 and 1.3 respectively. In general, the number of observations decreases with depth. In Area I, except during June, July and November, the number of observations are, in general, satisfactorily high. Area II contains comparatively large number of observations in all months.

Oort and Vonder Haar (1976) utilised hydrographic and bathythermograph data averaged for 19 levels from surface to 1000 m for studying ocean-atmospheric heat balance. Average profiles of different oceanographic parameters for different regions have been worked out by

Table 1.2. Monthly and depthwise distribution of number of observations utilized
to get average profiles in Area I

DEPTH (m)	JAN	FEB	MAR	APR	MAY	JUN	JUL	AUG	SEP	OCT	NOV	DEC
0	7	16	30	21	6	4	3	65	11	23	4	13
10	7	16	30	21	6	4	3	67	11	23	4	13
20	7	16	31	21	6	4	3	69	10	23	4	13
30	7	15	31	21	6	4	3	71	11	23	4	13
40	7	15	31	20	6	4	3	71	11	23	4	13
50	6	15	30	20	6	4	3	70	11	23	4	12
60	7	15	30	20	6	4	3	69	12	22	4	11
70	7	15	32	19	6	4	3	69	12	23	3	9
80	7	15	32	19	6	4	3	68	12	21	3	8
90	7	15	32	19	6	4	3	68	12	22	3	8
100	7	15	32	18	5	4	3	68	12	23	3	7
110	6	15	32	18	5	4	3	67	12	21	3	5
120	3	15	31	18	5	4	3	67	12	22	3	5
130	1	15	32	16	4	4	3	67	12	22	3	4
140	1	16	28	14	3	3	3	66	12	22	0	0
150	0	16	28	14	3	2	3	66	12	22	0	0
160	0	16	28	14	3	2	3	65	12	21	0	0
170	0	16	27	14	3	2	3	64	12	22	0	0
180	0	15	27	14	3	2	3	63	12	22	0	0
190	0	14	27	14	3	2	3	61	12	23	0	0
200	0	15	27	14	3	2	0	56	11	21	0	0

Table 1.3. Monthly and depthwise distribution of number of observations utilized
to get average profiles in Area II

DEPTH (m)	JAN	FEB	MAR	APR	MAY	JUN	JUL	AUG	SEP	OCT	NOV	DEC
0	54	18	48	51	30	40	13	51	45	23	57	33
10	54	18	54	50	30	40	13	51	45	23	58	33
20	54	18	54	50	30	40	13	51	45	23	58	37
30	53	18	54	50	30	40	13	48	43	23	51	37
40	53	18	55	49	30	40	12	46	43	21	54	36
50	51	18	52	47	24	38	12	45	39	21	48	35
60	48	12	50	39	24	34	12	36	31	16	40	31
70	36	10	46	35	23	28	11	34	25	12	29	23
80	27	10	44	31	23	26	9	27	22	12	27	17
90	28	8	43	26	23	21	3	26	16	10	24	15
100	26	6	38	19	23	19	3	25	13	10	19	15
110	18	6	37	15	23	11	3	22	11	5	18	15
120	14	4	36	13	23	12	3	22	10	1	14	10
130	9	3	32	12	23	12	3	22	7	1	16	8
140	6	3	30	10	23	10	3	22	5	1	13	7
150	5	2	28	6	23	9	3	21	6	1	10	7
160	4	2	28	6	23	7	2	20	12	1	10	7
170	3	2	27	6	23	8	2	20	11	1	10	6
180	3	2	26	6	21	8	2	20	10	1	10	4
190	3	2	13	6	16	8	2	15	10	1	10	5
200	3	2	8	6	9	8	2	11	9	1	9	5

various authors (Fuglister, 1960; Merle, 1980; Lamb, 1981; Lamb and Bunker, 1982; Emery and Dewar, 1982; Levitus, 1984). Such detailed studies have been very few in Indian Ocean. Recently, Levitus (1987a) has presented the variation of zonally averaged heat storage for different oceans including Indian Ocean. Various problems encountered in obtaining such average profiles are discussed in Chapter 5 (Sec. 5.3) while describing the oceanic heat transport in north Indian Ocean.

Heat storage

Heat content in the different layers of upper ocean is evaluated from the average monthly temperature profiles using equation 1.12. The heat storage, Q_t , is given by

$$Q_t = \frac{\delta HC}{\delta t} \quad (1.17)$$

where HC is heat content in upper ocean and t is time interval.

The following equation has been used for evaluating heat storage.

$$(Q_t)_i = \frac{HC_{i+1} - HC_{i-1}}{2 \text{ months}} \quad (1.18)$$

where $(Q_t)_i$ is heat stored in i^{th} month and HC_{i+1} and HC_{i-1} are the heat contents in succeeding and preceding months respectively. Etter (1983), following Puttulo (1957) used this equation. Hastenrath and Merle (1986) and Levitus (1987a) also adopted this method. The heat storage in upper 150m in Areas I and II are compared with surface heat input adapted from the atlas by Hastenrath and Lamb (1979b). As the values in the atlas would have undergone some smoothening, the calculated annual cycle of heat storage have also been smoothened. Three point binomial filter is used

for smoothing. This method has earlier been employed by Etter (1983) for smoothing the annual heat storage cycle in Gulf of Mexico.

1.2.3. OCEANIC HEAT ADVECTION

Using the surface heat input (Q_o) and heat storage (Q_t) in upper 150 m, the heat transport through this layer is obtained as a residual of heat budget

$$Q_v = Q_o - Q_t \quad (1.19)$$

for both Areas I and II. Details of estimation of zonally averaged oceanic heat advection are given in Chapter 5.

1.2.4. MIXED LAYER HEAT BALANCE

Mc Phaden (1982) has used a model to simulate the monthly mixed layer temperature observed at Gan Island in equatorial Indian Ocean over a period of $2\frac{1}{2}$ years. This model was applied by Molinari et al (1985 and 1986) for studying the evolution of SST during FGGE 1979 (First Garp Global Experiment) in Pacific and Indian Oceans respectively. Although these studies were carried out for monthly data extending over a year or more, in the present study, an attempt has been made to employ the same method in the case of climatological data in Areas I and II.

Following Mc Phaden (1982), from the depth integrated heat balance of ML, the fluctuations can be expressed as

$$\begin{aligned} \frac{\partial \theta}{\partial t} - \frac{1}{\partial t} [\theta(t_1) - \theta(t_0)] + \left(u \frac{\partial \theta}{\partial x} + v \frac{\partial \theta}{\partial y} + w \frac{\partial \theta}{\partial z} \right)' + \left(\frac{1}{h} W_e \Delta \theta \right)' \\ = \int_{w}^c \left[\left(\frac{Q_o}{h} \right)' - \left(\frac{Q_h}{h} \right)' - \left(\frac{I_o}{h} e^{-r^* h} \right)' \right] \end{aligned} \quad (1.20)$$

The primes indicate the deviations from mean. Θ is surface temperature, t is time and $(t_1 - t_0)$ is the total duration of study period. h is MLD and u , v and w are velocity components. W_e is the entrainment velocity and $\Delta\Theta$ is the temperature jump at the base of ML due to entrainment and Q_h is the heat diffused through the base of ML. I_0 represents penetrative radiation and γ^0 determines its attenuation with depth.

As pointed out by Mc Phaden (1982), the fluctuations in SST contributed by various processes alone are considered and the actual temperatures are not predicted in this model. He has further observed that penetrative radiation accounts only a small percentage of variability in temperature. It is also observed that contribution from heat diffusion through base of ML is not significant (Mc Phaden, 1982; Molinari et al, 1986). Hence, this is ignored in the present study.

The second term in the equation is given as a correction for any trend in the time series of temperature. However, since the present study considers monthly data based on climatological average, the question of trend does not arise.

Integration of the above equation, under these assumptions yields

$$\begin{aligned} \Theta_E(t) = & \Theta(t_2) + \frac{1}{\rho_w c} \int_{t_1}^{t_2} \left(\frac{Q_0}{h} \right)' dt - \int_{t_1}^{t_2} \left(\frac{1}{h} W_e \Delta\Theta \right)' dt \\ & - \int_{t_1}^{t_2} \left(u \frac{\partial \Theta}{\partial x} + v \frac{\partial \Theta}{\partial y} + w \frac{\partial \Theta}{\partial z} \right) \end{aligned} \quad (1.21)$$

Here $\Theta_E(t)$ represents the estimated SST. $\Theta(t_2)$ is an arbitrary constant of integration chosen in such a manner that mean of estimated time series of SST is equal to the mean of the observed time series. Thus, as noted

earlier, this heat balance equation gives only the fluctuations and not the actual temperatures. The second term on the right hand side gives the effect of surface heat exchange.

The third term gives the contribution due to entrainment. In mixed layer models, the entrainment is parameterized from external inputs. In present study, the entrainment is evaluated from the observed characteristics of thermal structure. Mc Phaden (1982) estimated entrainment velocity, W_e , as the sum of rates of change of depths of mixed layer and some isotherm below it. Since the observed thermal structures show large vertical excursions of isotherms, it is thought that MLD alone should be considered to find out W_e . Since entrainment always deepens ML, it is not defined during shoaling of the layer. Thus

$$W_e = \frac{d(h)}{dt} \text{ for } \frac{d(h)}{dt} > 0 \quad (1.22)$$

$$= 0 \text{ for } \frac{d(h)}{dt} < 0 \quad (1.22)$$

The temperature jump at the base of ML may not always be well defined in the vertical profiles and can be approximated as

$$\Delta\theta = \Delta h \frac{\partial\theta}{\partial z} \quad (1.23)$$

where Δh is the change in ML depth over the time interval dt . Dividing by dt , this expression yields

$$\Delta\theta = W_e dt \frac{\partial\theta}{\partial z} \quad (1.24)$$

$\frac{\partial\theta}{\partial z}$ is taken as the temperature gradient in a 20 m layer just below ML.

The fourth term on right hand side of 1.21 gives the effect of advection. Horizontal advection of heat has been adapted from Molinari et al (1986) near the respective areas. From their figures, the differences in temperature estimated using models with and without horizontal advection are noted and are used as the contribution from this term. Vertical advection of heat has been evaluated using the vertical velocity derived from the rate of change of the depth of selected isotherm (20°C) in the thermocline. A fixed vertical temperature gradient of 0.08°C/m has been considered.

Procedure of calculation

For calculating the estimated temperature, the effects of different factors are added one by one. For the discussions, these are termed as schemes 1, 2, 3 and 4.

In scheme 1, surface heat flux is considered. The annual mean of Q_0/h is obtained and the fluctuations from the mean are obtained as $(Q_0/h)'$. The values $\int \frac{1}{\rho_w c} (Q_0/h)' dt$ are evaluated. The mean of these is subtracted from mean of observed SST. This difference was added to the estimated values. This process has rendered the mean of observed series same as that of the estimated series. The root mean square (r.m.s.) deviation between observed and estimated series as well as the linear correlation coefficient between the two series have been evaluated.

The effect of entrainment is also incorporated in scheme 2. The fluctuations due to entrainment are subtracted from those due to surface flux (scheme 1) to obtain the fluctuation under the influences of both. Same procedure as in scheme 1 has been followed to obtain the estimated series of surface temperature and other related parameters.

In scheme 3, since the contributions from horizontal advection have been extracted from published work, these values are only algebraically added to the fluctuations in scheme 2 to get the temperature fluctuations under the influence of surface heat flux, entrainment and horizontal advection. The estimated temperature and other parameters are evaluated.

Vertical advection is also included in the 4th scheme. Temperature fluctuations due to vertical velocity are subtracted from those in third scheme for obtaining the fluctuations under the influence of all the four processes considered. Estimated series of temperature and other related parameters have been worked out.

Since these evaluations involve lengthy, repetitive computations, necessary computer programmes have been developed.

Error estimation

The estimated series of temperatures have been examined in the light of the uncertainties due to observational errors and errors in parameterization of surface heat fluxes. Method for estimating the errors, considering all the terms in equation (1.21) to be independent, has been presented by Mc Phaden (1982).

If $\overline{\sigma_{\Delta\theta}}$ is the expected r.m.s. error in the first term (ie. $\frac{1}{\int_w^c} \frac{Q_0}{h} dt$) due to inaccuracy, $\overline{\sigma_h}$ in MLD, then

$$\overline{\sigma_{\Delta\theta}} \approx \frac{1}{\int_w^c} \frac{\overline{Q_0}}{h} \left(\frac{\overline{\sigma_h}}{h} \right) \Delta t \quad (1.25)$$

where bars indicate mean quantities and Δt indicates time interval viz., month, in the present case.

Similarly, the error in the first term due to uncertainties in surface heat flux can be estimated as

$$\overline{\sigma_{\Delta\theta}} \approx \frac{1}{\rho_w c \bar{h}} \overline{\sigma_{Q_0}} \Delta t \quad (1.26)$$

The total error from the first term in the estimated SST is the sum of above two.

Similarly the errors due to other terms can also be worked out.

Uncertainty in net surface heat exchange exceeds 20 W/m^2 (Hasternath and Lamb, 1979b). Mc Phaden (1982) considers an error of 20 W/m^2 and Molinari et al (1986) indicate that the error varies between 25 and 30 W/m^2 . In the present study, this uncertainty is taken as 25 W/m^2 . Following Molinari et al (1986), the uncertainties in entrainment velocity, temperature jump at the base of ML and thermocline depth are taken to be $5.5 \times 10^{-6} \text{ m/s}$, 0.5°C and 10 m respectively. For this uncertainty of 10 m in thermocline depth, uncertainty in vertical velocity, estimated for monthly interval is $3.8 \times 10^{-6} \text{ m/s}$. Uncertainty in vertical gradient is not considered, since a constant gradient of 0.08°C/m is used.

Averages of different factors for Areas I and II have been worked out. The expected errors in estimated SST, based on the averages and above uncertainties for both areas are also evaluated.

CHAPTER 2

SHORT-TERM VARIATIONS

Data collected during MONEX-79 are utilised to examine the air-sea energy exchange and upper ocean thermal structure on a day-to-day basis in central east Arabian Sea during pre-onset and after the onset of southwest monsoon. Data from two fixed stations located at 9°N , 68°E and 15°N , 65°E have been studied (see Fig. 2.1). These stations are referred to as 'S' and 'N' respectively in the following discussions. Although the observations are, in general, simultaneous, there are occasions when one or the other station has not been occupied. Further, there are few days when subsurface data have not been collected. Periods of observation are given in Table 2.1.

The weather conditions during MONEX-79 have been summarized by Sikka and Grossman (1980). During May 1979, anticyclonic circulation prevailed over Arabian Sea. This weakened by 10 May and reappeared around 16th to persist till 5 June. A cyclonic cell, the monsoon onset vortex, which was noticed on 14 June, intensified into a depression around 14°N , 70°E . Between 16-18 June, a core of strong winds of 60-70 knots was seen along 8° - 10°N . On moving northwestwards, the depression intensified into a storm and crossed the Arabian coast by 20 June. Mukherjee and Paul (1980) noted that the above system appeared first as a trough over Lakshadweep on 7 June.

2.1. AIR-SEA INTERACTION

Variations of different parameters of air-sea interaction at station S are presented in Figs. 2.2a and b.

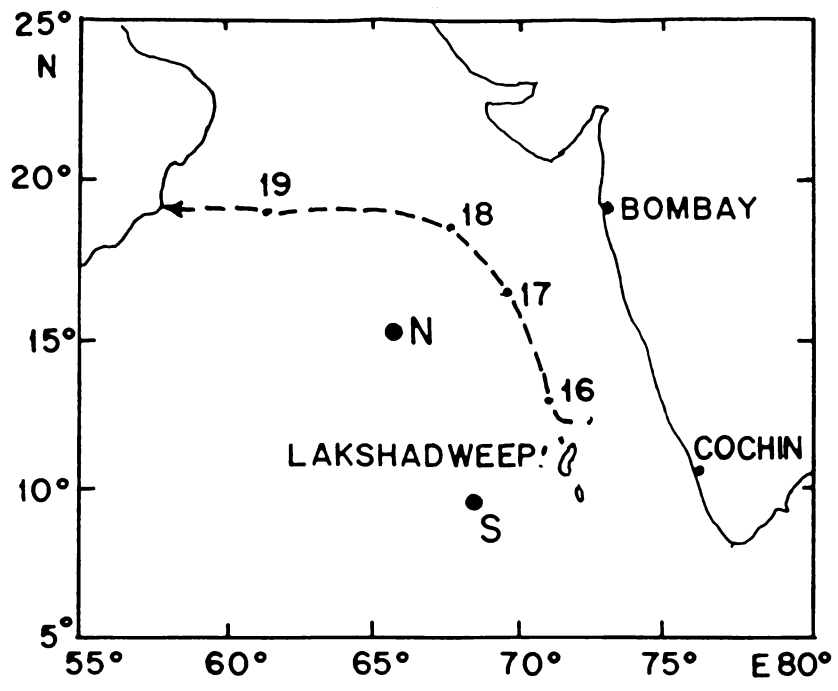


Fig. 2.1 Station locations.
Track of monsoon onset vortex, with dates, is also shown.

Table 2.1. Observations at the 2 stations during MONEX-79, utilized in the study of short-term variations

St. No.	Station	Location	Duration	
			Surface meteorological data	Bathy thermograph data
1	S	9° N 68° E	2-12 May	2-12 May
2	S	9° N 68° E	26 May - 3 June	26 May - 3 June
3	S	9° N 68° E	21 - 23 June	21 - 24 June
4	N	15° N 65° E	17 May - 8 June	17 May - 8 June
5	N	15° N 65° E	19 - 25 June	20 - 24 June

At S, during early May, atmospheric pressure was about 1011 mb (Fig. 2.2a) which progressively decreased from 6 May to reach 1008 mb on 12 May. During late May, pressure again became high and decreased during early June by about one mb. After the onset of monsoon, in the wake of onset vortex, atmospheric pressure decreased to 1010 mb.

Vapour pressure difference between sea surface and atmosphere was about 11 mb on 2 May and increased gradually to 13 mb on 7 May. After decreasing by 2 mb in next 2 days it again increased slightly. During late May, at S, vapour pressure difference was generally 11 mb with slightly higher values on 26 May. Towards early June it decreased to 9 mb. After monsoon onset, sharp drop to about 3 mb was seen on 21 June which increased to around 8 mb in next 2 days.

Wet bulb depression, at S, was about 3.5°C on 2 May and increased in the following two days to 5°C and decreased by about 1°C after 7 May. During late May and early June, wet bulb depression was around 4°C . After the onset of monsoon, it dropped to about 1.2°C on 21 June indicating very moist condition which is also reflected in the fall in vapour pressure difference. Wet bulb depression again increased in the following days.

At S, sea surface was, in general, warmer than air by about 1°C during early May. After 10 May, SATD increased due to a fall in air temperature. On 26 May, SATD was about 1.5°C which decreased in the following days and increased again in early June. The decrease was due to a fall in SST and also an increase in air temperature. After the onset of monsoon, sea was slightly colder than air on 21 June and became warmer by about 1°C in the following days.

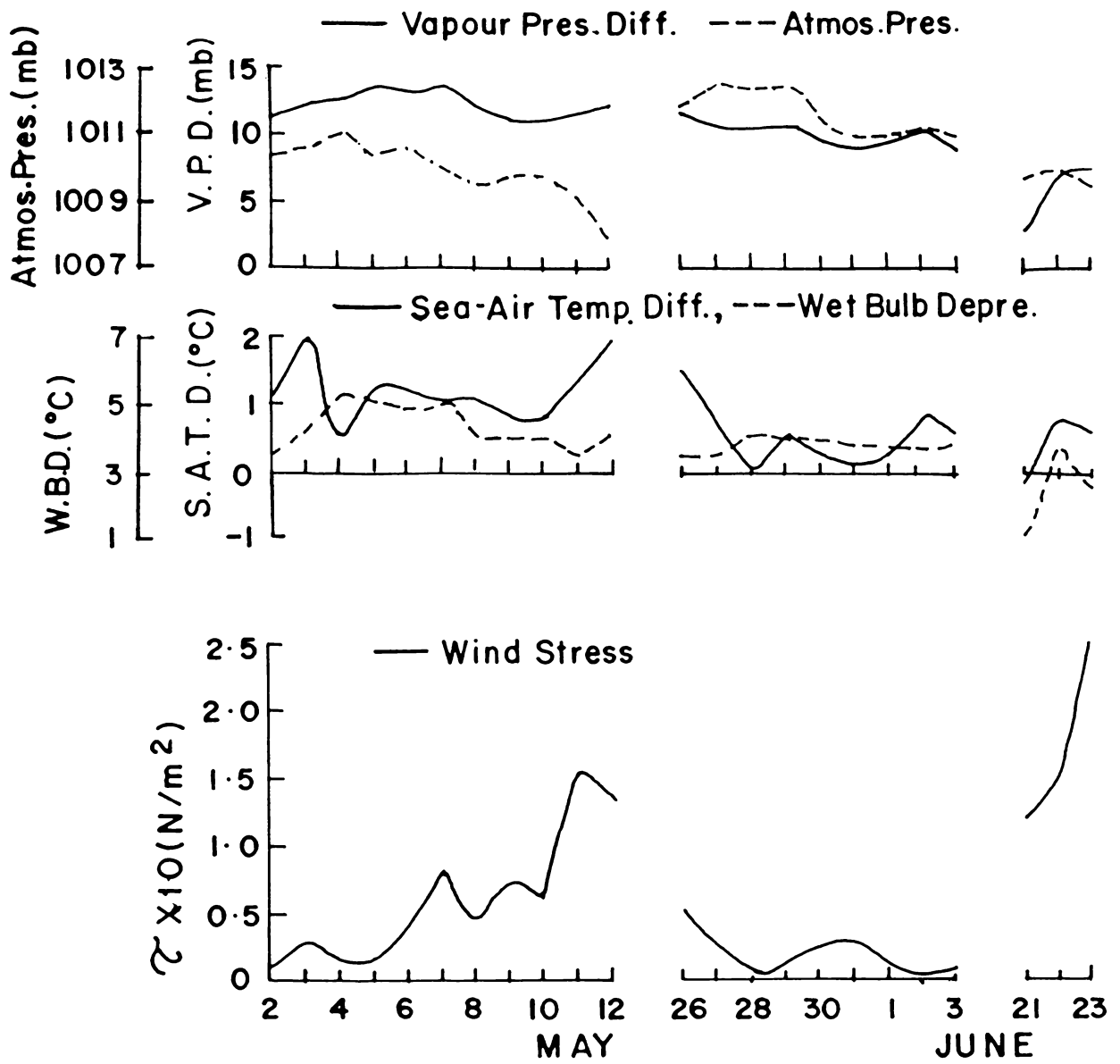


Fig.2.2(a) Daily variation of meteorological parameters and wind stress at S.

Cloudiness was generally less than 4 octa, during early May, at S and increased steadily after 6 May and reached about 7 octa on 12 May. During late May, the cloud amount was, in general, very low. After the onset of southwest monsoon, cloudiness increased to nearly overcast conditions.

At S, during early May, the wind stress (τ) was generally low ($<0.02\text{N/m}^2$) and increased after 6 May to 0.15N/m^2 during 11-12 May. During late May and early June, the wind stress was, in general, very low. When the station was occupied after the onset of monsoon, higher values of τ were noticed (0.11 to 0.25N/m^2).

At this station, the short wave radiation varied, during the first half of May, between 120 and 260W/m^2 . A progressive decrease was noticed during 7-12 May (Fig. 2.2b). During late May and early June, short wave radiation ranged from 145 to 245W/m^2 . After the monsoon onset, short wave radiation decreased (110 - 140W/m^2). As compared to short wave radiation, back radiation was throughout low and the net radiational flux followed the pattern of short wave radiation.

Latent heat, in general, followed the pattern of τ . During early May, latent heat was low ($\sim 60\text{W/m}^2$) and increased after 4 May and reached about 270W/m^2 during 11-12 May. During late May and early June, latent heat was generally about 70W/m^2 . Higher rate of evaporation on 26 May (200W/m^2) was caused by the slightly higher wind speed and vapour pressure gradient on 26 May. After the monsoon onset, the rate of evaporation was more. Latent heat was 75W/m^2 on 21 June and increased to about 210W/m^2 on the next 2 days.

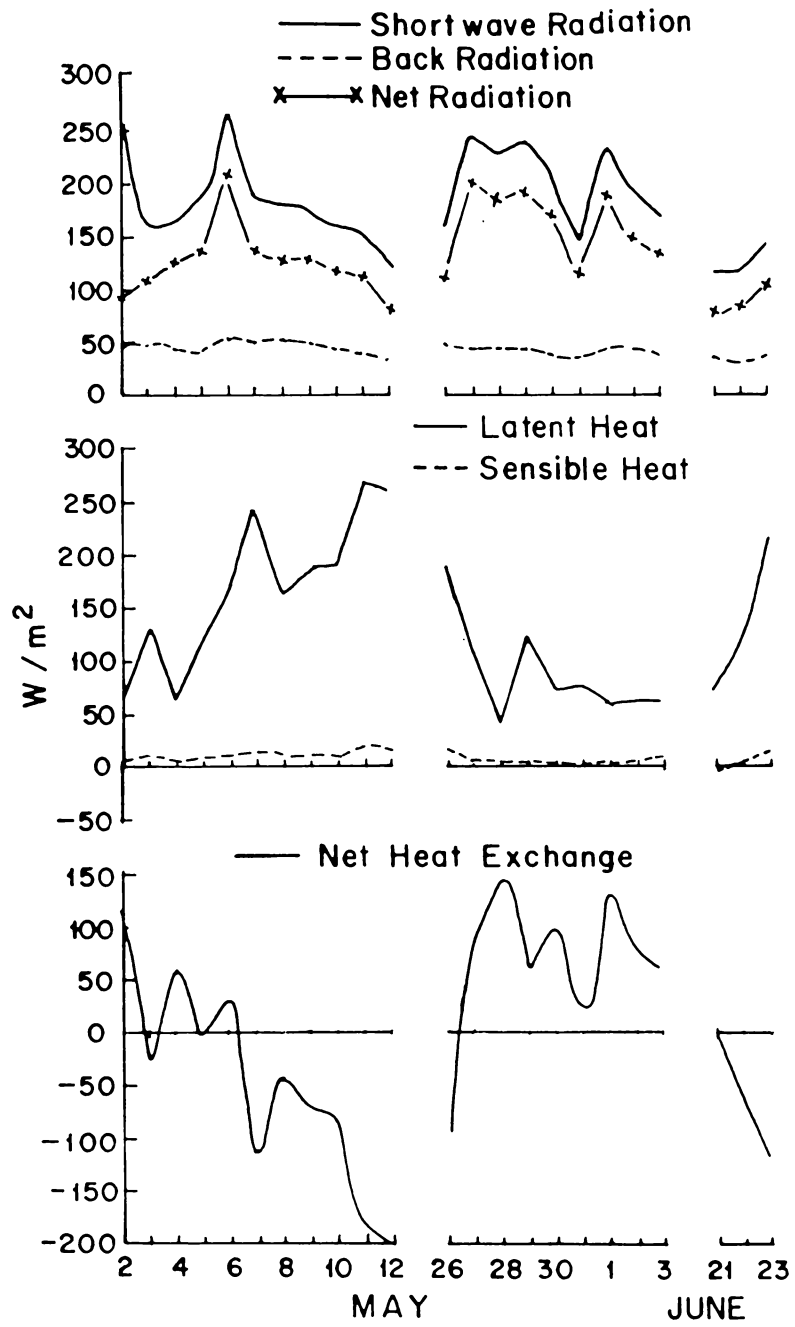


Fig.2.2(b) Daily variation of heat budget components at S.

Sensible heat flux which also followed the pattern of τ , was an order of magnitude less than latent heat. During pre-monsoon, sensible heat was lost from sea surface, while after the onset, mild gain was noticed on 21 June.

The net surface heat exchange at station S showed wide fluctuations. There was generally heat gain upto 6 May and a heat loss subsequently. The loss gradually increased to reach about 200 W/m^2 on 12 May. Heat loss observed on 26 May was a result of the high rate of evaporation on that day. On the following days, sea gained heat varying between 25 and 145 W/m^2 . After the onset of monsoon, sea lost heat and the loss increased to about 120 W/m^2 on 23 June.

Variations of different parameters of air-sea interaction at station N are given in Figs. 2.3a and b.

At this station, atmospheric pressure remained high (1010-1013 mb) from mid-May till 29 May and subsequently decreased progressively. By 8 June, the pressure decreased to about 1005 mb (Fig. 2.3a). After the monsoon onset, pressure was 1001 mb on 19 June and increased to about 1004 mb on the following days.

At N, vapour pressure difference was about 10 mb from mid-May to 4 June and showed a decrease of about 5 mb by 8 June. At this station, after the monsoon onset, there was no decrease in the vapour pressure difference. This feature is different from the finding at southern station where a decrease was noticed.

Wet bulb depression was mostly around 4°C during mid-May to early June. A slight reduction was noticed ($\sim 1^\circ \text{C}$) after 5 June towards

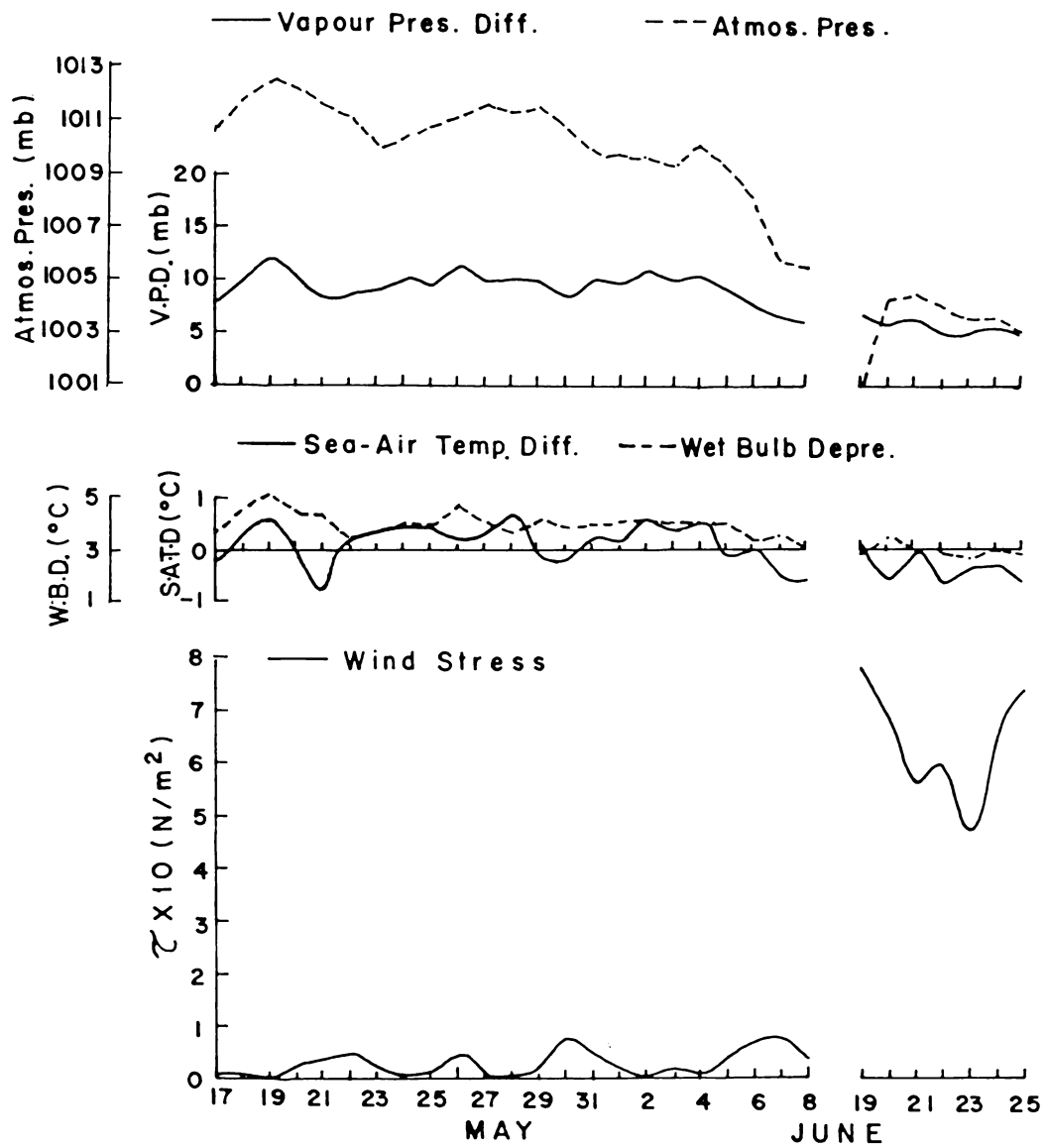


Fig.2.3(a) Daily variation of meteorological parameters and wind stress at N.

the end of the observation period. Unlike at southerly station, here the wet bulb depression did not show any decrease after the onset and remained to be about 3°C during 19-25 June.

At this station, sea surface was, in general, warmer than air during mid-May to early June ($\sim 0.5^{\circ}\text{C}$). However, after 4 June, together with the fall in vapour pressure, atmospheric pressure and wet bulb depression, the SATD also decreased. During this time, air became warmer than sea surface. After monsoon onset, sea surface was generally colder by about 0.5°C . This is unlike station S where sea surface was warmer on 21 June, after monsoon onset.

At N, during mid May to June, very low cloud amount was noticed (~ 2 octa). After monsoon onset, cloudiness increased which, however, was less as compared to S.

At this station, low wind stress varying between 0.002 and 0.08 N/m^2 was noticed from mid-May to 8 June. The fluctuations in wind stress showed a periodicity of 3-4 days. After the onset of monsoon, wind speed increased and stress varied between 0.45 and 0.80 N/m^2 during 19-25 June.

During the pre-onset phase of monsoon, short wave radiation at N ranged between 205 and 310 W/m^2 (Fig. 2.3b). Considerable reduction in incoming radiation was noticed after monsoon onset when it varied between 110 and 175 W/m^2 . The back radiation was comparatively low and the net radiational flux followed the pattern of short wave radiation. The net radiation ranged between 160 W/m^2 and 260 W/m^2 during pre-onset and between 95 W/m^2 and 155 W/m^2 after the onset.

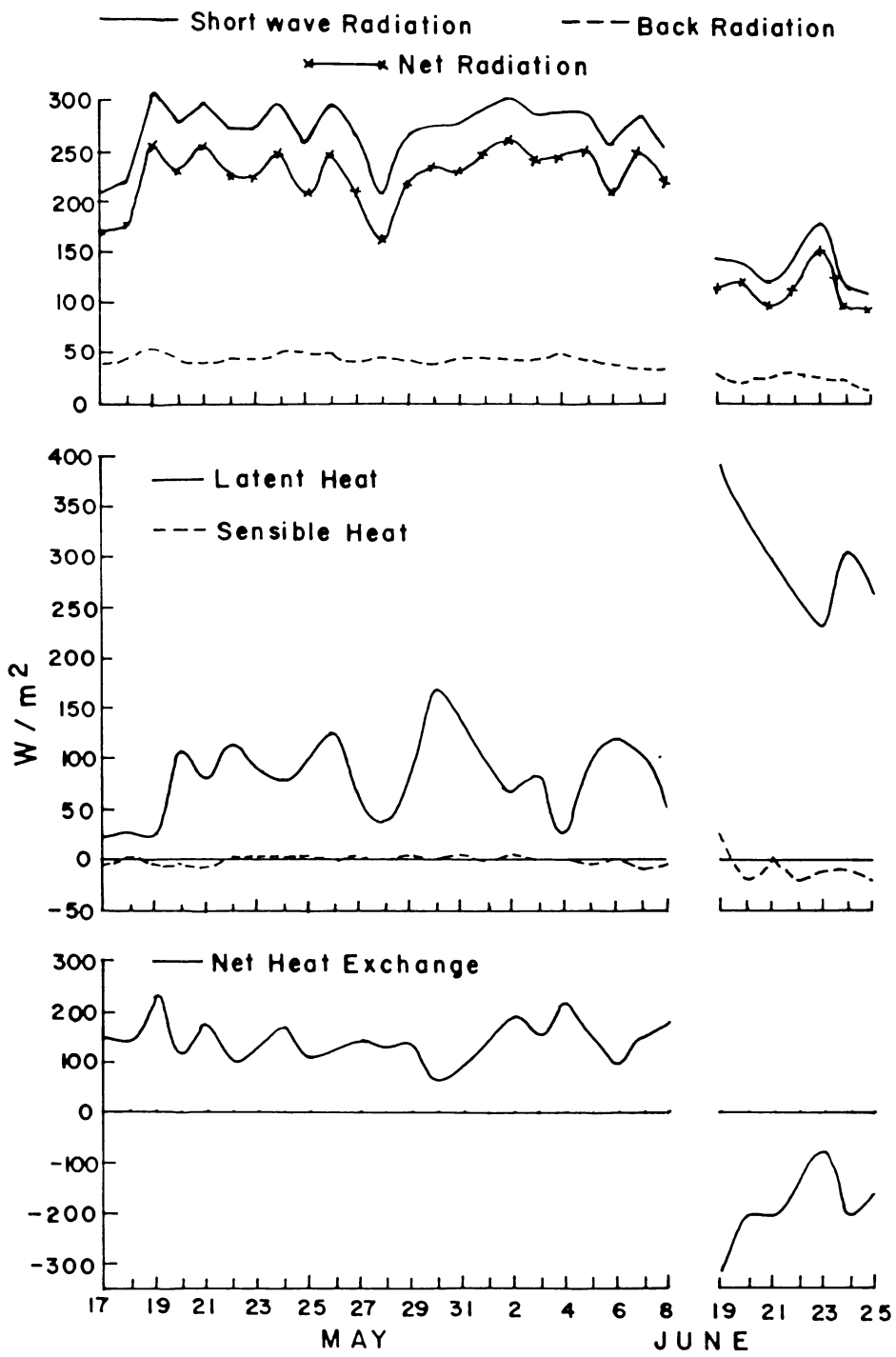


Fig.2.3(b) Daily variation of heat budget components at N.

Latent heat of evaporation, in general, followed the pattern of τ . From mid-May to June, it varied between 25 and 170 W/m^2 . The maximum value was observed on 30 May. After the onset of monsoon, higher rates of evaporation were noticed. Latent heat was about 395 W/m^2 on 19 June and decreased progressively to a minimum of about 230 W/m^2 on 23 June and increased again slightly during the next 2 days.

Sensible heat transfer was comparatively low (mostly 5 W/m^2) during pre-onset and was generally a loss from sea surface. However, during 4-8 June, heat gain was noticed. This was due to a slight fall in SST and an increase in air temperature. After the monsoon onset, generally, sea gained sensible heat by about 20 W/m^2 . This increased heat gain was due to increase in wind speed and the decrease in SST due to the onset vortex.

Net heat gain at station N varied between 65 and 225 W/m^2 during pre-onset phase. Lower values were registered towards the end of May when evaporation had increased. After the onset of monsoon, there was heat loss. Highest loss of about 310 W/m^2 was noticed on 19 June which decreased to 70 W/m^2 on 23 June and increased thereafter.

The above results shall now be analysed in relation to atmospheric processes and in the light of earlier studies.

A severe cyclone formed on 5 May in southern Bay of Bengal (7°N , 90°E) and moved northwest to cross the east coast of India near Nellore town (14.5°N , 80°E) on 12 May (Sikka and Grossman, 1980). Under its influence during 9-12 May, the atmospheric pressure dropped. The cloudiness increased and hence the net radiation decreased. Also the turbulent fluxes increased and consequently the sea lost heat during this period.

At the station S, after the passing of the onset vortex, the evaporation observed on 21 June was similar to that during earlier undisturbed weather conditions. The evaporation was low, despite slight increase in wind speed. This might have been due to the presence of moist air as deduced from wet bulb depression. While wet bulb depression was mostly about 4°C during undisturbed weather, it decreased to about 1.3°C on 21 June (Fig. 2.2a). However, on the following days, the wet bulb depression increased and this, together with increasing wind speed, resulted in the increase of evaporation.

The air, in general, was less moist at station N during the observations after the monsoon onset (wet bulb depression of about 3°C ; Fig. 2.3a). This, along with higher wind speeds, caused the comparatively higher rates of evaporation at station N. This difference in atmospheric moisture could have been due to the differential interaction with sea of the vortex at the two stations or might have been a feature of main monsoon flow. The present data, however, are not sufficient to draw definite conclusions. Using atmospheric observations during this period, Holt and Sethuraman (1987) noted that the region around N was comparatively more convective than S.

At N, after the monsoon onset, wind stress showed a minimum on 23 June. This agrees, in general, with the finding of Nyenzi (1980). Studying meridional time sections, he observed along 65°E (longitude of N) high westerly winds at 850 mb from 14 June till the end of the month with a break on 24 June. Meridional sections of wind, further east (70°E) did not exhibit this decrease. At southerly station S, which was located at 68°E , decrease was not noticed and instead an increasing trend was seen from 21 to 23 June.

Table 2.2. Average Fluxes during pre-onset and after-onset of monsoon

(Positive values of latent and sensible heats are considered as heat loss from sea surface)

Parameter	Pre-onset	After-onset
Wind stress (N/m^2)	0.04	0.53
Net radiation (W/m^2)	190	104
Latent heat (W/m^2)	105	262
Sensible heat (W/m^2)	4	-4
Net heat transfer (W/m^2)	79	-147

The average fluxes during pre-onset and after-onset phases of monsoon are presented in Table 2.2. Average fluxes increased considerably after the onset. Wind stress increased to about 0.53 N/m^2 . Similar values have been reported by Pant (1977) in association with increase in monsoon activity. The average heat losses due to fluxes of latent heat and sensible heat were about 105 W/m^2 and 5 W/m^2 respectively during pre-onset and became 265 W/m^2 and -5 W/m^2 respectively after the onset. Daily average fluxes with values similar to those observed after onset have been reported earlier from this area during Indo-Soviet Monsoon Experiment (Pant, 1977). Present fluxes after monsoon onset are higher than the climatological average for the month in this area (Hastenrath and Lamb, 1979a, b) and the average for monsoon months of certain years (Saha, 1970a; Saha and Suryanarayana, 1972). It may be noted that the present observations have been made soon after the passing of the vortex. Studying GATE data, Senguin and Kidwell (1980) observe that synoptic scale fields contain large fluxes.

2.2. UPPER OCEAN THERMAL STRUCTURE

Depth-time sections of temperature at stations S and N are presented in Figs. 2.4 and 2.5 respectively. Isotherms are drawn at 1°C intervals. MLD is shown by dashed line.

At S, SST varied between 29.5° and 30.8°C during first half of May and MLD ranged between 40 and 60 m. (Fig. 2.4). Vertical oscillations of isotherms could be due to the presence of internal waves. The isotherms were closely spaced between 100 and 150 m, indicating the layer of higher temperature gradient. After 8 May, at S, MLD deepened together with a slight decrease in SST of about 0.5°C . During late May

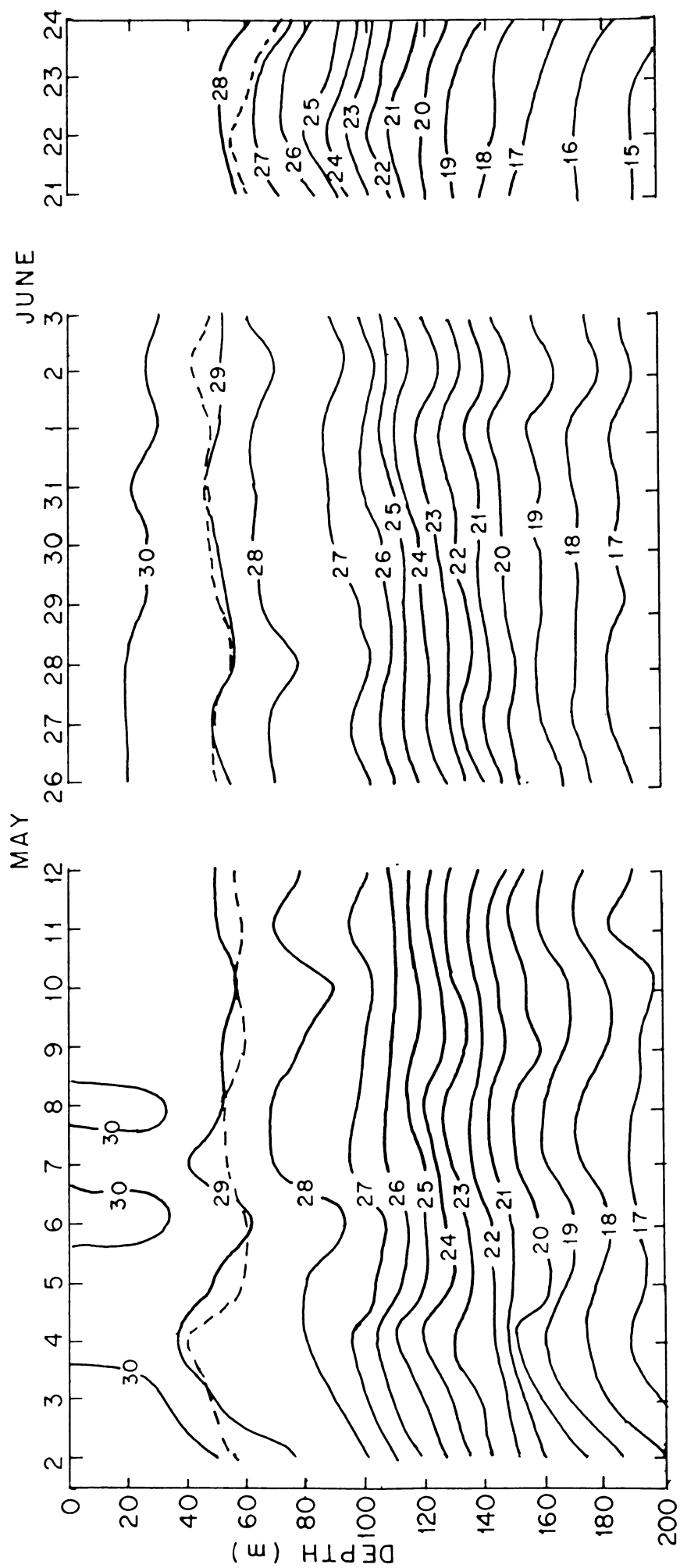


Fig.2.4 Depth-time section of temperature at S. Isotherms are drawn at 1°C intervals. MLD is shown by dashed line.

and early June, SST was, in general, higher ($> 30^{\circ}\text{C}$) and MLD was shallower by about 10 m. During this period, some readjustments in thermal structure seemed to be occurring at S. A layer of higher temperature gradient with an approximate thickness of 25 m appeared just below mixed layer. The deeper layer of higher gradient still persisted. Further, isotherms in the thermocline progressively rose during this period.

After the onset vortex of monsoon, drastic changes in the thermal structure were noticed at S. SST dropped by about 1.5°C to become about 28.7°C on 21 June and decreased by 0.5°C in next 3 days. MLD was about 60 m on 21 June. After mild shoaling on the next day, the ML deepened further to about 75 m on 24 June. Temperature at all levels were found to be less than that during pre-onset phase. However, during this period the isotherms, in general, showed a deepening tendency with the progress of observations.

At the northerly station (N), SST varied between 29.8° and 30.5°C from mid-May to 8 June (Fig. 2.5). From mid-May onwards, MLD was, in general, about 35 m and increased by about 10 m on 28 May. Mixed layer shoaled on 31 May and deepened again to 50 m on 2 June and remained around 55 m during 6-8 June. The oscillations of the isotherms in the thermocline might be due to the presence of internal waves. As in the case of station S, at N also thermocline was found to consist of two layers during mid-May. One layer with a thickness of about 25 m was seen just below ML. Below this, a layer of reduced gradient was observed followed by the second layer with an approximate thickness of 40 m. Temperature gradient gradually decreased below 160 m. This pattern persisted till the end of May and subsequently got modified slightly. With the deepening of ML in early June, the gradient just below ML decreased.

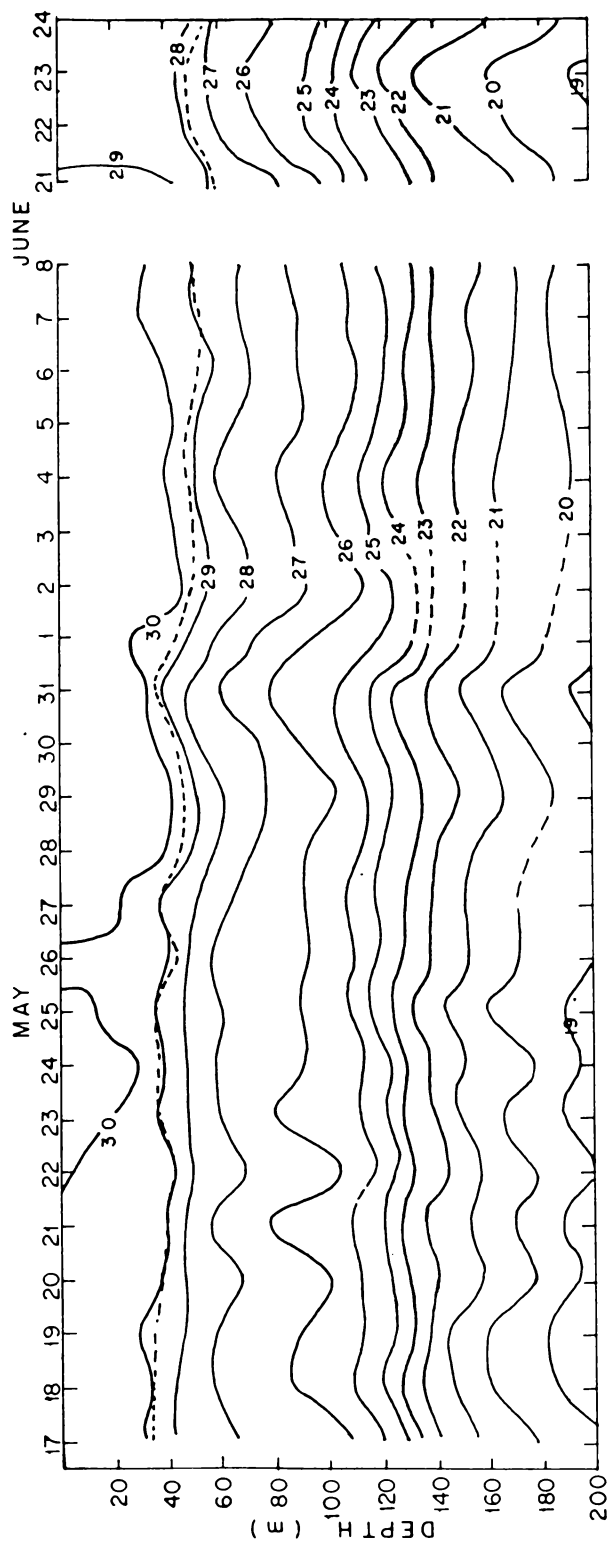


Fig.2.5 Depth-time section of temperature at N. Isotherms are drawn at 1°C intervals.
MLD is shown by dashed line.

After the passing of onset vortex, at N also SST decreased by about 1°C to become 29°C on 21 June and decreased further by about 0.8°C in next 4 days. ML deepened by about 5 m from its pre-onset depth to reach 60 m on 21 June. After mild shoaling on the next two days, ML deepened again. While there was a decrease in temperature from pre-onset values at all levels, this decrease was less than that observed at S. At subsurface also, the isotherms shoaled till 23 June and deepened on 24 June. The amplitude of oscillations of isotherms was found to increase with depth.

Time-depth sections of vertical temperature gradient for the stations S and N are presented in Figs. 2.6 and 2.7 respectively. Isolines are drawn at intervals of $0.5^{\circ}\text{C}/10\text{ m}$. To examine the evolution of temperature profiles, the 3 day average profiles for these stations are given in Figs. 2.8 and 2.9 respectively.

During the first half of May, at S, two layers with higher temperature gradient were noticed (Fig.2.6). In the upper part, weak gradient ($0.5^{\circ}\text{C}/10\text{m}$) was seen. During 2-6 May, this layer deepened from around 40 m to about 55 m. The deeper layer had higher gradient of $1.5^{\circ}\text{C}/10\text{m}$ in the core. This core which was initially located at about 150 m gradually rose in the following days to reach about 120 m on 12 May. During late May, this core continued to rise and was centred around 110 m by early June. Together with this, the gradient in the upper layer increased and also the upper layer thickened, leaving a thin region separating the two high gradient layers. During this period, a mild gradient was generated close to surface indicating atmospheric heat input. From the average profiles (Fig. 2.8), it can be seen that from surface to 40 m, temperature observed during late May and early June is more than

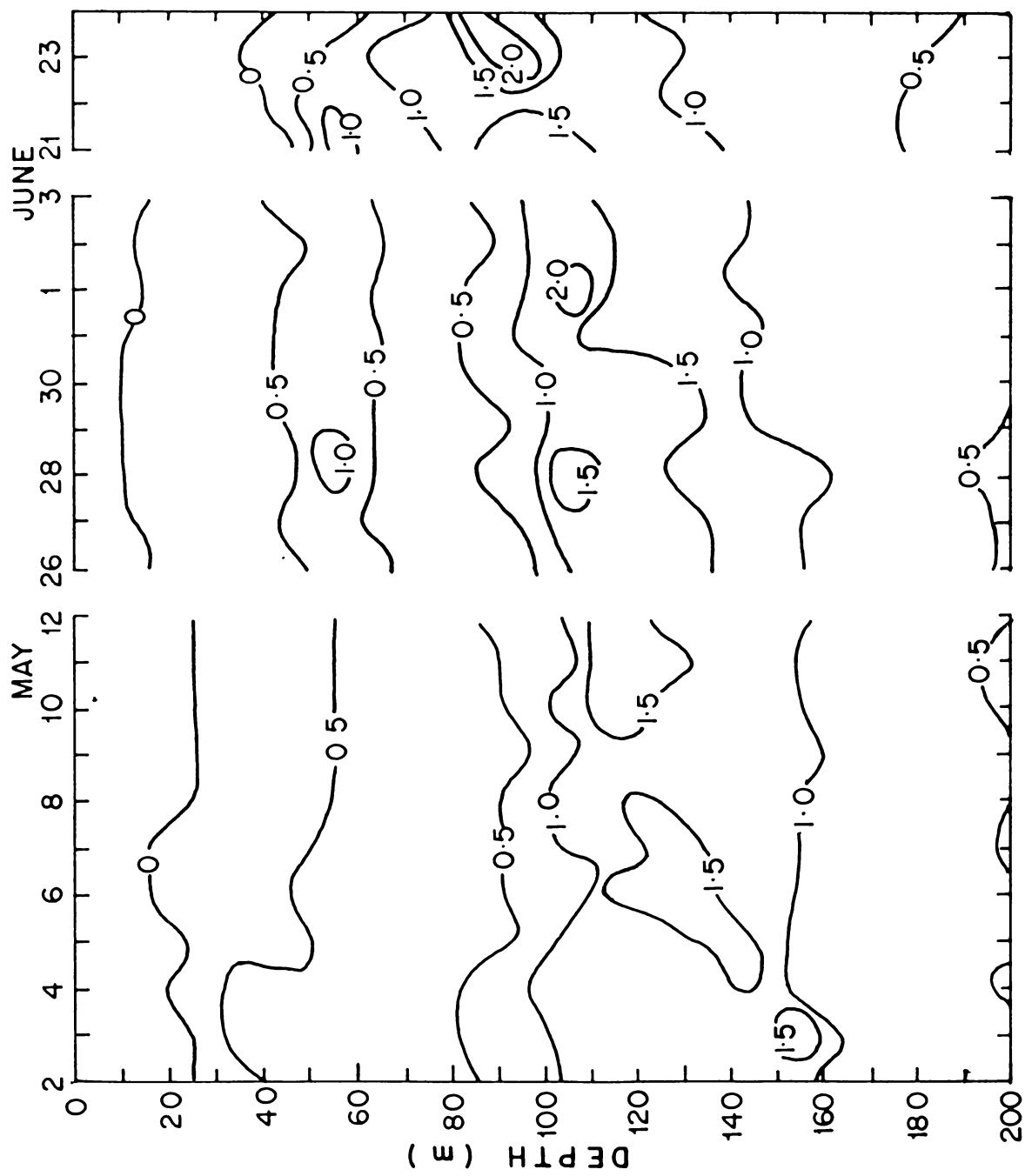


Fig.2.6 Depth-time section of vertical temperature gradient ($^{\circ}\text{C}/10\text{m}$) at S.

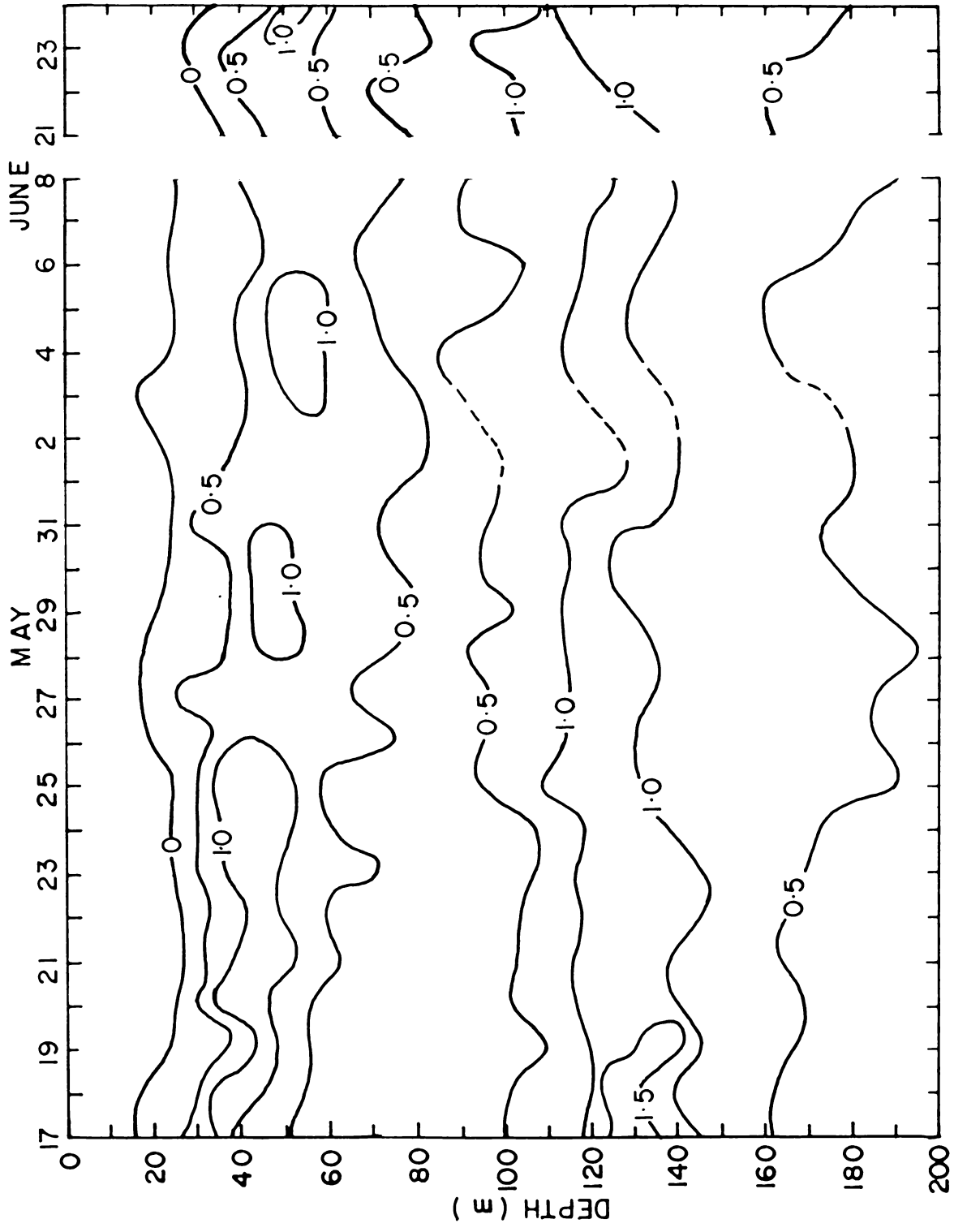


Fig.2.7 Depth-time section of vertical temperature gradient ($^{\circ}\text{C}/10\text{m}$) at N.

that during early May while at 60 m, there has been a fall in temperature compared to early May values. This resulted in the thickening of the upper gradient region mentioned above.

After the vortex, at S, with the deepening of ML, very weak negative gradient was noticed around 45 m on 21 June, indicating convective mixing generated by surface heat loss. During this period, the upper layer of higher gradient had also deepened. Another feature observed was that the core in the lower layer of higher gradient moved further upwards by about 10 m. The average profile after the storm (Fig. 2.8) shifted to lower values indicating cooling at all levels.

At N also, two layers of higher temperature gradient were observed during pre-onset (Fig. 2.7). The core in the upper gradient which was located around 30 m during mid-May deepened progressively to reach about 50 m in June. As in the case of S, at N also this layer thickened towards June. In the deeper gradient layer, centred around 130 m, the gradient and thickness were lesser than at S. Another conspicuous difference at N was that the lower layer did not progressively rise during pre-onset phase but remained around 130 m. It is interesting to note from the evolution of temperature profiles (Fig. 2.9) that at N, while there has been an increase in temperature in June (prior to the monsoon onset) in surface layer, this surface layer of uniform temperature has deepened with the progress of pre-onset observations. The increase in temperature was found to extend to still deeper parts also.

After the vortex, at N, the lower layer of higher gradient moved slightly upwards. However, unlike at S, the upper gradient layer had not deepened. Although, the average profile shifted to lower values (Fig. 2.9) indicating cooling throughout the depth, the extent of shift was less than at S.

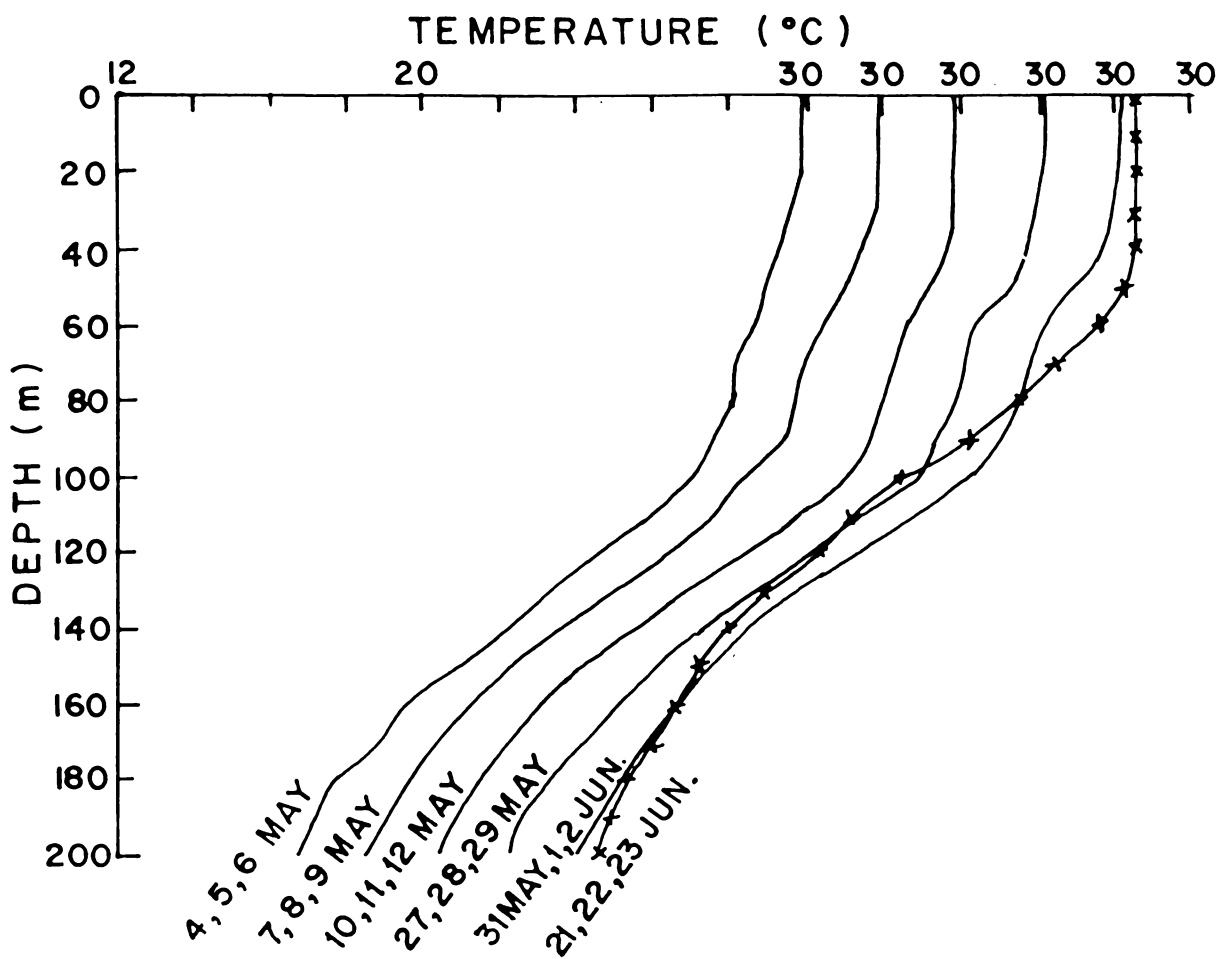


Fig.2.8 Three-day average profiles of temperature at S. Profiles are progressively shifted to the right.

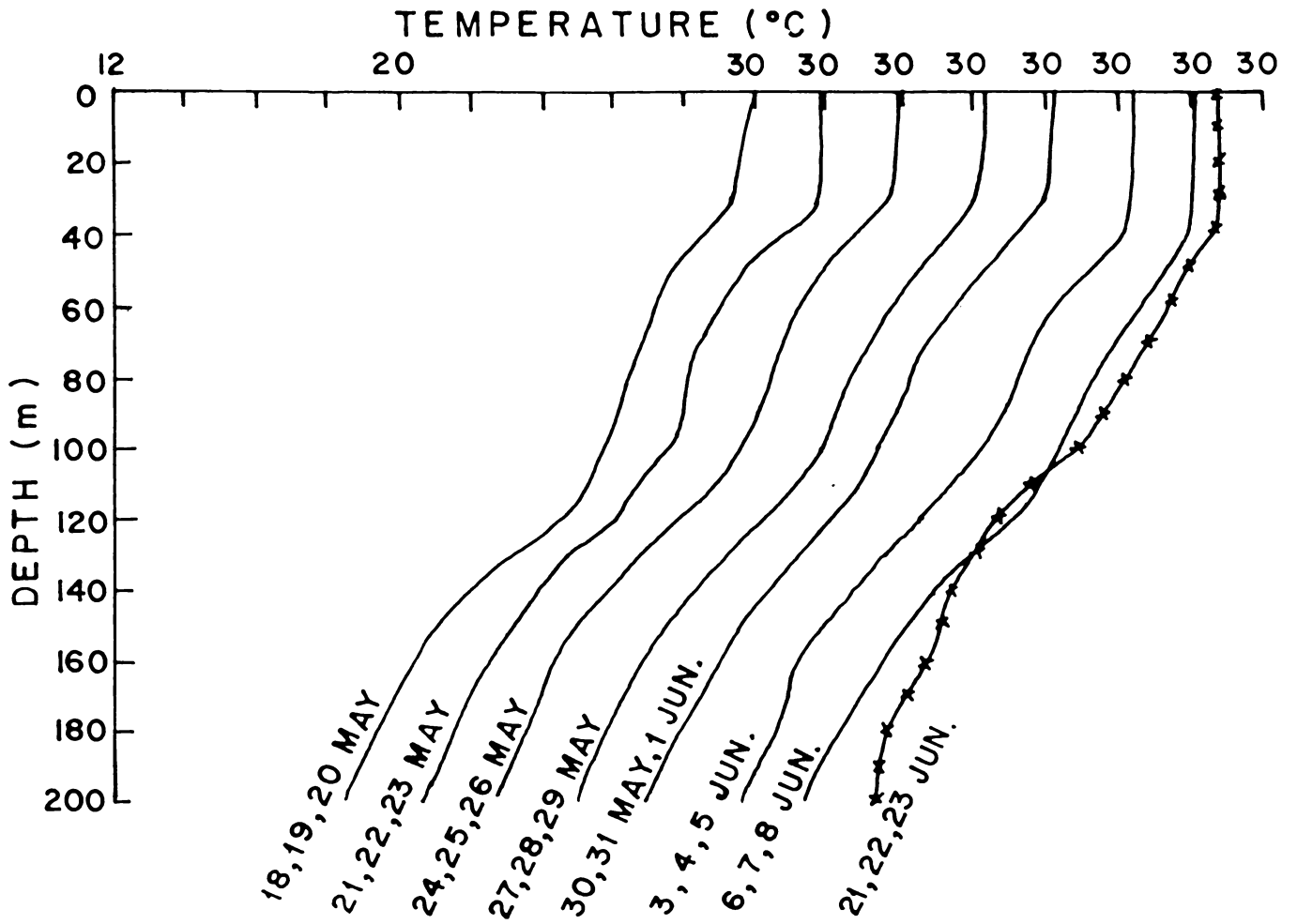


Fig.2.9 Three-day average profiles of temperature at N. Profiles are progressively shifted to the right.

Heat content and cyclone heat potential

Heat content in 4 different layers of 50 m thickness from surface to 200 m at stations S and N are presented in Figs. 2.10 and 2.11 respectively.

At S, during early May, the heat content in the upper 50 m varied between 60.0×10^8 and 62.5×10^8 J/m² (Fig. 2.10). Fluctuations were noticed in the subsurface layers due to vertical excursions of isotherms. Maximum fluctuation of about 4.0×10^8 J/m² was noticed in the two layers between 100 and 200 m.

During late May and early June, heat content of upper 50 m was about 61.0×10^8 J/m². During this period, a progressive depletion of heat was noticed at intermediate layers. Maximum decrease was noticed in 100-150 m where it fell from 49.0×10^8 J/m² on 26 May to about 45.0×10^8 J/m² on 3 June.

After the passing of the onset vortex, the heat content decreased at all layers. The decrease during the intervening period (3 June - 21 June) was about 2.1×10^8 J/m² in 0-50 m and 50-100 m layers while it was more in the deeper layers. In upper 50 m, heat content decreased slightly in the following three days while it decreased first and then increased in deeper layers. Maximum variation was noticed between 50-100 m.

At N, heat content in upper 50 m during mid-May was around 59.5×10^8 J/m². It increased to about 62.0×10^8 J/m² by late May (Fig. 2.11). Heat content decreased slightly after 5 June. At subsurface layers, the fluctuations in heat content were more which might be due

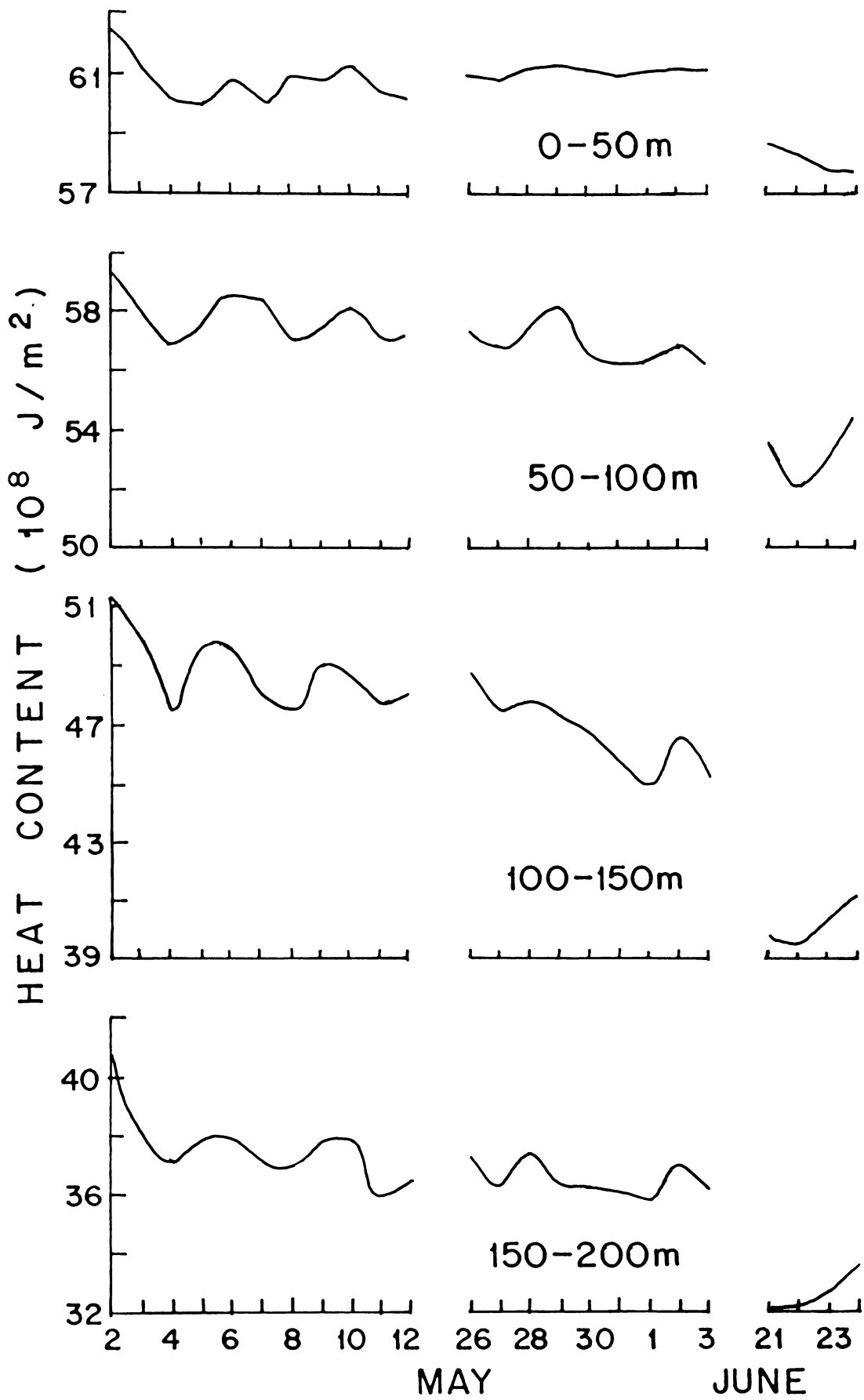


Fig.2.10 Daily variation of heat content in different layers at S.

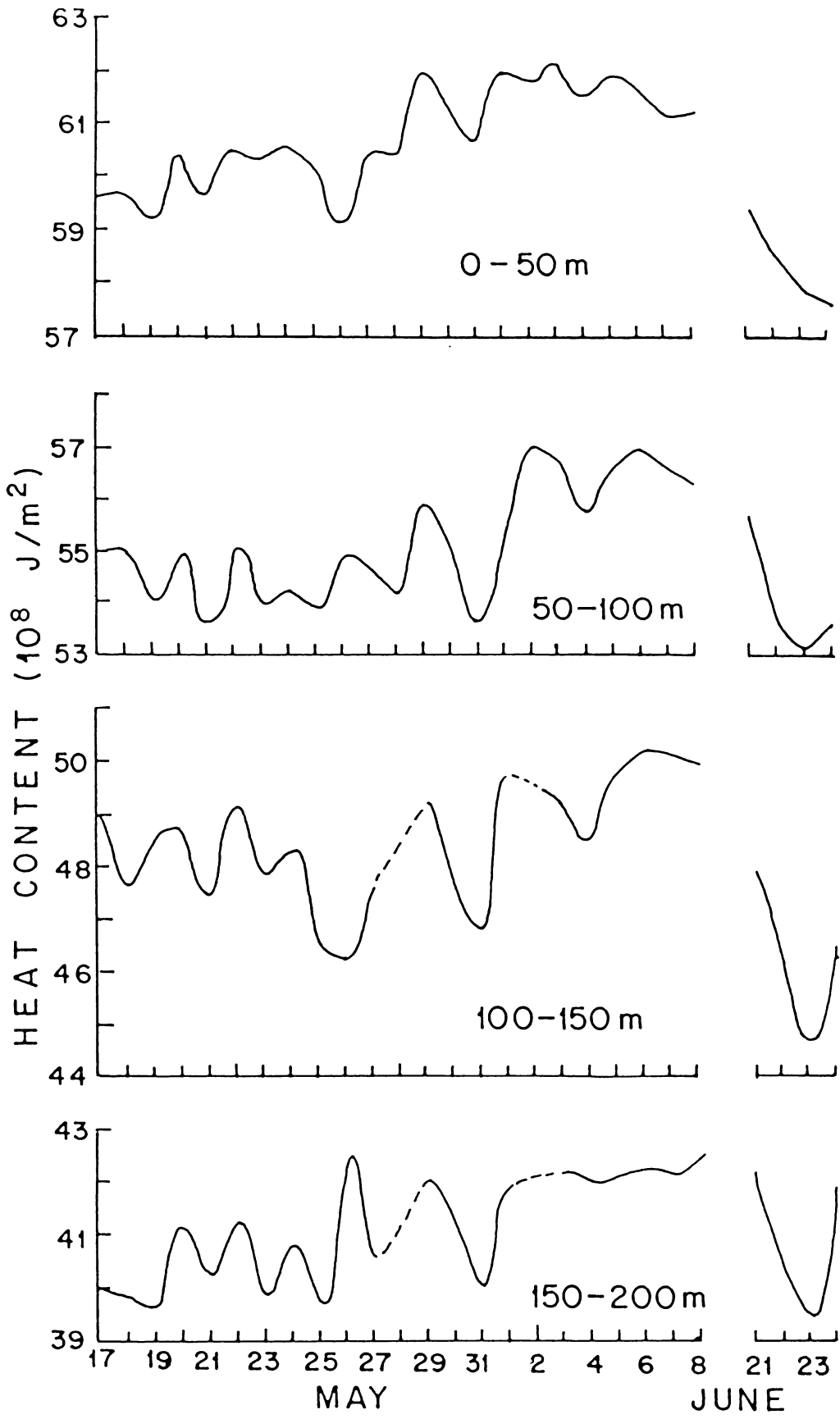


Fig.2.11 Daily variation of heat content in different layers at N.

to the presence of internal waves, as mentioned elsewhere. An increase in heat content on 1 June was noticed at all levels and this increase was more prominent between 50 and 100 m. This might be due to heat advection as shown later in this chapter.

Unlike S, at the station N, the decrease in heat content after the vortex from pre-monsoon values was generally less. In the upper 50 m, the reduction was about $1.9 \times 10^8 \text{ J/m}^2$. While between 50 and 150 m also heat content had decreased during this period, in the 150-200 m layer it did not show appreciable decrease. In the following three days, there was a decrease of about $1.6 \times 10^8 \text{ J/m}^2$ in the upper 50 m while in deeper layers heat content first decreased by about $2.5 \times 10^8 \text{ J/m}^2$ for 2 days and then again increased. Amplitude of variations increased with depth.

Cyclone heat potential calculated with respect to the 28°C is shown in Fig. 2.12. During early May, cyclone heat potential varied, in general, between 2.5×10^8 and $6.8 \times 10^8 \text{ J/m}^2$, at S. During late May and early June, variation in heat potential at this station was less.

At N, the heat potential progressively increased from mid-May and reached about $5.0 \times 10^8 \text{ J/m}^2$ on 20 May and decreased slightly till end of the month. At both S and N, the heat potential observed was almost equal during late May and early June. Subsequently at N the heat potential increased. The maximum of $5.4 \times 10^8 \text{ J/m}^2$ was observed on 3 June. This increase in heat potential was one of the favourable conditions for the formation and intensification of the monsoon onset vortex.

At both the stations, considerable decrease in heat potential was noticed after the vortex. Heat potential decreased to about $1.6 \times 10^8 \text{ J/m}^2$ at S and $2.2 \times 10^8 \text{ J/m}^2$ at N on 21 June. On the following

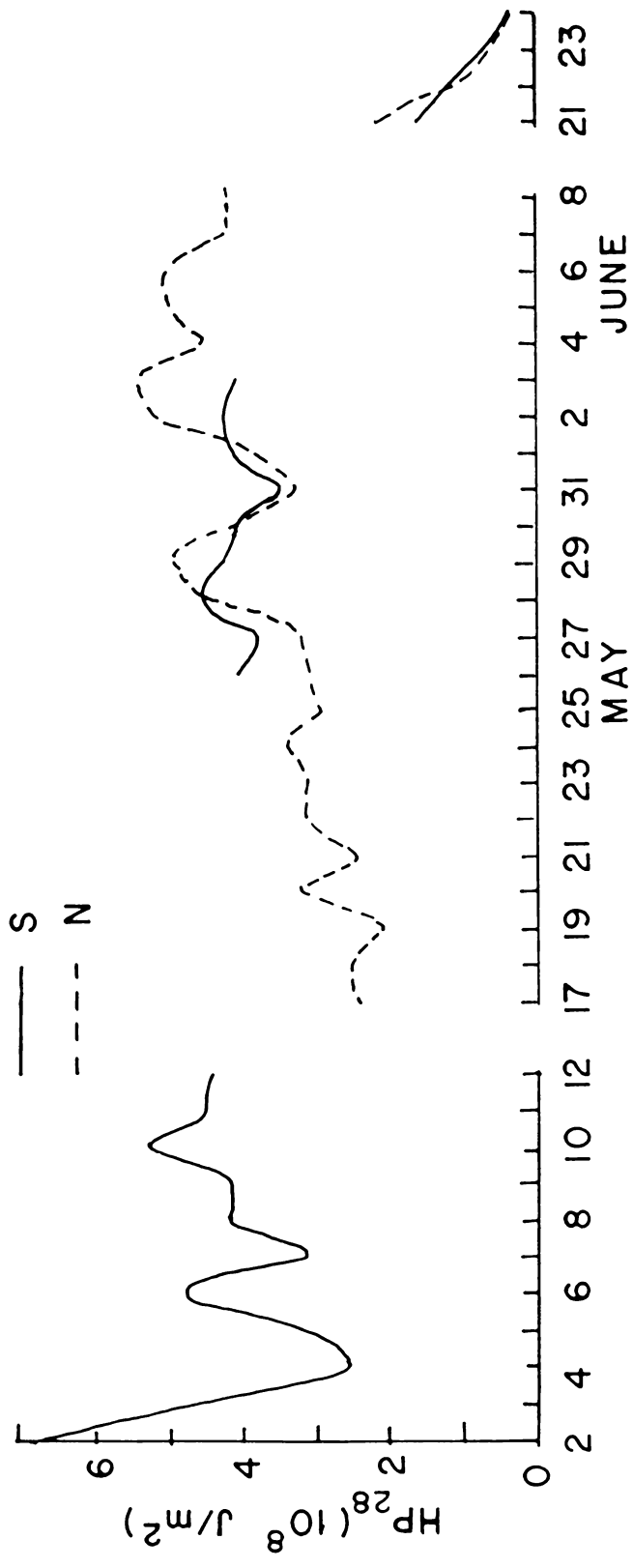


Fig.2.12 Daily variation of cyclone heat potential at the stations.

days, the cyclone heat potential decreased further by $1.0 \times 10^8 \text{ J/m}^2$ at S and by $1.5 \times 10^8 \text{ J/m}^2$ at N.

The results obtained on the various upper ocean thermal characteristics from above analysis are discussed in the following paragraphs.

The evolution of three day average profiles at S, during late May and early June (Fig. 2.8) indicates the formation of mild gradients close to surface. From surface to 40 m, the temperature was more than during early May, while at 60 m there was a reduction in temperature. This sudden decrease resulted in the thickening of the upper gradient regions discussed earlier.

At S, slight decrease in SST was noticed towards the end of observations in early May. During this period, the ML had also deepened slightly. These features indicate downward heat flux at the base of ML. Mixing might have been increased by surface heat loss and increase in wind speed under the influence of the cyclonic storm which occurred in the southern Bay of Bengal during this period.

A sudden increase in heat content, more conspicuously at subsurface layers was noticed on 1 June at N. During this period the isotherms had spread in the upper part of thermocline (Fig. 2.5). Thus, some oceanic readjustments appeared to be occurring before monsoon onset. As pointed out earlier, during this period, at N there was an increase in the temperature of surface layers. However, the ML showed slight deepening. It may be noted that during this period, there has been neither an increase in wind stress to induce mechanical mixing nor any surface heat loss for inducing convective mixing (Fig. 2.3). Hence, heat advection appears to be important in this area before the onset.

Observations at both stations after the passing of the vortex (21 June) have shown only a slight deepening of ML by about 10 m at S and about 5 m at N. The absence of an appreciable deepening, despite mixing due to storm, could have been the effect of upwelling. The three day average profiles for early June (1, 2, 3 June) and after the storm (21, 22, 23 June) at stations S and N are presented in Figs. 2.13a and b respectively. Both figures show an upward shift after the storm. The upward movement of isotherms can also be seen in vertical sections (Figs. 2.4 and 2.5). Upwelling due to passing storms have been well documented (Leipper, 1967; Ramage, 1972; Rao et al, 1983; Rao, 1984; Ramesh Babu and Sastry, 1984). Krishnamurti (1981) suggested that surface cooling in central and eastern Arabian Sea around 10° N in June 1979 was mainly due to upwelling caused by positive wind stress curl associated with monsoon onset.

Of the two stations, S registered more drop in temperature at all levels. This indicated more intense upwelling. The above storm (the onset vortex) which formed as a low pressure over Lakshadweep remained there from 8 to 13 June, before moving further north and intensifying (Mukherjee and Paul, 1980). The possible occurrence of positive wind stress curl for a longer period might have induced comparatively more intense upwelling here. Further, at this station, upward trend of isotherms was noticed and the core of high temperature gradient had progressively moved up during pre-onset itself (Figs. 2.4, 2.6). This tendency also may augment the upwelling.

Using numerical models, Chang and Anthes (1978) have shown that for slow moving hurricanes, the effect of wind mixing can be more than the upwelling effect. Near station S, the storm remained for longer

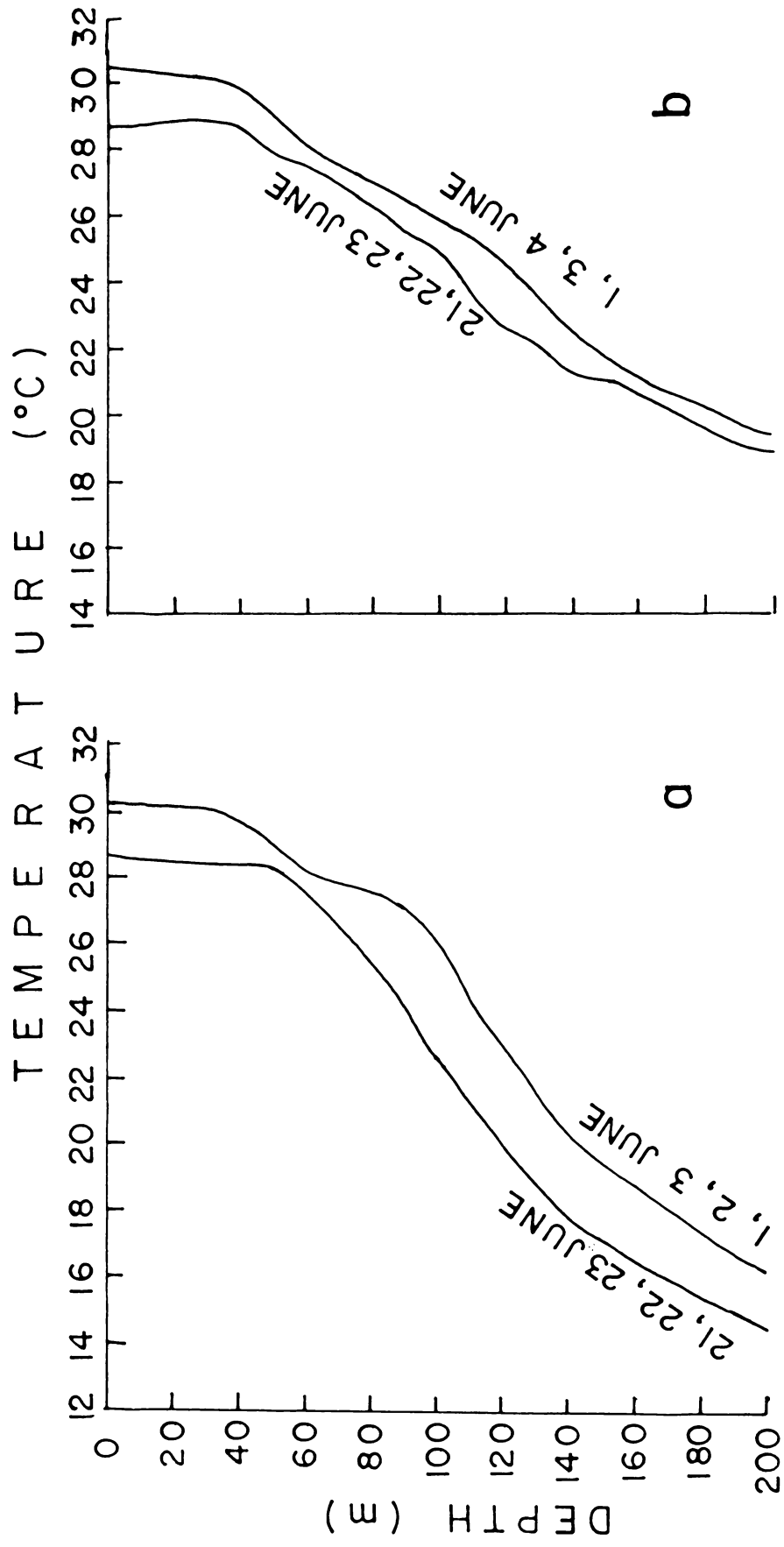


Fig.2.13 Three-day average profiles of temperature during early June and after the onset vortex.
a) at S and b) at N.

time, albeit with lesser intensity. These lesser wind speeds would not have been sufficient to induce mixing against the upwelling effect caused by diverging currents.

The present storm can, perhaps, be considered as a comparatively fast moving storm during 6-20 June (~ 6 m/s). Numerical experiments mentioned above have also indicated that for fast moving storms (~ 10 m/s), due to lesser time for mixing, the deepening of ML is reduced on either side of storm track and that upwelling is seen along the track of the storm. Since station N was located on the side of the track, the response to this storm, in terms of deepening of ML and upwelling, would be less intense.

After the storm, there were up and down movements of isotherms which appear to have been due to oscillations set up possibly by the storm. After the cessation of upwelling, the ML deepened on the following days probably due to mixing by persistent monsoon winds. As noted earlier, there was a deepening of isotherms at subsurface layers. This was manifest also in the increase in heat content in these layers with the progress in observations. This might be a consequence of the general circulation pattern. During southwest monsoon period, ocean circulation in Arabian Sea consists of a large anticyclonic gyre and under its influence, convergence and sinking can be expected in the central parts of Arabian Sea (Sastry and Ramesh Babu, 1985). This can lead to the deepening of isotherms when the effect of storm decreased. On examining the evolution of thermal structure during MONSOON-77, at 12.5° N and 68.0° E, Ramesh Babu and Sastry (1984) observed shoaling of ML due to storm and the subsequent deepening. They have suggested that with the progress of monsoon, entrainment of cold subsurface water also become important in ML deepening.

For better comparison, 3 day average profiles during pre-onset (early June) and after the vortex at both stations are given in Fig. 2.13. Mild deepening of ML after storm was not penetrative. The penetration of existing thermocline was prevented by the upward movement at subsurface. However, the tendency to deepen penetratively can be considered to be indicative of the effect of wind induced and convective mixing at the base of ML. The downward heat flux at the base of ML due to storm at station N is estimated elsewhere in this chapter.

2.3. UPPER OCEAN HEAT BALANCE

The relative importance of different processes in bringing about the observed decrease in heat content in upper layers (50 m) is examined. Since continuous data during the occurrence of onset vortex are not available, the bulk changes alone have been evaluated with necessary assumptions. Station N where continuous data for longer duration are available before storm has only been considered.

The decrease in heat content of upper 50 m from 8 June to 21 June was $1.90 \times 10^8 \text{ J/m}^2$. Murty et al (1983) obtained a decrease of $1.83 \times 10^8 \text{ J/m}^2$ in upper 40 m during 9-18 June in the locality. The decrease in heat content in ML observed by Rao (1984) from 2 June to 21 June was $2.7 \times 10^8 \text{ J/m}^2$. Seetharamayya and Mullen (1987) found a fall of $3.0 \times 10^8 \text{ J/m}^2$ in cyclone heat potential (HP_{28}) between 9 and 18 June.

For the evaluation of surface heat exchange, heat gain has been assumed till the occurrence of vortex (9-13 June) and heat loss during the vortex (14-20 June). Assuming not much change in atmospheric conditions, heat gain of the order of 150 W/m^2 can be reasonably arrived at as an average of previous 3 days (6-8 June). This works out to a total gain of $0.648 \times 10^8 \text{ J/m}^2$ for 9-13 June.

Surface heat loss due to vortex during 14-20 June is approximated in the following manner. Radiation flux, in this area, averaged for 12-20 June has been found to be about 90 W/m^2 (Smith et al, 1981). However, during the actual occurrence of vortex, it could have been still less. In this study radiative flux is assumed to be 75 W/m^2 . Evaporative loss on 19 June obtained in present study is 400 W/m^2 (Fig. 2.3b). Murty et al (1983) found loss due to evaporation of about 230 W/m^2 during 15-17 June and Shajahan (1980) reported high rate of about 580 W/m^2 on 14 June, at a station located south of station N. Evaporation at the rate of 350 W/m^2 appears to be a reasonable estimate for the period 14-20 June.

Sensible heat transfer can be negligibly small. Back radiation has been assumed to be 20 W/m^2 . The net heat loss during this period can thus be approximated as 300 W/m^2 which provides a total loss of $1.814 \times 10^8 \text{ J/m}^2$ for 7 days. Hence, during 9-20 June, the surface heat exchange can be obtained as a loss of about $1.17 \times 10^8 \text{ J/m}^2$.

Entrainment of heat has been evaluated as follows. MLD (h) has increased from about 55 m on 8 June to about 60 m on 21 June. Downward heat flux due to entrainment occurs during the deepening period. Entrainment velocity " w_e " can be obtained by dividing 5 m by the duration of entrainment (dt). Temperature jump, dT, in 10 m at the base of ML is found to be 1°C . Mixed layer being a region of homogenous temperature, the temperature drop, ΔT , in the 55 m water column due to entrainment is given by $w_e \times \frac{dT}{h} \times dt$. Since this drop has resulted in the formation of final ML of 60 m, heat flux due to entrainment has been obtained using the expression $\Delta T \times \int_w C \times 60$. The entrainment flux is estimated to be $0.22 \times 10^8 \text{ J/m}^2$.

Heat flux and entrainment accounts for a loss of about $1.39 \times 10^8 \text{ J/m}^2$. Heat advection, obtained as the residual, is $0.51 \times 10^8 \text{ J/m}^2$.

It can thus be seen that surface flux, entrainment and advection have accounted approximately 60%, 10% and 30% of the heat lost by surface layers, during the vortex.

Comparing the changes in heat content of ML between 2-21 June, Rao (1984) has found that surface heat exchange contributes to 50% of the heat loss and attributes the remainder to advection. Murty et al (1983) have found 40% of heat content changes in upper 40 m between 15-17 June to be due to surface heat loss and consider the remainder to be the heat flux to the interior of ocean. However, in both the above studies, entrainment has not been evaluated. Although the present analysis is at best only an approximation, it has been possible to bring out the relative importance of the three processes during the storm.

Camp and Elsberry (1978) have shown that during strong atmospheric events in early cooling seasons, heat flux at the base of ML can be 10 times the magnitude of surface heat loss and also that advection is not important during these events. However, in the present context, mild upwelling at N due to storm has inhibited the mixing. Further, as noticed earlier, the storm being comparatively fast moving one, the mixing might have been less effective. Another reason for the lesser downward flux can be the occurrence of comparatively deep ML before the storm.

Price et al (1978) have estimated, by model studies, these components of heat loss during storms and have found the surface flux, entrainment and horizontal advection for a winter time case to be 61%, 13% and 26% respectively while for a summer time case, these are 30%, 62% and 8% respectively. Entrainment is found to dominate during summer case, when ML is shallow. The present estimates agree more with the former when ML is deeper.

2.4. CONVECTIVE MIXING IN UPPER OCEAN

Since the mixing in the upper ocean is caused by the energy derived from wind stress and surface buoyancy flux due to air-sea exchange, an attempt has been made to examine the relative predominance of these during pre-onset and after-onset of monsoon. Following Shay and Gregg (1986), the various related parameters have been estimated for S and N and are presented in Figs. 2.14 and 2.15 respectively.

At S, (Fig. 2.14) wind energy (E) was found to be low during early May ($< 0.1 \text{ W/m}^2$) which increased after 6 May and reached $> 1.0 \text{ W/m}^2$ on 11 and 12 May. The increase was due to the effect of the storm which formed over Bay of Bengal during this period. Towards the end of May and early June, low values, less than 0.1 W/m^2 , were generally observed. After the onset of monsoon, energy increased and varied between 1.0 and 2.2 W/m^2 during 21-23 June. Friction velocity of about $0.4 \times 10^{-2} \text{ m/s}$ observed during early May progressively increased to about $1.2 \times 10^{-2} \text{ m/s}$ due to the storm. After monsoon onset, friction velocity increased to more than $1.0 \times 10^{-2} \text{ m/s}$.

Buoyancy flux at S, during pre-onset was generally positive (heat gain by sea) except when the area came under the influence of the storm in Bay of Bengal. Negative buoyancy flux increased to about $-1.0 \times 10^{-7} \text{ W/kg}$ by 12 May. After the onset of monsoon it was negative ($-0.6 \times 10^{-7} \text{ W/kg}$). Monin-Obukhov length (L) was generally positive during pre-monsoon when fair weather conditions prevailed. However, during storm period (May 7-12), negative L indicating convective condition was observed and it varied from -25 to -50 m. After monsoon onset, higher values of |L| (-120 to -150 m) were seen. There were certain observations when L could not be defined due to nearly zero heat transfer at sea surface.

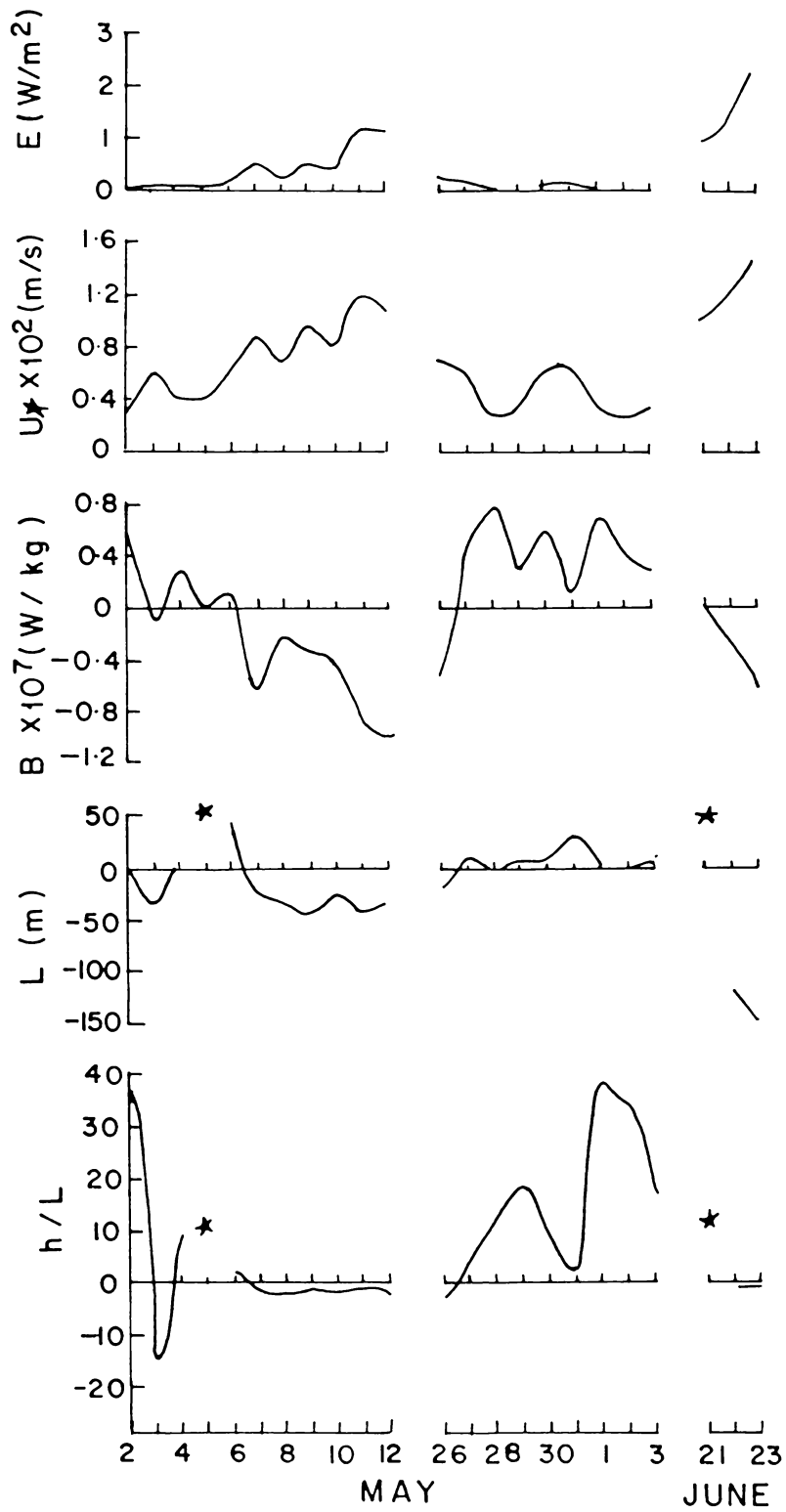


Fig.2.14 Daily variation of wind energy, friction velocity, buoyancy flux (+, heat gain at sea surface), Monin-Obukhov length (+, stable condition) and h/L at S.

During pre-monsoon, at S, when convective conditions did not occur, h/L where h is MLD, was generally positive. However, when the layer became convective due to storm, h/L was about -2.0 . After monsoon onset, although convective mixing was observed, $|h/L|$ was very small (~ -0.4). During certain days, h/L was not realistic, either due to very low wind speed or near - zero heat transfer at sea surface.

At N, during pre-onset, wind energy was generally negligible, maximum observed being 0.6 W/m^2 (Fig. 2.15). After monsoon onset, energy increased and was about 12 W/m^2 on 21 June. It decreased to 5 W/m^2 on 23 June and increased again on the following days. Friction velocity was less during pre-onset ($< 1.0 \times 10^{-2} \text{ m/s}$). Friction velocity increased after monsoon onset and varied between 2.0×10^{-2} and $2.8 \times 10^{-2} \text{ m/s}$.

At N, positive buoyancy flux varying between 0.3×10^{-7} and $1.2 \times 10^{-7} \text{ W/kg}$ was observed during pre-onset, indicating absence of convective mixing. After monsoon onset, buoyancy flux became favourable for convective mixing due to surface heat loss and the flux ranged from -0.4×10^{-7} to $-1.6 \times 10^{-7} \text{ W/kg}$. Monin-Obukhov length was positive and very small during pre-onset and became negative after monsoon onset when it varied between -300 and -600 m . $|L|$, after onset were higher than at S where the wind speeds were lesser. These values are considerably higher than in the warm core ring of Gulf Stream during cold air outbreaks observed by Shay and Gregg (1986). Although their observations showed wind energy comparable with the present case, the buoyancy flux was large resulting in smaller $|L|$. It is possible that during the period of occurrence of the onset vortex, surface heat loss might have been more and consequently, $|L|$ would have been lesser.

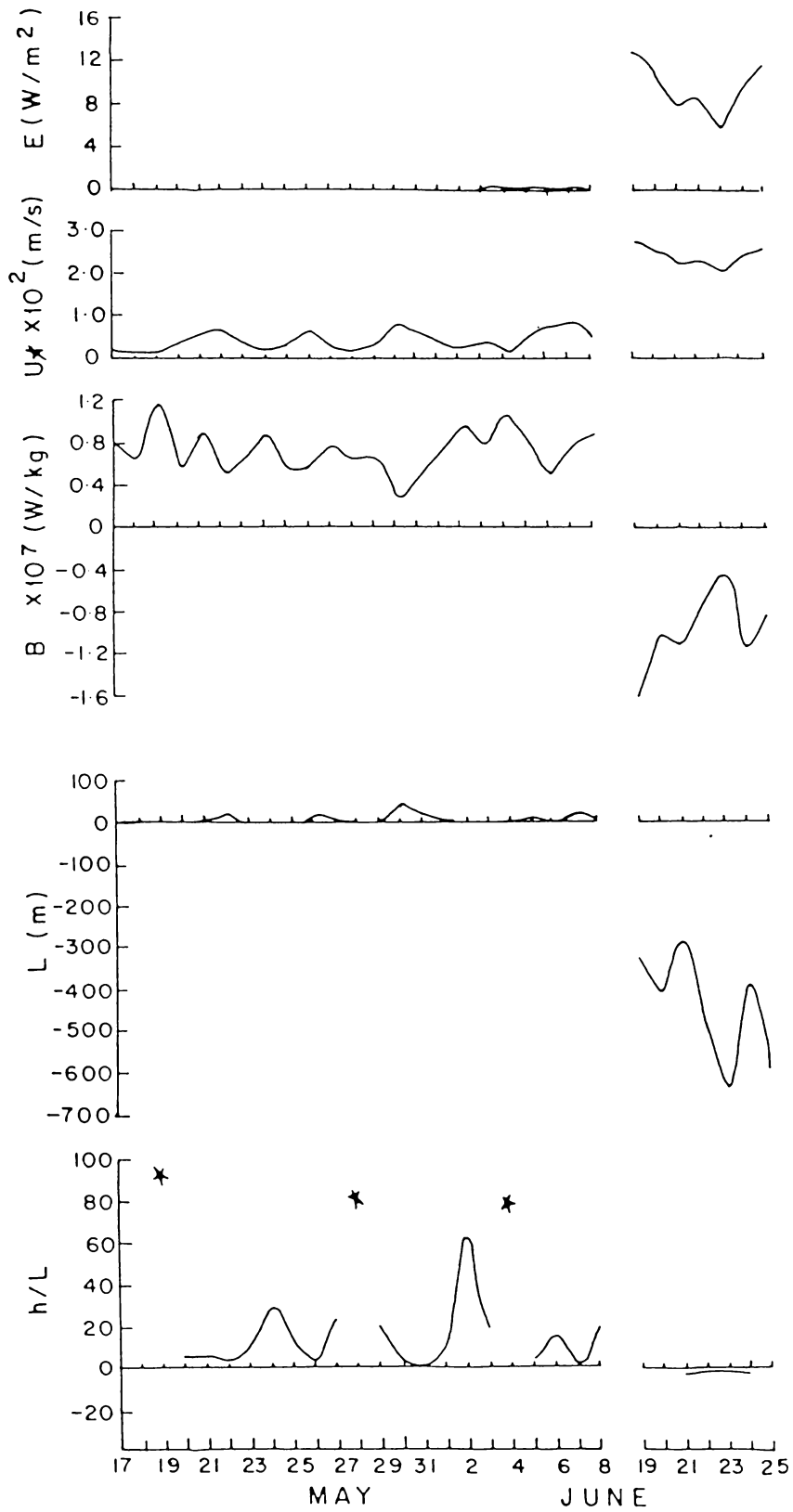


Fig.2.15 Daily variation of wind energy, friction velocity, buoyancy flux (+, heat gain at sea surface), Monin-Obukhov length (+, stable condition) and h/L at N.

h/L at N , during pre-onset was positive. After monsoon onset it became negative (~ -0.1) indicating convective mixing. There were few observations without realistic values of h/L when L was very small due to negligible wind speed.

From the foregoing, it can be seen that convective mixing was absent during pre-onset, except when the area had come under the influence of a storm in Bay of Bengal. Wind energy was also less during pre-onset. In the absence of wind stress, the mixing in the upper ocean might have been caused by the convection due to surface heat loss during night time cooling. Shay and Gregg (1986) observe that, at night, convection erodes the stable zone and penetrates the restratified layer. Diurnal variations are, however, not included in the present study.

Convective mixing was observed under the influence of storm in Bay of Bengal and also after monsoon onset. During the storm, $h > L$ and the reverse was true after monsoon onset. This indicates that buoyancy mixing has been predominant in the former case while wind mixing has been important in the latter. In both cases h/L , which can be considered as a stability parameter, was low compared to that in the warm core ring of Gulf Stream observed by Shay and Gregg, (1986). After monsoon onset, h/L was -0.1 to -0.4 while under the influence of the storm in Bay of Bengal it was about -2.0 . These two situations are compared using the schematic presentation by Nicholls and Readings (1979).

Fig. 2.16 represents the importance of the two aspects viz., wind stress and buoyancy flux in inducing mixing. Diagonal lines are drawn for different values of h/L . Each quadrant of the space stands for different situations. In the lower left quadrant, wind stress is dominant and in the upper right quadrant buoyancy forcing is the important

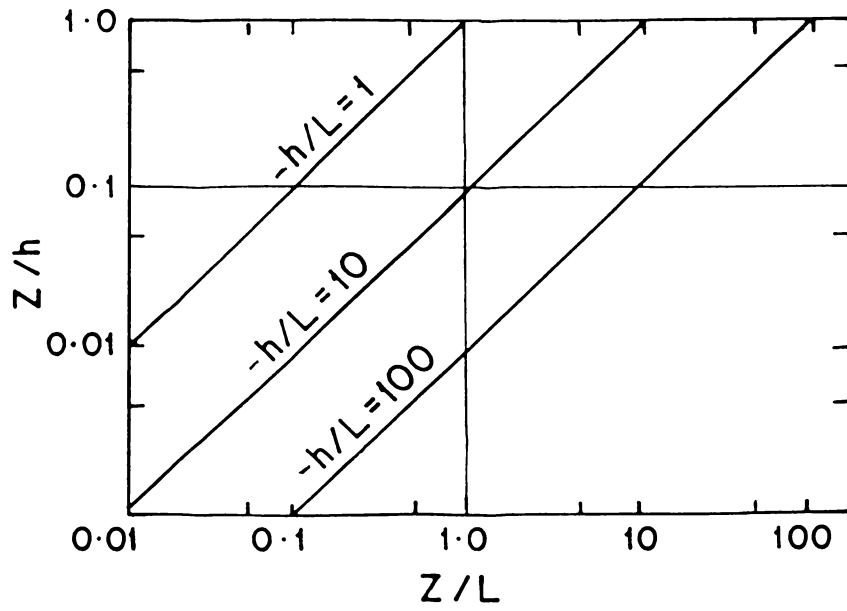


Fig.2.16 Schematic diagram adapted from Nicholls and Readings (1979) indicating the quadrants where wind and buoyancy flux are important in mixing. Explanation is given in the text.

factor. The lower right quadrant is termed as free convection region where both wind stress and buoyancy are not applicable. The upper left quadrant is a condition where both aspects are important.

In the present data, h/L was about -2 during the period of convective mixing due to effect of storm that occurred in the Bay of Bengal. For the observed MLD, this falls in the upper right quadrant. Hence, as expected when $h > L$, in this case also convective mixing is predominant.

h/L , obtained after monsoon onset (-0.2 to -0.4), will fall in the upper left quadrant of Fig. 2.16. This shows that although $h \ll L$, the effect of buoyancy cannot be neglected in the mixed layer. These effects have earlier been noticed in the 3 day average temperature profiles as a tendency to deepen penetratively. Atmospheric data over oceans were also found to fall in this quadrant indicating a deep atmospheric boundary layer where in addition to the effect of buoyancy flux, the effect of wind stress is also important (Nicholls and Readings, 1979).

Thus we can distinguish the situations in Arabian Sea during pre-onset and after the monsoon onset. Before monsoon onset, convective mixing does not occur because of surface heat gain. Convection may, however, be taking place during night time, maintaining the ML. Under the influence of a storm in the Bay of Bengal, the mixing in upper ocean in eastern Arabian Sea is dominated by buoyancy forcing while after the monsoon onset, mixing is induced by the combined effect of buoyancy and wind forcing.

CHAPTER 3

UPPER OCEAN THERMAL STRUCTURE IN AREA I (NORTHERN PART OF SOMALI CURRENT AREA)

Area I of the present study which is located in the western Arabian Sea (Fig. 1.1) is situated on the northern part of Somali current region. Somali current is of considerable interest for two reasons. Firstly, with the onset of southwest monsoon, the current in this area reverses to become a swift northeasterly current parallel to the east African coast. The second reason is the presence of intense upwelling during southwest monsoon season in this area. As a result of upwelling, cold subsurface water is brought to the surface layers near the shore which spreads over extensive areas of Arabian Sea. Different aspects of the upper ocean thermal structure in this area are discussed in the various sections of this chapter.

Somali current is a seasonal current which is set up in response to the southwest monsoon and flows northwards along the coast of east Africa. Observing that the current reverses northwards by late April at 2°S , Leetmaa (1973) points out that this is the reason why the Arab sailors waited until the third week of April to begin their sail northwards. Warren et al (1966) and Swallow and Bruce (1966) have reported detailed results on these currents based on data from International Indian Ocean Expedition. These works, however, give the picture only in August, after the formation of Somali current. Studies of limited spatial extent in Somali current region have been made, using drouges (Leetmaa, 1972, 1973) and by moored instruments (Düing and Schott, 1978). Mathematical models employing different assumptions, in general, succeeded in generating

reversal of currents in this area in response to the southwest monsoon (Lighthill, 1969; Cox, 1970; Anderson and Rowlands, 1976; Luther and O'Brien, 1985). Das et al (1987) found from model studies that both curl and divergence of wind stress are important in generating upwelling off Somali coast during monsoon.

Multiship oceanographic programme together with moored and satellite observations were carried out in 1979 to gain better understanding of the current and the thermal response to the southwest monsoon. This programme, known as Indian Ocean Experiment (INDEX), formed part of First GARP Global Experiment (FGGE) and coincided with MONEX-79 (Swallow, 1980). Various preliminary results of this study have appeared in a single issue of SCIENCE (Vol. 209, 1980). Details of current reversal, current and thermal structures, water masses, upwelling and many other aspects associated with Somali current have been presented subsequently (Leetmaa et al, 1982; Quadfasel and Schott, 1982; Schott and Quadfasel, 1982; Swallow et al, 1983).

Sastry and D'Zouza (1971) have inferred from geostrophic computations that during the southwest monsoon season the coastal current turns offshore at the northern Somali Basin as part of an anticyclonic eddy. Several workers have reported the presence of this eddy which Findlay (1866) called the "great whirl". More recent studies have, however, shown that during southwest monsoon season, there are two eddies in the Somali Basin instead of one, the second being located south of the "great whirl" (Bruce, 1973, 1979; Evans and Brown, 1981; Swallow and Fieux, 1982; Swallow et al, 1983). Towards the end of southwest monsoon season these two eddies merge into one and the great whirl alone will be present. Coalescing of these eddies has been studied by Evans and Brown (1981) and Bruce and Beatty (1985). The present study Area I is

located in the region of the northern Somali eddy observed during the southwest monsoon season.

3.1. SEA SURFACE TEMPERATURE

The annual variation of sea surface temperature (SST) is presented in Fig. 3.1. Net heat transfer at sea surface is also included. SST shows double maxima in this area (Fig. 3.1). From March to May, SST increases from about 26° to 29° C. Schott and Quadfasel (1982) observed a gradual warming of the surface layer by about 2.6° C from March to early May during 1979. After May, the SST decreases, which is due to the effect of southwest monsoon. The SST continues to decrease until August, in spite of the increase in atmospheric heat input. This fall in SST is due to the cooling associated with upwelling. Beyond August, there is a warming because of the cessation of upwelling and also due to increased surface heat input. Upwelling and sinking in this area are discussed in detail elsewhere in this chapter. In winter, SST registers a fall due to decrease in atmospheric heat input. Climatological cycle of SST in a smaller portion of Area I, has been presented by Molinari et al (1986), based on a paper by Reynolds (1983). The double maxima in the annual cycle agrees with the findings of the present analysis. However, the minimum observed in the present study in August, is about 2° C less than that presented by Molinari et al (1986). Somali Basin being a region of sharp horizontal gradients during southwest monsoon, the average values will be very sensitive to the area selected for averaging. During summer monsoon, SST and MLD vary significantly within short distances in Somali Basin (Reverdin and Fieux, 1987). The smaller subarea in the study of Molinari et al (1986) might have contributed to the difference observed. Annual cycle of SST in a region located slightly away from the coast also shows a similar double maxima as in present study but

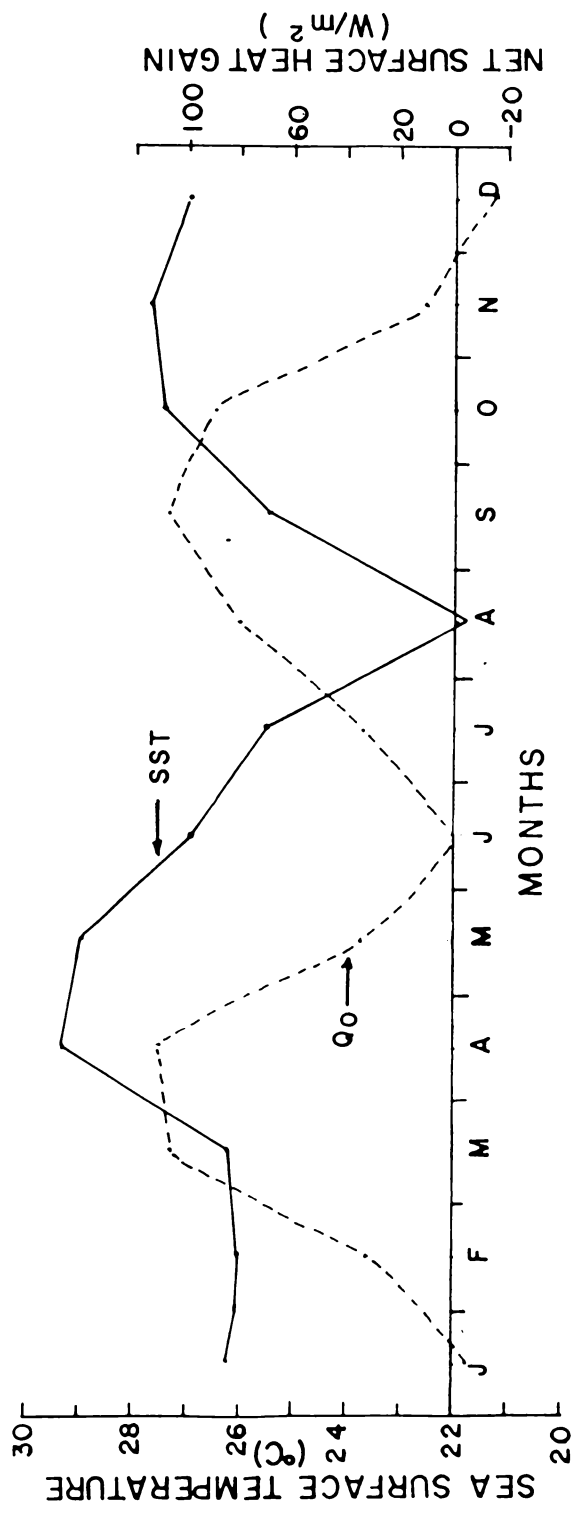


Fig.3.1 Average monthly variation of sea surface temperature and net surface heat exchange, in Area I.

with reduced amplitude (Reverdin and Fieux, 1987).

3.2. SUBSURFACE THERMAL STRUCTURE

Annual variation of subsurface thermal structure is presented in Fig. 3.2. In January and February, deep mixed layer (ML) extending to about 70 m depth is observed. From January to February, isotherms above 100m, generally, do not show much variation in depth. However, slight deepening is noticed between 100-150 m. This agrees with the increase in depth of 20°C isotherm in February in this area observed by Quadfasel (1982). From the topography of 20°C isotherm in western Indian Ocean, Quadfasel has inferred the existence of a weak southerly current at these depths all along Somali coast during January - February. After February, the surface layers warm to attain maximum temperatures by April-May. Schott and Quadfasel (1982) have observed gradual warming of surface layers by about 2.6°C from March to early May in 1979 which, in general, agrees with the findings of the present analysis based on climatological data. Along with this warming, a shallow temperature gradient develops and the ML shoals. Coinciding with this, there is a deepening of isotherms. This increase in depth of isotherms at subsurface layers may be associated with southerly coastal current in this area. Southwesterly undercurrent at about 200 m has been noticed by Schott and Quadfasel (1982) in this area before the onset of monsoon in 1979.

In May, the mixed layer shoals to a depth of 40 m. In 1979 also similar observations have been reported by Schott and Quadfasel (1982). Cooling is observed ($1^{\circ} - 2^{\circ}\text{C}$) upto a depth of 150 m, during this month. Although the cooling close to the surface may have been due to a reduction in atmospheric heat input associated with the advance of southwest monsoon, in the layers below, some other mechanism also may have contributed to

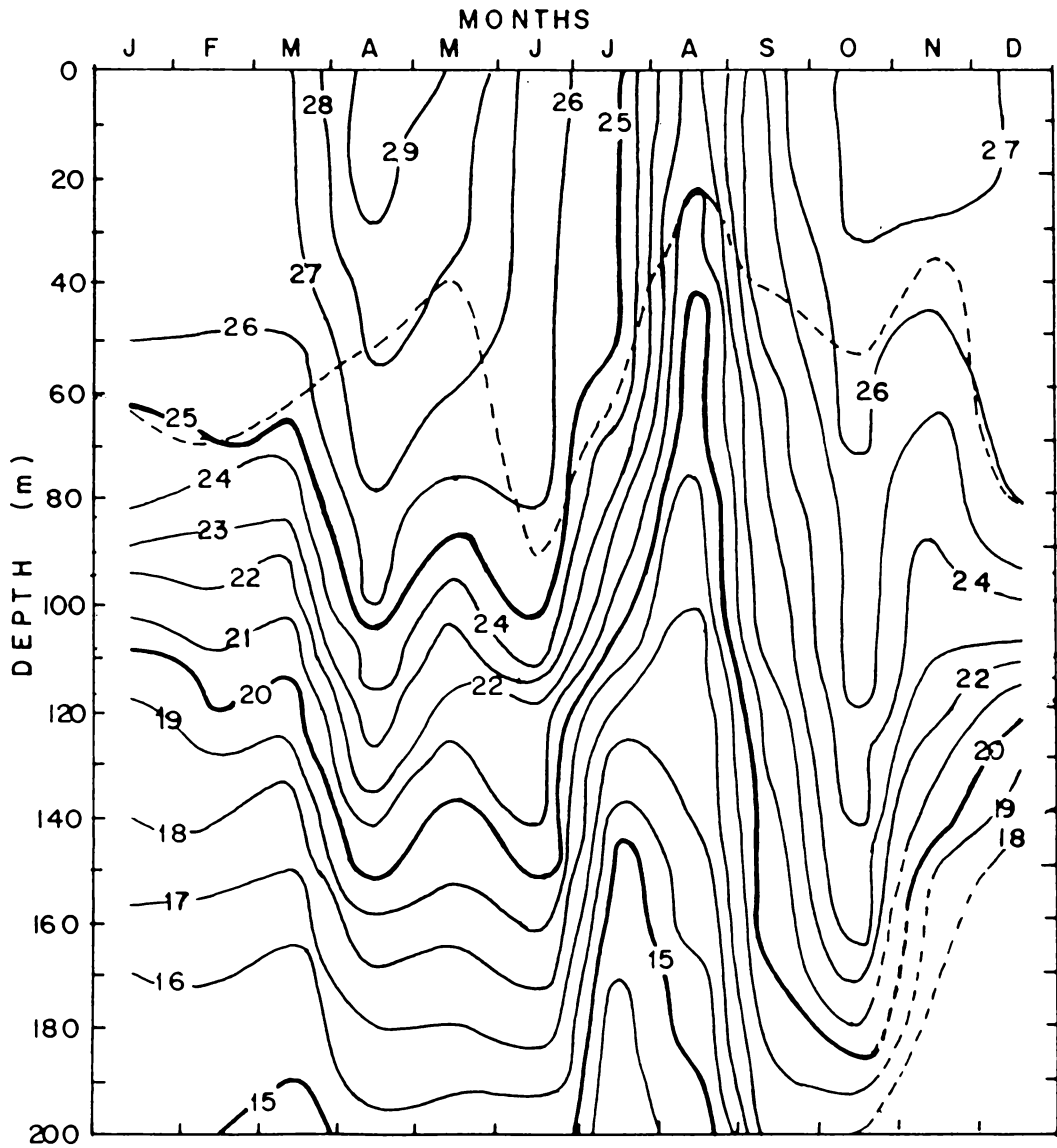


Fig.3.2 Average vertical-time section of temperature, in Area I. Isotherms are drawn in °C. MLD is shown by dashed line.

this. Schott and Quadfasel (1982) reported a decrease in temperature at depths between 110 and 135 m, by about $3-5^{\circ}\text{C}$ during pre-monsoon (March to May) in 1979. This feature may be related to the easterly equatorial jet during this period. Slight decrease in the depth of 20°C isotherm, similar to that found in present study, has been attributed by Quadfasel (1982) to the equatorial jet. Along the equator during transition periods between monsoons, April-May and October-November, narrow easterly surface jet is set up (Wyrтки, 1973). Since the jet is fed from the western part, it causes an uplift of thermocline near the shore leading to the observed fall in temperature. Düing and Schott (1978) have attributed same reason for the cooling south of equator in western Indian Ocean during pre-monsoon. Slight spreading of isotherms in the thermocline, observed after April, is indicative of downward heat flux.

During June, a fall in temperature is noticed in the upper layers together with considerable deepening of mixed layer. The 20°C isotherm deepens to about 160 m. Deepening of isotherms around June is seen in the section presented by Colborn (1975), but he has not attempted to offer an explanation for this feature. The lowering of temperature in the surface layers can be due to sudden fall in surface heat input. Mild deepening of isotherms in the upper thermocline, observed in June, may be related to the slackening of the above mentioned easterly equatorial jet. As this jet weakens during southwest monsoon, water is no more fed from the western coast, resulting in the relative deepening of thermocline.

The thermal structure indicates that upwelling does not commence in June in the present study Area I. As will be discussed later in this chapter, upwelling in this region is generated by the current turning offshore. Analysing historical data, Fieux and Stommel (1977) have shown that the onset of monsoon is not gradual in all years. In some years,

after its onset in May, the monsoon stops for some days before the final onset - termed as "multiple onset". Schott and Quadfasel (1982) have shown that, during 1979, the monsoon onset was multiple with 2 phases. The first phase occurred on 5 May when the wind became parallel to the coast. After a weakening of the wind, the monsoon revived around 10 June, with a drastic increase in wind speed.

The response of ocean currents in Somali Basin to such events of monsoon is not simultaneous everywhere. Looking for evidence for a two gyre current system during southwest monsoon from historical information, Swallow and Fieux (1982) find that in early May, the current moves offshore around $2-4^{\circ}$ N as part of the southern anticyclonic eddy. However, offshore movement of the northern eddy appears only after many days (see Table 3.1).

Thus it appears that from May to mid-June, upwelling of the surface layers has not commenced in study Area I. At the same time, the equatorial jet has weakened and hence, the upward tilt of the thermocline reverses contributing to the observed deepening of isotherms at subsurface levels.

It is also possible that this deepening of isotherms by mid-June provides a favourable condition for the spin up of the northern gyre along with the onset of southwest monsoon. In 1979, the northern eddy appeared to have developed rapidly with the second onset of monsoon (Leetmaa et al, 1982). Schott and Quadfasel (1982) find that there has been no change in the circulation north of 4° N, after first onset. Moreover, after the second onset, northern eddy spins up rapidly away from shore and then propagates shorewards (Fig. 3.3). They conclude that the northern

Table 3.1. Dates of appearance of wind and current events
 (from Swallow and Fieux, 1982)

Year	Southerly winds off Somalia		Earliest evidence of current turning off shore. 2° - 4° N	Earliest evidence of current turning off shore 7° - 10° N
	Absent	Present		
1934	Apr 27	May 4	May 28	May 31
1936	Apr 24	May 9	May 11	Jun 4
1937	May 4	May 8	May 10	Jun 6
1953	May 16	May 10	May 19	Jun 19
1954	May 1	May 3	May 12	Jun 7
1955	Apr 11	Apr 13	--	Jun 18
1963	Apr 28	May 5	May 6	Jun 16
1966	-	May 12	May 20	Jun 9

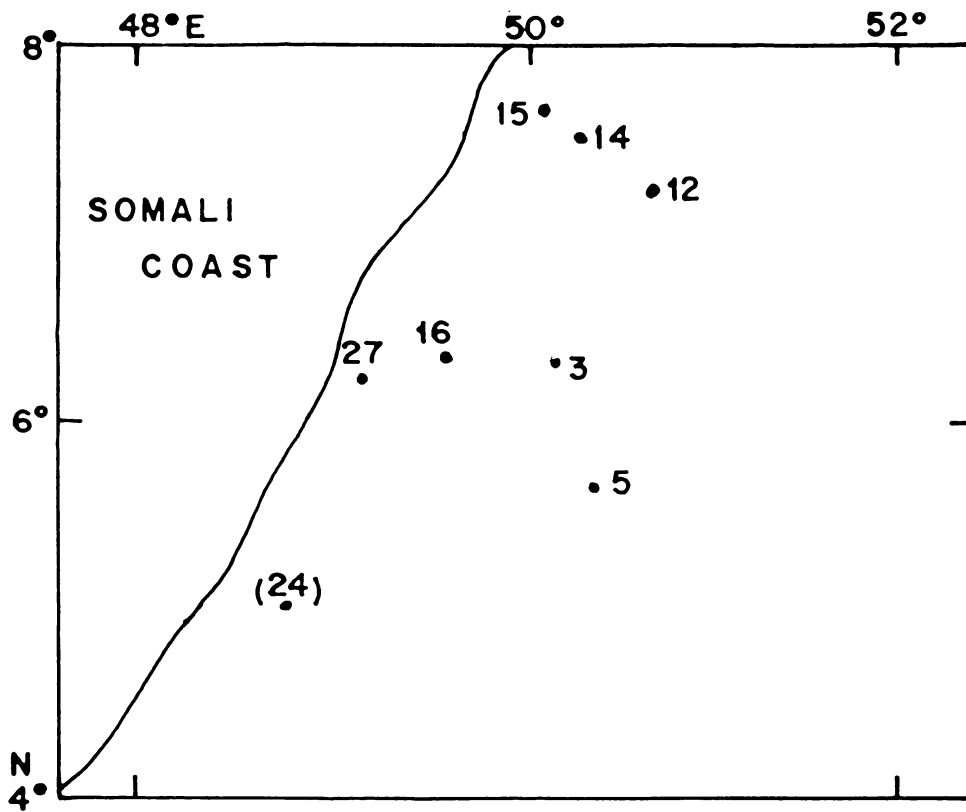


Fig.3.3 Response time of currents at different current meter moorings, counted in days after the final onset on 10 June in 1979 (From Schott and Quadfasel, 1982)

gyre is locally generated by anticyclonic wind stress curl over northern Somali Basin. It is then possible that the deepening of isotherms in early June as seen in the present study, indicating warming, may be conducive for the above local response to the second onset of monsoon.

Thermal structure during the next two months (July and August) clearly indicates intense upwelling. Upward tilt of isotherms begins in late June from more than 200 m depth. This may extend to depths of 425-600 m (Wooster et al, 1967). Between June and July, upwelling is more intense below about 100 m. This depthwise variation in intensity of upwelling may be due to the variations in current structure. As noted earlier, upwelling in Somali region is the result of the north easterly current turning offshore. Two regions of upwelling are observed, one at 2° - 4° N and the other at 8° - 10° N. SST fields during southwest monsoon 1979 (Brown et al, 1980), reproduced in Fig. 3.4 show the cold wedges due to the upwelling regions. These are the two places where the northern arms of two gyres move offshore. Present study Area I comes in the northern upwelling region resulting from the northern gyre. Hence, it appears that there may be depthwise difference in the northern gyre.

Referring to the observation of Bruce and Volkman (1969) on subsurface anticyclonic eddy during northeast monsoon season to be a remnant of the previous southwest monsoon circulation, Leetmaa (1972) suggests that it is this gyre that surfaces when the northeast monsoon weakens. The present study on thermal structure also suggests that a gyre may have occurred first at subsurface layers and have resulted in an upward tilt of isotherms. However, it does not appear to be the remnant of the circulation of previous southwest monsoon. Had it been so, the upwelling associated with eddy would have been a continuous process. Present analysis shows that upwelling starts only around June.

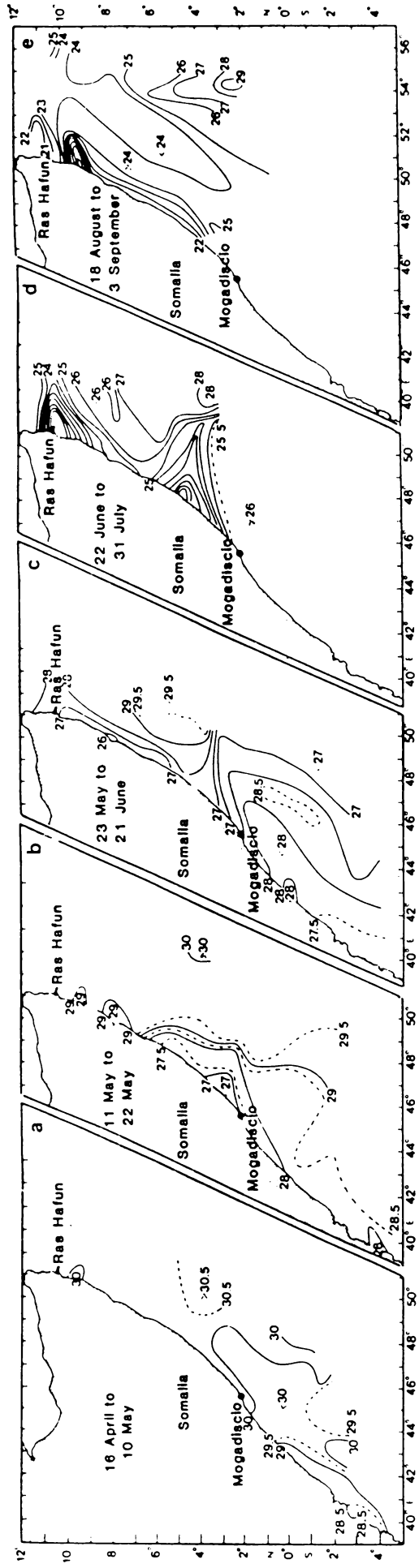


Fig.3.4 Sequence of SST fields showing cold wedges due to upwelling (From Brown et al., 1980)

At intermediate levels, at about 700 m, an anticyclonic eddy was observed by Quadfasel and Schott (1982) in May 1979, in this region. From watermass analysis they have found that salinity in the eddy is similar to that in equatorial region (less than 35.1‰), much less than that in the region of well developed Somali current indicated by Warren et al (1966). Quadfasel and Schott (1982) speculate that this eddy is generated at the equatorial region due to subsurface westerly current. When the westerly equatorial subsurface current meets the shoreline, eddies are generated which drift north and south of the equator. They have also observed an eddy south of equator simultaneously. This means that, at intermediate depths, the eddy is not generated in response to local monsoon winds. It is possible that an anticyclonic eddy occurs first at subsurface and is responsible for the intense upward tilt of isotherms at subsurface layers as observed in the present study.

By mid July, SST decreases to about 25°C . Although the mixed layer started shoaling, it still remains as deep as 60 m. Schott and Quadfasel (1982) are of the opinion that the initial decrease of SST after the onset of southwest monsoon, observed during 1979 at 6°N and 10°N , is due to upwelling produced by winds parallel to the coast. They argued that if mixing were important in cooling, the cold water must not be confined close to the shore as observed by them. Present studies show that mixed layer to be deep in July also, although a shoaling tendency due to upwelling can be seen. Since the upwelling off Somali coast is attributed to coastal currents turning offshore at two locations viz. 2°N and 8°N (Warren et al, 1966; Bruce, 1979; Brown et al, 1980; Evans and Brown, 1981; Swallow et al, 1983), the maximum cooling must be at these two areas and not all along the coast. Preceding discussions

have shown that upwelling alone does not provide surface cooling in July. Thus, wind mixing cannot be neglected. The increased wind and wave action can generate mixing with cold upward moving water. This results in cooling of surface layers, still retaining somewhat deep mixed layer. However, classical upwelling as suggested by Schott and Quadfasel (1982) also may have contributed to the cooling. The observed mild shoaling of isotherms together with surface cooling may be the combined effect of these processes.

By the middle of August, the lowest surface temperature of about 22°C is observed. During this period, intense cooling is seen above 120 m. Warming is observed below this depth. This indicates the presence of upwelling in upper layers and sinking in the lower layers. Thermocline rises to surface and the mixed layer becomes very shallow (~ 20 m). Permanent thermocline is found to outcrop the sea surface. This agrees with the observation by Colborn (1975).

There can be two reasons for the very intense upwelling during this period. The northern eddy - 'prime eddy' according to the terminology of Bruce (1968, 1979) - continues to be strong. From the topography of 20°C isotherm, Quadfasel (1982) finds that the northern eddy reaches full strength by August/September and continues to be so in October. Observations during 1-4 August, 1979 have shown that 20°C isotherm reaches close to surface, near the northern eddy (Swallow et al, 1983). Apart from the effect of northern eddy, the southern eddy, due to its change in position, also might have contributed to this feature. The southern eddy moves northward as monsoon progresses and together with this, the southern upwelling area also moves northwards. In 1970, the southern eddy moved from 5°N to 6°N during August before it merged with northern

eddy during September (Bruce, 1979). Using satellite derived data, Evans and Brown (1981) also noticed similar northward translations during certain years. The southern upwelling region which is located south of study Area I in the beginning of monsoon, moves into this study Area during August. Due to the combined effect of the two upwelling regions, very intense cooling of waters is observed in the upper part.

During this period of intense upwelling in upper layers, sinking is seen below this. By this time, the eddy at subsurface, discussed earlier, may have drifted further north of the region under study. The entering of onshore arm of the above eddy into study area may have resulted in the observed sinking. Moreover, during this period, new eddies are not generated and transported into study area because of the disappearance of equatorial surface easterly jet and consequently the subsurface westerly current (Cane, 1980; Quadfasel, 1982). The dynamic situation in Area I during this period can result in vertical transport of heat as seen from a spreading of isotherms.

After the middle of August, very sudden warming in surface layer is noticed (Fig. 3.2). Intense sinking is noticed which appears to extend deeper than 200 m discussed in this study. Quadfasel (1982) also noticed deepening of isotherms in September. Swallow et al (1983) have found that by the end of August, circulation pattern changes rapidly. Their figure for 5-25 August 1979 shows considerable deepening of 20°C isotherm in this area. It is surprising that sinking is taking place in spite of the presence of the northern eddy, "the prime eddy", during this period. Bruce (1979) finds the presence of northern eddy in October. Similar finding of Quadfasel (1982) has been pointed out earlier. The evolution

of SST in Somali Basin during southwest monsoon of 1979, presented by Brown et al (1980) shows that the northern and southern eddies and the associated upwelling areas coalesce by late August and reach as north as 10° N. Bruce (1973), analysing thermal structure during southwest monsoon of 1970, shows that by September, the two upwelling areas merge and northern anticyclonic cell becomes weak. Large temperature changes in the thermal structure of upper 200 m is seen within short time interval towards the end of monsoon. Changes upto 10° C in observations separated by 2 weeks to one month are noticed in the study region. Large changes in flow paths and associated regions of upwelling may occur over a period of one month (Bruce, 1973).

Presenting the details of upwelling off Somalia using data for 1963, Bruce (1974) also observed changes in upwelling areas from August to September. While during August, coldest water of temperature $< 16^{\circ}$ C is found at $8^{\circ} 30'$ N, within ten days the cold water shifts to north of latitude of Ras Hafun (10.5° N). Considering the 20° C isotherm to be northern limit of east flowing arm of Somali northern eddy, it has been found that this current shifts from 9° N to about 10° N during August to September (Bruce, 1974).

The northward translation of eddies was studied for some years by Evans and Brown (1981) from the propagation of thermal front during the course of southwest monsoon. In 1976 and 1979, the northward translation of southern eddy took place in phases during one month and finally coalesced with the northern eddy between 8° and 10° N. In 1978, while the southern thermal front moved northward, the northern front moved further and without merging, translated past Socotra and disappeared in Arabian Sea. The evolution of frontal development in 1979 from

satellite data presented by Swallow et al (1983) also indicates such northward translations.

From the various studies discussed above, it can be seen that although there are year to year variations, on a climatological scale the eddies coalesce into one, the great whirl, by September. The great whirl turns offshore at a region located north of 10° N. South of that, in present Area I, sinking takes place due to the onshore arm of the great whirl. That upwelling takes place north of 10° N during this period, is confirmed by the shoaling of isotherms in the time depth section presented by Colborn (1975).

Colborn (1975) suggests that the sinking (in the present Area I) may be due to change in direction of wind that blows onshore by October. However, since upwelling and sinking occur at the same time, in adjacent areas along the coastline, the wind does not appear to be the reason for the sinking. It may be noted that Colborn had not considered eddies and their changing positions in the processes of upwelling and sinking in Somali Basin.

Sinking is found to continue through October (Fig. 3.2). The 20° C isotherm sinks further to a depth of about 180 m. During this period, mixed layer also deepens to about 45 m while SST continues to increase as a result of the combined effect of sinking and the surface heat input. Using bimonthly data, Colborn (1975) has noticed that thermocline reaches the deepest position in September - October.

In November and December, an upward tilt of isotherms is seen below 120 m. The 20° C isotherm is at about 145 m and 125 m during November and December respectively. Similar observations have been made in this

area by Quadfasel (1982). This upward tilt can be due to the equatorial easterly jet discussed earlier, during transition between the two monsoons (Wyrski, 1973) which is fed from east African coastal waters. It may also be noted that during this time, the eddies generated in Somali current also cease to exist.

The difference in thermal structure between subsurface and surface layers in December is another notable feature. While an upward tilt is seen below 120 m, surface cooling as well as a deepening of mixed layer can be noticed above this depth. As can be seen from net heat input (Fig. 3.1), winter cooling is responsible for the convective mixing and the formation of deeper mixed layer. Also, the favourable winds of northeast monsoon generate sinking of surface waters.

3.3. HEAT CONTENT AND HEAT STORAGE

As a result of the complex nature of the variation in thermal structure as discussed above, large changes take place in the heat content of the water column as well as in the monthly heat storage during the course of the year. There are different factors that contribute to such variations. The net heat flux at sea surface, convective and wind mixing, advection of heat by ocean currents, upwelling and sinking and vertical movements associated with ocean currents are the processes that influence the thermal characteristics.

Heat content in different 50 m layers is presented in Fig. 3.5. Annual variations of heat content occur even upto 200 m, although with lesser variations in the 150-200 m layer. At all the layers the maximum heat content is, generally, found during April. This is followed by a decrease during the southwest monsoon season and an increase during

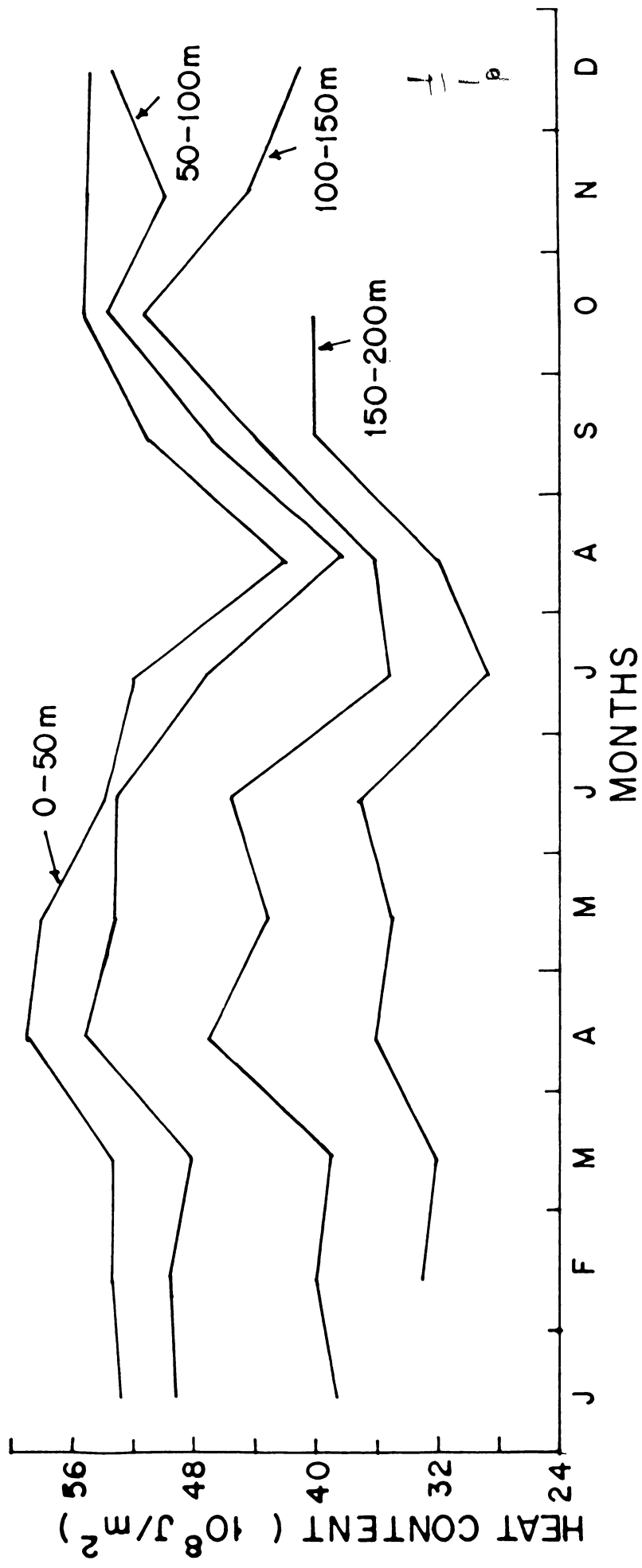


Fig.3.5 Average monthly variation of heat content in different layers, in Area I. Due to lack of data, heat content in 150-200 m Layer is not estimated for some months.

post-monsoon. Above 100 m (0-50 m and 50-100 m layers), the minimum occurs during August. However, in deeper layers, the minimum occurs one month earlier. In the upper 50 m, heat content varies between 42×10^8 and 59×10^8 J/m². In the next 50 m, the variation is between 38×10^8 and 55×10^8 J/m². Between 100 and 150 m, the heat content ranges from about 35×10^8 to 51×10^8 J/m². Although data for some months are not available for the 150-200 m layer, it is seen that the variation in heat content decreases in this layer, the minimum and maximum being 29×10^8 and 40×10^8 J/m² respectively. Considerable warming by mid-October followed by cooling till the end of the year in 100-150 m layer is a conspicuous feature.

After attaining maximum in April, the heat content in upper 50 m decreases while the layers below do not show much variation till June. This appears to be due to downward flux of heat stored in upper layers. Using data averaged for the entire Somali Basin, Bruce (1987) observes pronounced downward flux of heat. He has noticed that with the progress of southwest monsoon, intense warming occurs below 100 m which is almost equal to the heat loss in upper 100 m. In the present study heat loss is noticed upto 200 m till July. After July, while upper 100 m continues to cool by about 20×10^8 J/m² in a month, the warming between 100 and 200 m during this month is about 5×10^8 J/m². Thus, some downward flux takes place in Area I.

In the upper 200 m, the maximum values of total heat content of about 200×10^8 J/m² are found during pre-monsoon (April) and post-monsoon (October). The minimum of about 150×10^8 J/m² is observed towards the latter part of southwest monsoon (August). The annual range of about 50×10^8 J/m² is more than the range observed in Pacific Ocean by Bathen (1971).

Heat storage in different layers is shown in Fig. 3.6. Due to paucity of data, it was not possible to compute the annual cycle for depths below 150 m. Heat storages in different layers show bimodal variation. Similar semi-annual signal has not been noticed in the heat stored in the different zonal belts of Atlantic Ocean by Lamb and Bunker (1982). While large annual variations are noticed in extra-tropical north Atlantic zones, in the tropical Atlantic, storage cycles are irregular with smaller amplitudes.

In the upper 50 m (Fig. 3.6), cooling of about 25 W/m^2 occurs in January while warming of about 80 W/m^2 occurs in March. In April, warming decreases and by early May, this layer starts cooling. Maximum cooling occurs during June - July (150 W/m^2). This is followed by a sudden warming and by September maximum heating of 140 W/m^2 is seen. Warming reduces subsequently and this upper 50 m layer cools in December by about 25 W/m^2 .

Although the heat storage cycle in 50-100 m layer follows, in general, the pattern of the layer above, the annual range is found to be slightly higher. This layer exhibits slightly more cooling in January and lesser warming in February compared to the layer above. Comparatively larger warming during April and lesser cooling during May are noticed. Maximum cooling of about 170 W/m^2 observed in July is also more than that in the upper 50 m layer. Maximum warming ($\sim 155 \text{ W/m}^2$) is observed during September. Mild cooling similar to the upper layer is seen in this layer during December.

In the 100-150 m layer, the heat storage varies between -135 and 190 W/m^2 . This layer undergoes cooling in January. More warming compared to upper layers is seen during the pre-monsoon season. A

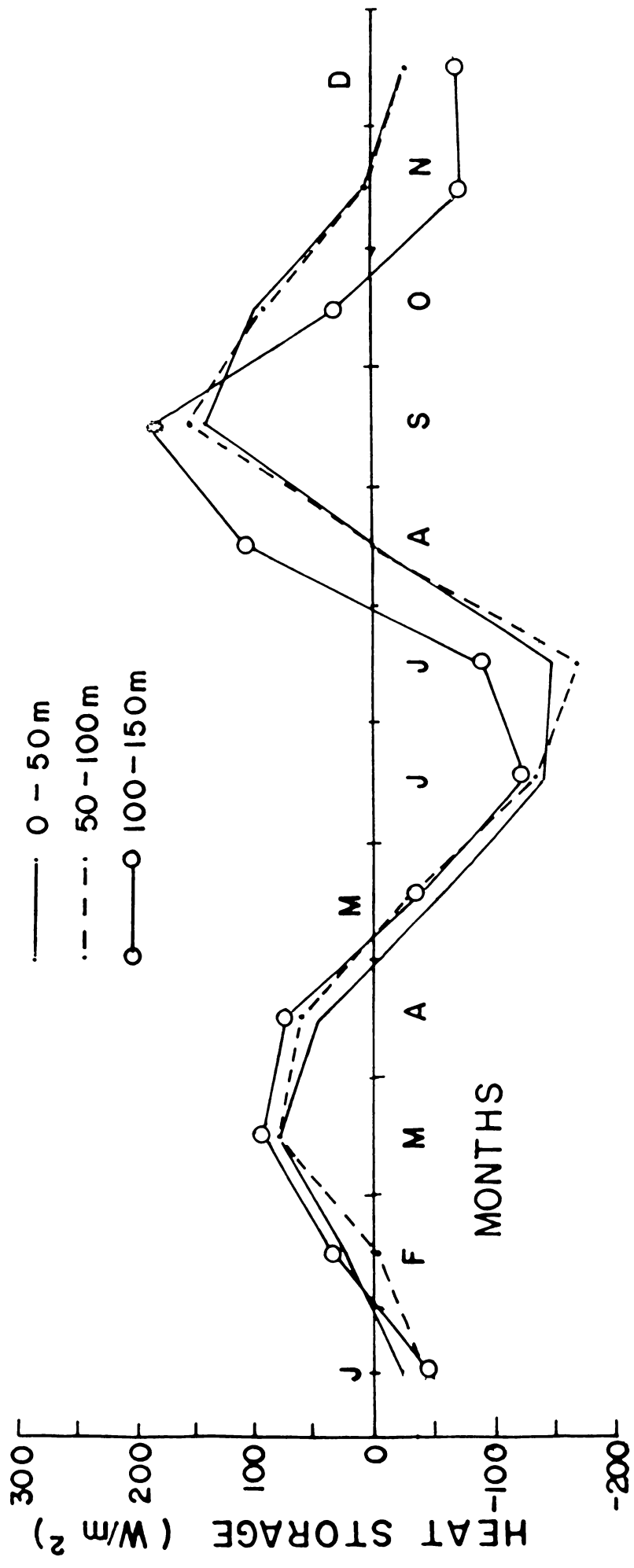


Fig.3.6 Average monthly variation of heat storage in different layers, in Area I.

conspicuous difference observed in this layer is that the maximum cooling during southwest monsoon season is advanced by one month. Consequently, the change over to warming, after the effect of southwest monsoon, is also advanced. However, maximum warming occurs in September coinciding with upper layers. Another interesting feature is the larger cooling ($\sim 125 \text{ W/m}^2$) observed during November-December.

Present observations on heat storage in Area I are different from those by Rao (1988), in central Arabian Sea, who has found that the magnitude and amplitude of variations in the top most 50 m is not similar to that in deeper layers and also that the semi-annual variations are clearly seen only in the upper 50 m.

The annual cycle of total heat storage in upper 150 m is included in Fig. 3.8. Cooling of about 110 W/m^2 is observed in January. Warming increases to about 250 W/m^2 in March. Maximum cooling exceeding 400 W/m^2 is encountered in June and July. While in June the entire water column contributes to this cooling, in July the contribution from 100-150 m is considerably reduced (see Fig. 3.6). Maximum warming observed in September ($\sim 500 \text{ W/m}^2$) has a slightly higher contribution from 100-150 m layer. A notable feature is that the cooling of the order of 125 W/m^2 in November is almost entirely provided by 100-150 m layer while some contributions from the upper layers are also encountered in December.

3.4. HEAT EXCHANGE AT SEA SURFACE

Monthly variation of different components of heat exchange at sea surface is presented in Fig. 3.7, the data for which have been obtained from Hastenrath and Lamb (1979b). Net radiation varies between 120 and 170 W/m^2 . The minimum radiation is encountered during winter which increases to reach a maximum in April. Radiation reduces slightly during

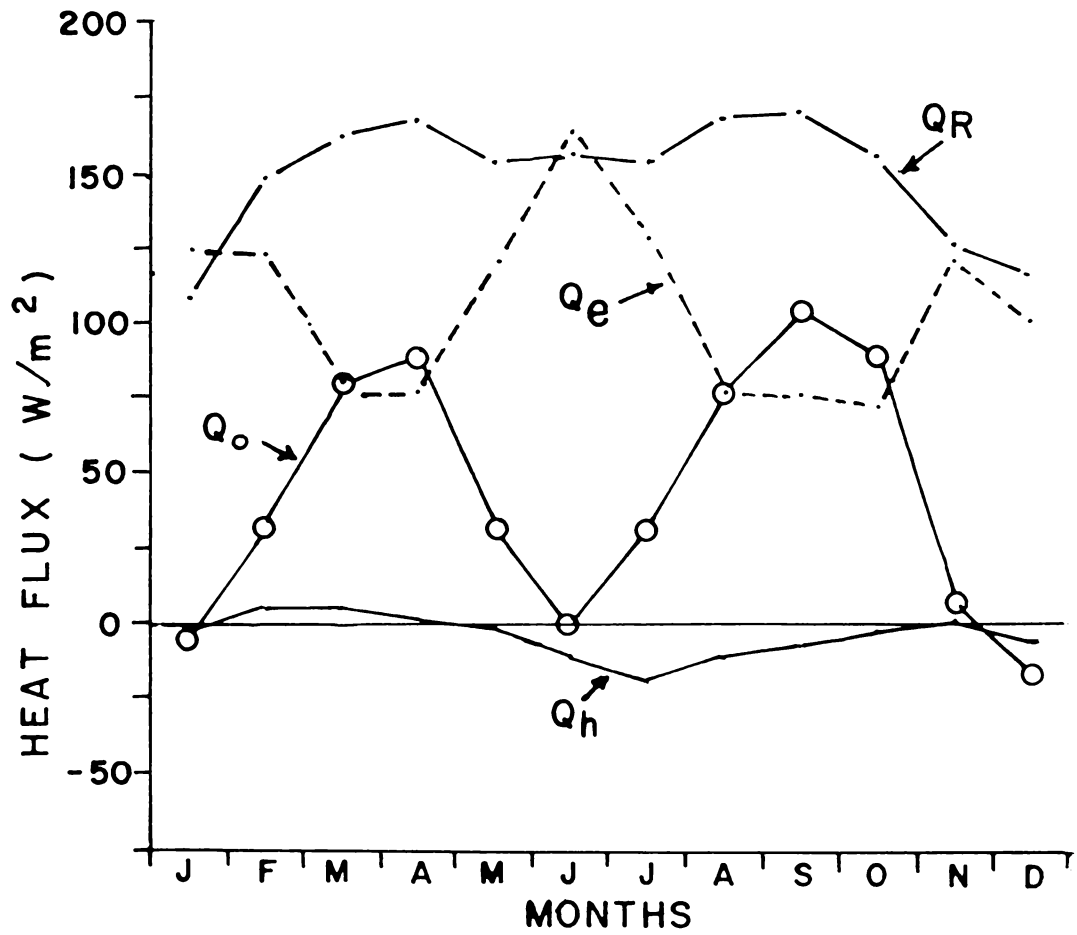


Fig.3.7 Average monthly variation of surface heat budget components in Area I. Positive values of Q_o and Q_R indicate downward transfer and those of Q_e and Q_h indicate upward transfer.

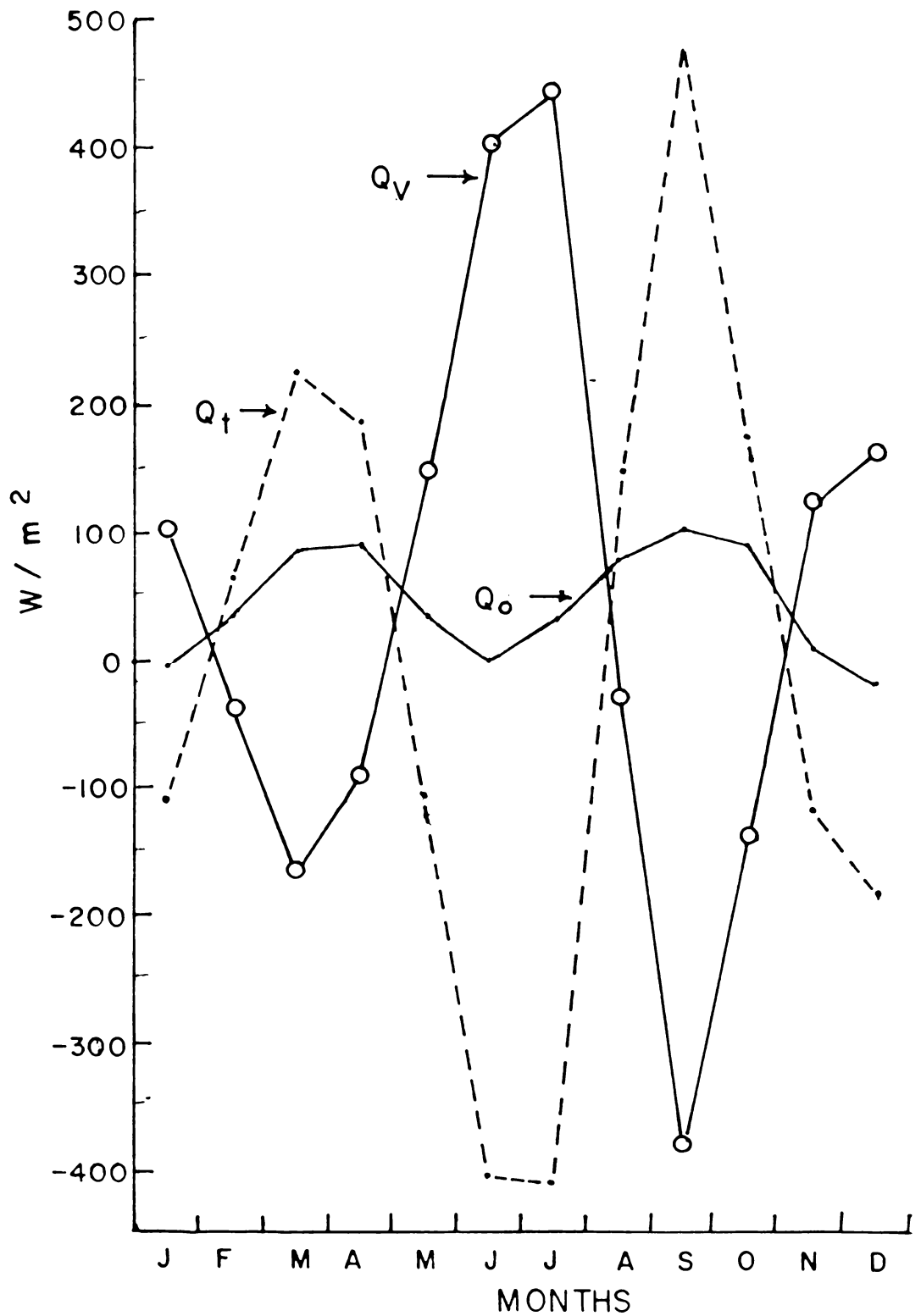


Fig.3.8 Average monthly variation of net surface heat exchange (Q_o), heat storage in upper ocean (Q_t) and heat advection (Q_v), in Area I. Heat advection out of the area (export) is positive.

the early southwest monsoon season and increases after July. A conspicuous feature is the absence of drastic decrease during the southwest monsoon season. This unexpected picture may, probably, be due to the absence of intense cloudiness in this region, as a feed back from the oceans as shown by Hastenrath and Lamb (1980). Intense upwelling and associated fall in SST stabilize the atmosphere and hence inhibit convection. This causes a fall in cloud cover and results in high values of net radiation.

Evaporation shows very clear double maxima (Fig. 3.7). During January-February, latent heat of evaporation is about 125 W/m^2 and decreases during the pre-monsoon season to about 75 W/m^2 . This decrease is mainly caused by a fall in wind speed associated with the retreat of northeast monsoon. In the early stages of southwest monsoon, sharp increase in evaporative heat loss is seen which is caused by the increase in wind speed. However, after June, in spite of the monsoon activity, evaporation decreases. This is again an effect of intense upwelling. Decrease in SST causes fall in vapour pressure gradient and reduces evaporation. Evaporation continues to be low during post-monsoon when, the decrease in wind speed contributes to the low values. Sensible heat exchange is very low except during southwest monsoon season when sea gains heat by about 15 W/m^2 . The increase in wind speed and fall in SST due to upwelling produce this gain of sensible heat.

Net heat exchange shows double maxima (Fig. 3.7). The loss of heat from sea surface during winter is followed by gain during pre-monsoon with a maximum gain of about 90 W/m^2 in May. With the onset of southwest monsoon, the heat gain decreases and becomes nil during June as a result of increased heat loss by evaporation. After June, heat gain

again increases to reach another maximum of about 105 W/m^2 in September in consonance with fall in evaporation and increase in radiation flux. Subsequently, the net gain decreases. At this area, sea surface gains heat annually at a rate of about 45 W/m^2 and this heat must be exported away from this region by different processes.

3.5. OCEANIC HEAT ADVECTION

Heat divergence through the upper layer (advective term in oceanic heat budget) obtained as a residual of surface heat input and oceanic heat storage, is also included in Fig. 3.8. Maximum export of 445 W/m^2 in July and import of 375 W/m^2 in September are observed. These are associated with intense upwelling and sinking respectively during different stages of southwest monsoon. It may be noted that these values are about four times the maximum heat input from atmosphere. These export and import are considerably higher than the average for northern hemisphere oceans in upper 250 m, reported by Oort and Vonder Harr (1976).

Heat export of about 100 W/m^2 noticed in January is due to cooling of water, which increases slightly with depth (see Fig. 3.6). During February through April, in spite of increase in surface heat input, import of heat is seen. While in February, this heat is generally not used to warm middle layer (50-100 m) during March and April, the entire 150 m column is warmed (see Fig. 3.6). During southwest monsoon season, large heat export from this area is also noticed. This is caused by negative heat storage resulting from intense upwelling. While this export cools the entire column equally in June, cooling in July is largely in the upper 100 m.

In August, mild import is encountered which is largely utilized to warm the 100-150 m layer. Although surface heat input increases in September, this is overbalanced by excessive warming resulting in large heat import. A drastic fall in heat import is noticed during October due to fall in heat storage. In November and December, heat export from this region is noticed. In November, this cools mainly 100-150 m. Cooling, albeit mild, is noticed in upper layers also during December (see Fig.3.6).

The distribution of heat during different heating and cooling seasons is considered. During pre-monsoonal warming period (February-May), surface heat input of about $24 \times 10^8 \text{ J/m}^2$ is almost completely used for warming by about $22 \times 10^8 \text{ J/m}^2$ in 0-100 m. Transfer of heat to deeper layers is very limited. Between 100 and 150 m, heat gain of approximately $17 \times 10^8 \text{ J/m}^2$ is noticed which is largely due to lateral advection possibly from equatorial regions. Large import of heat to Somali Basin, through layers below 100 m, has been noticed by Bruce (1987).

During southwest monsoon season (June-September), vertical excursions of the thermocline, due to upwelling and sinking, causes large changes in heat storage. Heat loss of about $31 \times 10^8 \text{ J/m}^2$ between surface and 100 m and gain of nearly $7 \times 10^8 \text{ J/m}^2$ in 100-150 m layer are noticed. Thus only a portion of heat loss is transferred vertically. If the surface input during this period of about $23 \times 10^8 \text{ J/m}^2$ is also included, heat export by horizontal advection becomes approximately $47 \times 10^8 \text{ J/m}^2$. Since for the entire Somali Basin, considerable vertical transfer of heat takes place to deeper layers (Bruce, 1987), the laterally advected heat from present Area I is finally transferred to the interior of ocean outside the area. It may, however, be noted that in the present analysis storage estimates are limited to upper 150 m.

During October-December, surface heat gain is about $7 \times 10^8 \text{ J/m}^2$ which is almost wholly used to warm 0-50 m layer. While mild warming of about $6 \times 10^8 \text{ J/m}^2$ occurs in 50-100 m layer, cooling of nearly $17 \times 10^8 \text{ J/m}^2$ is seen between 100-150 m. This agrees with the large heat export below 100 m from Somali Basin during November-December (Bruce, 1987).

Monthly variation of depth of 20°C isotherm is presented in Fig. 3.9. The depth of 20°C isotherm in the equatorial western Indian Ocean adapted from Quadfasel (1982) is also included. In Area I, semi-annual cycle superimposed with minor fluctuations is observed. During January to March, the depth is about 115 m. In the following month, isotherm deepens considerably to reach 150 m and continues to be around the same depth even after the onset of southwest monsoon. Drastic decrease is noticed in the following months and the minimum depth of about 40 m occurs in August. Swallow et al (1983) found that in 1979, 20°C isotherm had reached surface in August. The decrease is due to the vertical movement associated with intense upwelling. In the next month, an equally rapid increase associated with sinking is noticed. Maximum depth of 180 m is noticed in October. Towards the end of the year, slight decrease in depth of 20°C isotherm occurs. Variation in this area of study is quite different from further south where maximum depths are observed in February-March and August-September (Fig. 3.9).

The response of this area (Area I) to the southwest monsoon has been discussed in earlier sections. Quadfasel (1982) has presented amplitudes and phases of 12 monthly and 6 monthly cycles of 20°C isotherm depths in western Indian Ocean using long-term data. He has used $1^\circ \times 1^\circ$ squares in his analysis. Maximum amplitude of annual cycle is

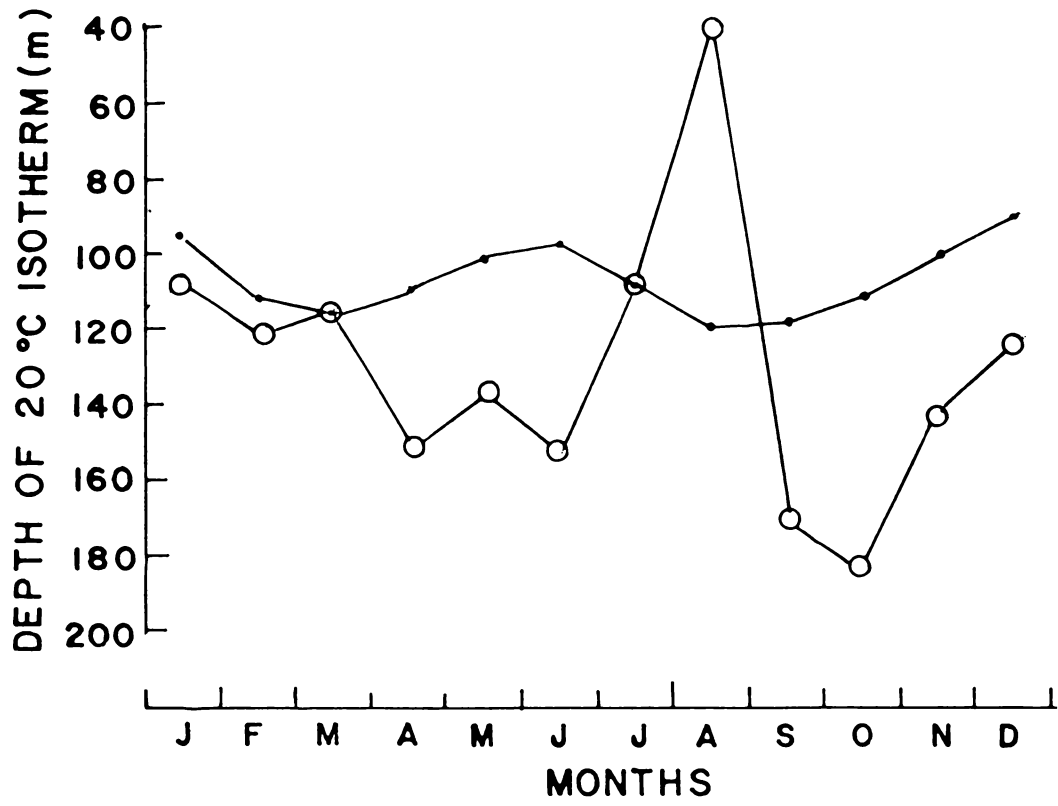


Fig.3.9 Average monthly variation of the depth of 20°C isotherm, in Area I (○-○) compared with that in the area 5°N-5°S and the coast to 65°E (—) by Quadfasel (1982).

located very close to present area. However, different regions of the present area of study show different phases. While close to the shore, maximum depth is during January-February, further offshore, this is shifted to July-August. Similarly, in the case of half yearly cycle, in most of western Indian Ocean, maximum amplitudes occur during periods January-February and July-August. However, in a small part of study Area I, maximum amplitudes do not occur during these periods. It may be the combined effect of the different phases of annual and semi-annual cycles in different portions of study Area I, that has contributed to the observed variation in the area under study. The annual cycle of 20°C isotherm depths presented by Moinari et al (1986) also gives variations somewhat similar to that in present study, although the range of variation is less.

3.6. SIMULTATION OF SEA SURFACE TEMPERATURE

The evolution of SST was simulated using different schemes explained in Chapter 1. SST simulated from schemes 1 and 2 are presented in Fig. 3.10a and those from schemes 3 and 4 are given in Fig. 3.10b. Observed SST is also included in these figures. The r.m.s. differences between the observed and estimated series and correlation coefficients are given in Table 3.2.

Uncertainties in simulated SST due to uncertainties in different parameters of the processes considered (see Chapter 1) are indicated in Table 3.3. The averages obtained for Area I which are utilized to estimate the uncertainties are 45 W/m^2 , 56m , $45.65 \times 10^{-7} \text{ m/s}$ and $1.33 \times 10^{-5} \text{ m/s}$ for surface heat flux, MLD, entrainment velocity and vertical velocity respectively.

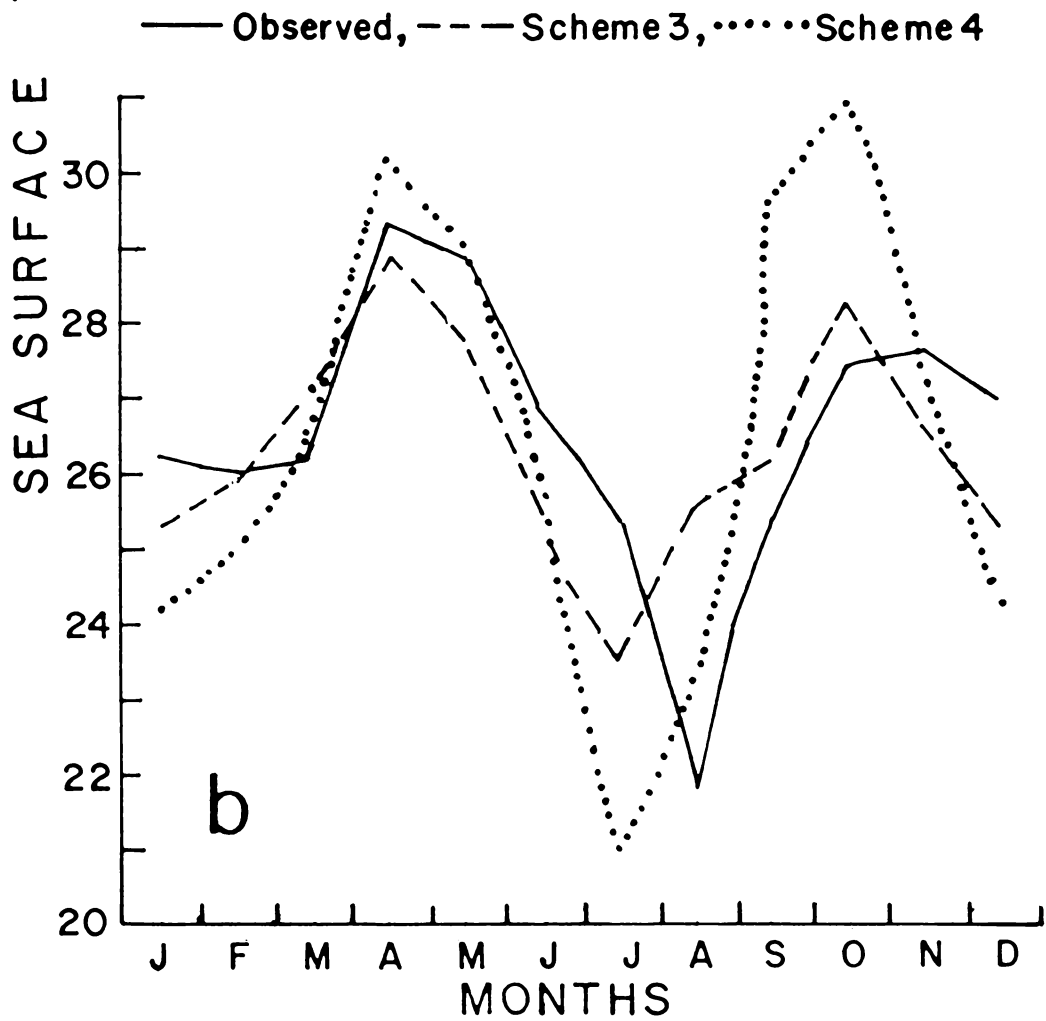
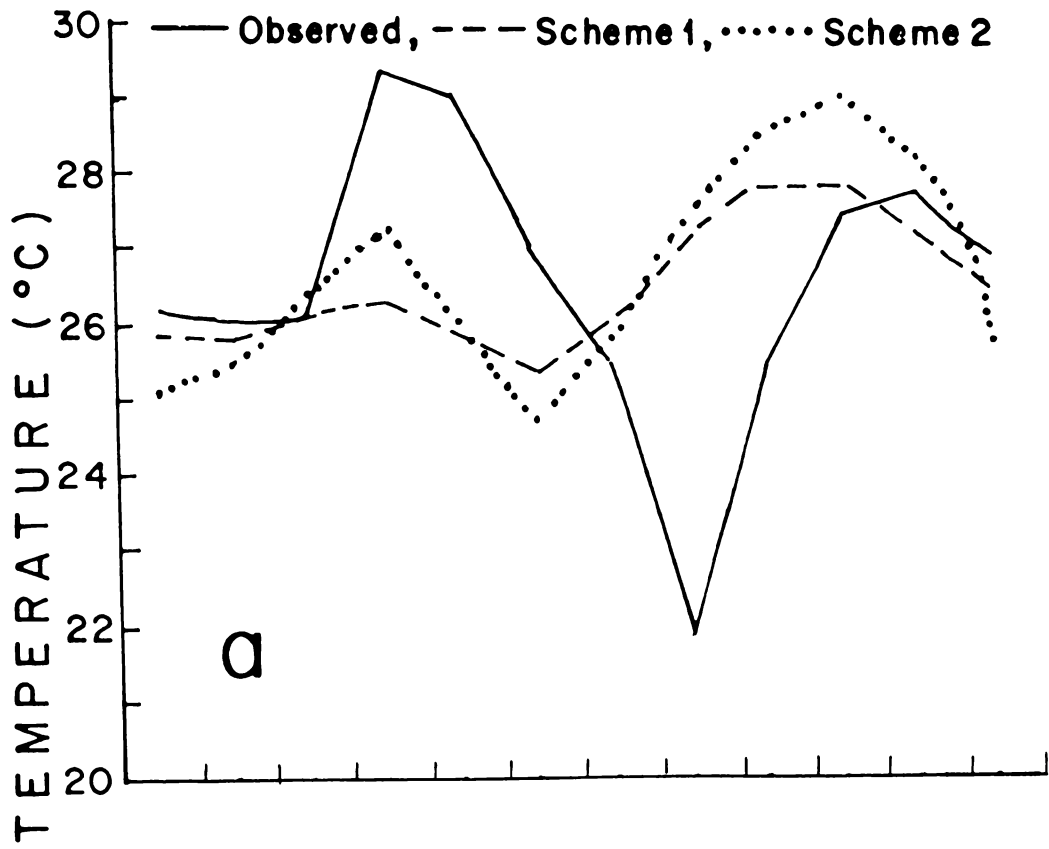


Fig.3.10 SST simulated by different schemes. Observed SST is also included.

Table 3.2. r.m.s. difference and correlation coefficient
between observed and estimated monthly SST

Scheme No.	Processes considered	r.m.s. difference (° C)	Correlation coefficient
1.	Surface heat flux	2.18	-0.24
2.	Surface heat flux and Entrainment	2.37	-0.10
3.	Surface heat flux, Entrainment and Horizontal advection	1.43	+0.63
4.	Surface heat flux, Entrainment, Horizontal and Vertical advection	2.43	+0.58

Table 3.3 Error in estimated SST due to uncertainties in different processes, in Area I

Process	Surface heat flux	Entrainment	Horizontal advection	Vertical advection
Error (°C)	0.36	0.43	0.62 (After Molinari et al, 1986)	0.81

Surface heat flux (Scheme 1) does not produce the observed variation of SST. Warming during pre-monsoon and the subsequent cooling obtained in scheme 1 are very much less than observed variations. During southwest monsoon, the simulated SST increases after June while the observed SST continues to decrease. The r.m.s difference between the observed and the estimated series is 2.2°C and the correlation coefficient between these two is very low and negative (-0.24). The coefficient of variation (r^2) is 0.06 which shows that variance of observed series is not accounted by the surface flux. This agrees with the finding by Molinari et al (1986) that in this area no correlation between the surface heat flux and SST existed in the monthly variations of 1979.

Not much improvement is noticed by including entrainment (Fig. 3.10(a), Table 3.2). As in earlier case, simulated warming during pre-monsoon is less than observed. Also, comparatively more heating is simulated during the observed monsoonal cooling. During 1979 also discrepancies have been noticed by Molinari et al (1986) between observed SST and that estimated with surface heatflux and entrainment. Mc Phaden (1982) has also noticed that on a monthly scale, entrainment is not important.

Slight improvement is noticed in March-April because of detrainment which accumulates heat in the shallow surface layer. Discrepancy in scheme 2 during southwest monsoon is understandable. In the model, the shoaling of ML during southwest monsoon is accounted as detrainment which can generate warming. The process which shoals the ML during this period, on the other hand, is upwelling which does not warm the waters.

On including horizontal advection (scheme 3), there is a reduction in r.m.s. difference by about 1.0°C . This appears to be good in view of the uncertainty of 0.62°C in SST, contributed by horizontal advection (averaged for western Indian Ocean; Molinari et al, 1986). Correlation coefficient increases to 0.63 which means that about 40% of the variance in observed cycle is accounted.

Molinari et al (1986) have observed that on including horizontal advection, the monsoonal cooling in this area is reproduced. In the present study, although the estimated SST shows persistence of low temperatures during monsoon, the amplitude of monsoonal cooling is less than that observed. The plausible reason for the difference between the present and earlier studies can be the difference in the types of data utilized. Molinari et al (1986) uses all model parameters of 1979 alone except the horizontal advection which has been derived from climatological data, while in present study only the climatological data are considered.

A remedy for the difference between estimated and observed cooling during southwest monsoon may be to include vertical heat advection (scheme 4). Vertical velocities derived from the movement of isotherm indicate maximum upward speed of 2.62×10^{-5} m/s and downward speed of

4.63×10^{-5} m/s. It is seen that scheme 4 reproduces the amplitude of cooling during southwest monsoon. As seen earlier in section 3.2, intense upwelling during this period lifts subsurface water which reaches sea surface. However, in spite of this improvement, the model degrades the prediction on the annual scale. The r.m.s. difference increases and the correlation coefficient decreases. The largest discrepancies are noticed during the warming after southwest monsoon season. It is seen that unless subsurface water is lifted upto the surface, the vertical movements at subsurface do not influence SST. Emery (1976) has noted that the temperature variations at the surface and deeper levels may not be caused by the same processes. Mc Phaden (1982) has also indicated that vertical oscillations may have little influence on SST variation. Merle (1980) has suggested that seasonal oscillations in the thermocline are not related to the surface processes and are in response to the ocean currents as a geostrophic balance.

Results of different schemes presented here show that not any one process can be identified as important throughout the year in the evolution of SST. Different processes assume importance during the course of the year. Surface heat flux is found to be important during winter. Horizontal advection seems to be important throughout the year. On the other hand, effect of vertical advection is predominant during southwest monsoon season.

CHAPTER 4

UPPER OCEAN THERMAL STRUCTURE IN AREA II (CENTRAL EASTERN ARABIAN SEA)

Area II, located off the central part of the west coast of India, is influenced by the reversing monsoons. As a result, the ocean currents also undergo reversal in direction during the course of the year in this area. During the southwest monsoon season, coastal current in this area is southerly as part of a general clockwise coastal circulation in the Arabian Sea. The current becomes northerly during the northeast monsoon season as part of an anticlockwise coastal circulation. Unlike the Somali current region (Area I), information on current measurements in the eastern Arabian Sea are meagre. Knowledge of dynamics of Somali Basin has achieved considerable advance since the International Indian Ocean Expedition, as could be seen in the preceding chapter. In contrast, the rest of the Arabian Sea remains less explored (Shetye, 1986).

In a study on currents off Bombay during February, Varma and Gopinathan (1977) have indicated the possibility of eddies in the basic coastal circulation. Varkey et al (1978) examined the currents off Bombay during March. Varkey (1980) finds that spectral energy of currents, off Bombay is predominantly in the frequency of tides.

Information on the annual variation of currents off west coast of India, available in atlases, are derived from ship drift data (Anon, 1952; Gorshkov, 1978). Surface currents off the west coast of India start flowing to south by February and continue to be southerly till October. The currents reverse to a northerly direction during the remaining part of the year. On an average, the speeds of the southward currents are less than 40 cm/s (Anon, 1952) which is considerably less than the swift

north flowing Somali current during the southwest monsoon season. The northerly currents, which set in as part of the counter clockwise coastal circulation in response to the northeast monsoon are very weak.

4.1 SEA SURFACE TEMPERATURE

Monthly variation of SST is shown in Fig.4.1. Net heat gain is also included in the figure. In this region, SST varies between 27.0° and 30.5° C. The range of variation is considerably less than that observed in Area I where the dynamic situation is much different. From February onwards SST increases, mainly due to increased surface heat gain and attains a maximum of 30.5° C in May. In the following months, SST decreases by about 3° C due to effect of the summer monsoon, when sea loses heat at sea surface. However, low values of SST continues even towards the fag end of monsoon when the sea surface gains heat from atmosphere. This might be related to the upwelling in the upper layers which is discussed in the following sections. Slight increase in SST during post-southwest monsoon is a result of atmospheric heat input.

4.2 SUBSURFACE THERMAL STRUCTURE

Subsurface thermal structure in Area II, presented in Fig. 4.2 is less complex than that observed off Somalia (Area I). Annual periodicity appears to be a predominant feature of the oscillations of isotherms in Area II. Deep mixed layer of about 80 m depth and sharp thermocline are seen during January - February. During the pre-monsoon period, layers close to surface get warmed by about 1.5° C possibly due to surface heating. During this period, shallow thermocline is formed. Maximum temperature at all levels is attained in May. A reduction in the gradient at the top of main thermocline noticed during this period may have facilitated increased downward heat flux and warmed the subsurface

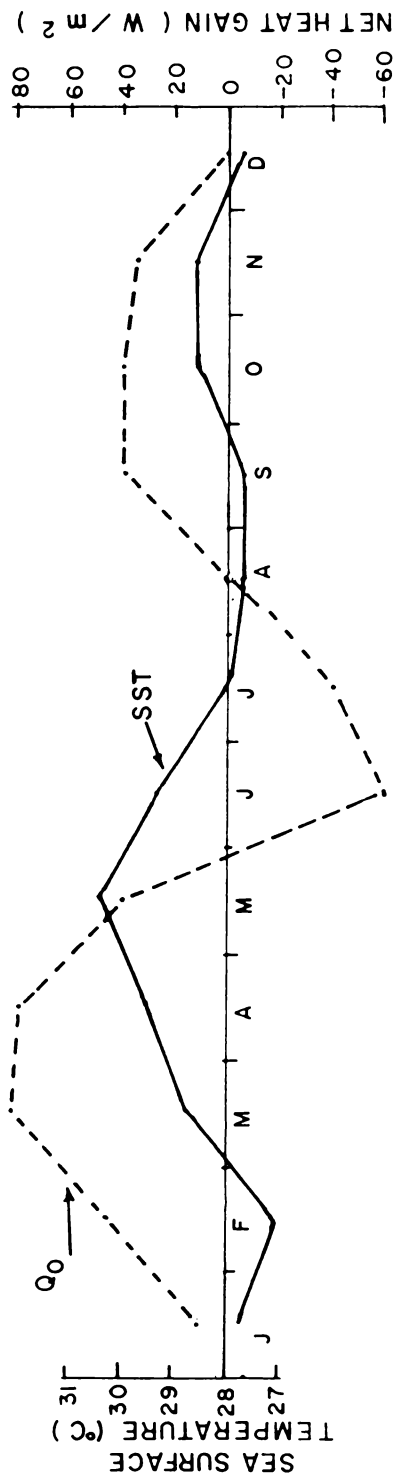


Fig.4.1 Average monthly variation of sea surface temperature and net surface heat exchange, in Area II.

layers. The subsurface processes also may be contributing to these. Coinciding with this, a mild deepening of ML is seen. Deepening of ML, immediately before the southwest monsoon season, has been reported earlier by Banse (1968).

While studying the hydrography along the west coast of India during pre-monsoon period of 1962, several vertical sections between Cape Camorin and Veraval have been presented by Patil et al (1964) and Ramamrithm and Patil (1965). Between Malvan and Bombay, 28°C and 23°C isotherms are situated roughly at depths 50-60 m and 100-110 m respectively. Further south, from Karwar to Goa, 28°C isotherm has been found to be very shallow over continental slope and sinks to about 50 m over the shelf region. The 23°C isotherm has been observed below 100 m. In the present study, in Area II which is situated south of Bombay, on an average, water temperatures of 28°C and 23°C are observed at about 45 m and 115 m respectively.

During April, mild upward tilt of isotherms is noticed below about 50 m (Fig. 4.2). Ramamrithm and Patil (1965) have suggested sinking to be taking place in April in this area. However, an examination of vertical section off Karwar (Fig. 16, Ramamrithm and Patil, 1965) indicates downward trend of isotherms only near the surface while at depths of 150-200 m, upward trend is seen. The same trend at these depths could be seen off Goa also although with lesser intensity. The present observations are in agreement with these findings. It may be noted that Rao et al (1974) have observed upwelling at subsurface layers in the continental shelf region off central west coast of India, during April.

After a mild downward trend for a period of about a month, by the end of May, an upward tilt of isotherms is observed below 50 m which

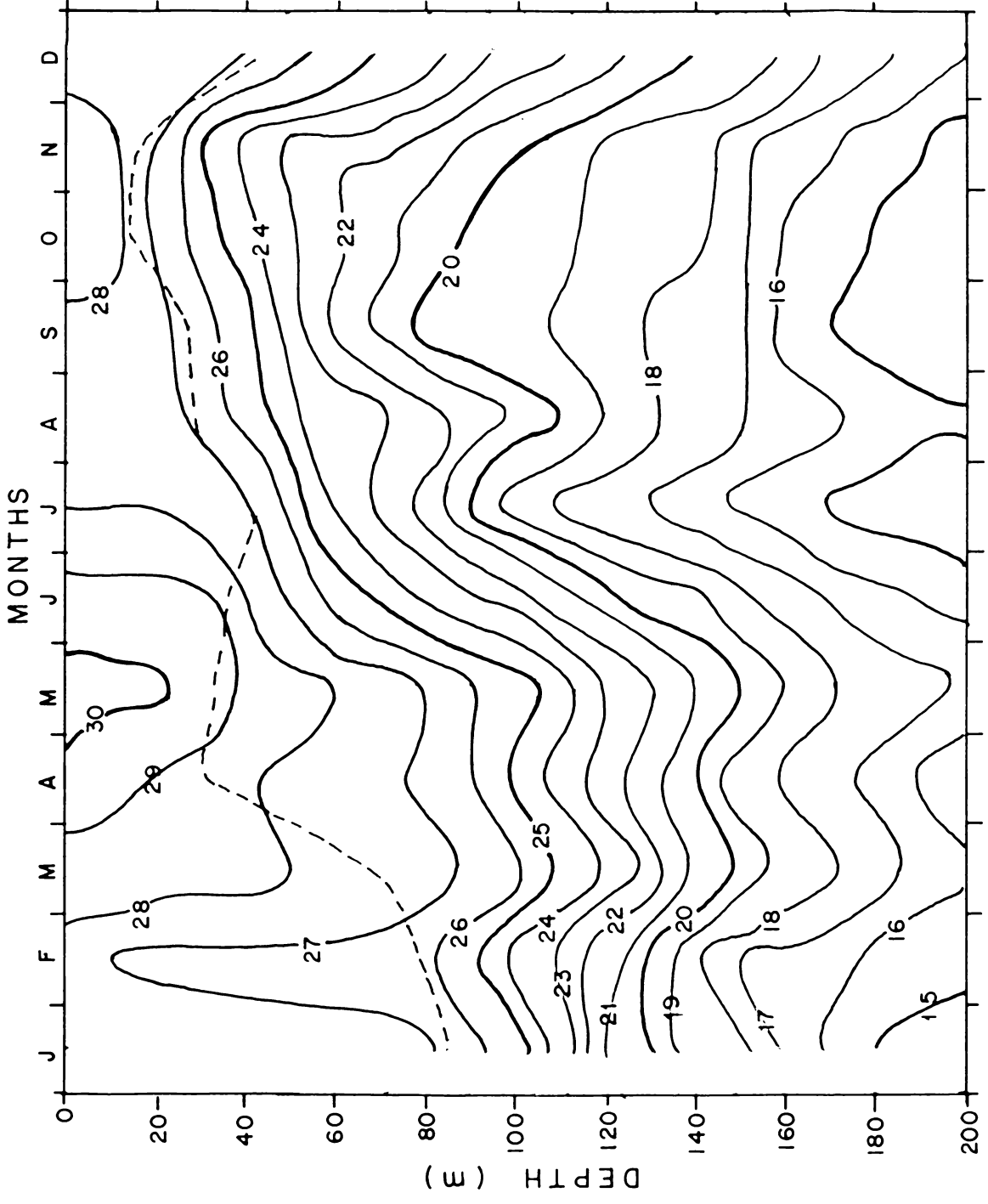


Fig.4.2 Average vertical-time section of temperature, in Area II. Units are $^{\circ}\text{C}$. MLD is shown by dashed line.

is indicative of upwelling. Upwelling off the west coast of India during southwest monsoon season has been reported by several authors (Jayaraman and Gogate, 1957; Carruthers et al, 1959; Ramasastry and Myrland, 1959; Banse, 1959, 1960, 1968, 1972; Ramamrithm and Jayaraman, 1960; Darbyshire, 1967; Sharma, 1966, 1968, 1978).

The present studies indicate that upwelling is not uniform throughout the depth studied (upper 200 m). Just before the beginning of the southwest monsoon season, the upward tilt of isotherms is very intense in the lower part (below about 100 m), while the intensity is considerably less above 60 m. Further, the duration of upwelling also shows a variation with depth. Below about 100 m, upwelling ceases early and the isotherms reach the minimum depths by the middle of July. In the upper layers, isotherms continue to rise even after July. These show that upwelling during the southwest monsoon season cannot be attributed to surface Ekman divergence alone. The coastal currents also appear to play a role in this phenomenon. This aspect is dealt with elsewhere in this section. The depthwise variation in upwelling gives an indication of the variation in dynamics, although it is much less intense and less complex than in Area I. In the deeper parts, in general, sinking is noticed after July which continues till the end of the year, though with lesser intensity.

In the upper parts, isotherms do not show an upward tilt during the beginning of the southwest monsoon season. The base of mixed layer retains nearly the same depth of about 40 m from April to July. From July onwards, the ML shoals and reaches the minimum depth of less than 20 m during October-November. In the upper layers, the minimum depths of isotherms are, in general, found during this period. This is followed

by a deepening of isotherms indicating sinking during December. The climatological data presented in this study for Area II agree, in general, with the observation on annual variation of thermal structure during certain years at a station located in present area (Anon, 1980). Vertical time section off Ratnagiri, for the years 1973, 1974 and 1975 are reproduced in Fig. 4.3. During all years upwelling commences at deeper regions before southwest monsoon season. A depthwise variation in upwelling is also noticed. Upwelling is found to continue even beyond the cessation of the southwest monsoon. The minimum depth of isotherms is, in general, found to occur in upper layers during October–November.

As in the case of Area I, off Somalia, in Area II also upwelling is associated with southwest monsoon. During this period, wind direction in this area is mainly southwesterly which is not favourable for classical wind-induced Ekman transport and consequent upwelling. As seen earlier, upwelling in Area I is a consequence of eddies of Somali current system which carries the water offshore, at the 'turning offshore' regions of eddies. Although, in the eastern part of Arabian Sea, presence of eddies has been observed during southwest monsoon season using geostrophic methods (Sastry and D'Zouza, 1971) and has been suggested during fair weather season (Varma and Gopinathan, 1977), these eddies are much weaker than those found off Somalia (Area I) during southwest monsoon season. Hence, the importance of eddies and their changing positions on upwelling/sinking as observed in Area I are not found off the eastern parts of Arabian Sea. However, the effect of mean coastal circulation should be important.

In subsurface layers, the current may be turning southerly as part of clockwise coastal circulation by May, before the onset of southwest

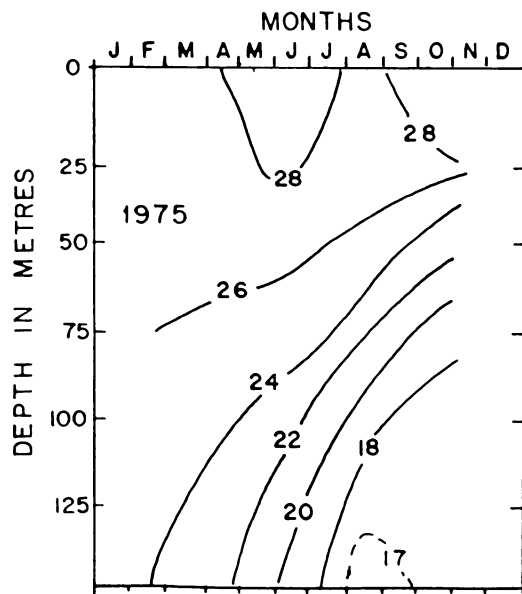
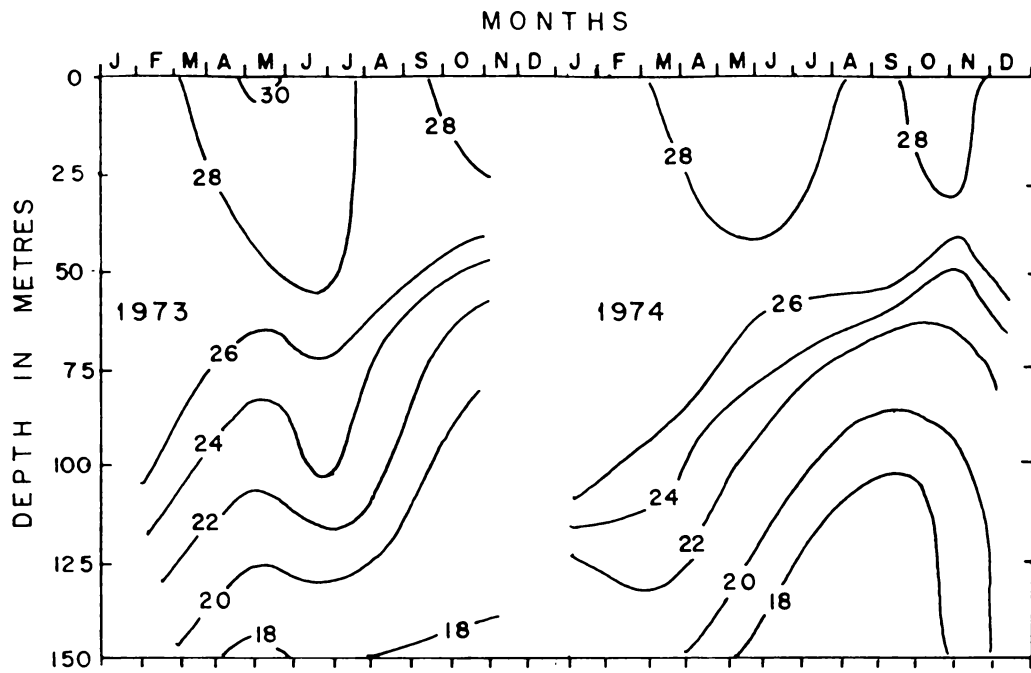


Fig.4.3 Vertical time section of temperature off Ratnagiri during 1973, 1974 and 1975 (Fron Anon, 1980).

monsoon. The geostrophic balance requires heavier water to the left of the flow, favouring upwelling (Varadachari, 1961). Banse (1972) found the depths of isotherms in June 1967 to be less than those found during pre-monsoon in some earlier years and concluded that upwelling occurs off Goa, before June. Probably, same is true off Bombay also. However, as explained earlier, in the upper regions, upwelling is not noticed during the early stages of southwest monsoon. This observation is not surprising, if the wind direction in this area is also considered. Wind stress components off Bombay, presented by Mathew (1982) are reproduced in Fig. 4.4. During the early stages of southwest monsoon season, the alongshore component of wind stress is towards north which is not favourable for upwelling. Thus upward movement close to the surface is absent during this period, inspite of the favourable current direction. Hence, cold subsurface water does not rise close to the surface. Towards the end of the southwest monsoon season, the winds become favourable for upwelling with a component towards equator, parallel to the coast. Maximum effect of upwelling occurs during post-monsoon or early northeast monsoon season in the upper layers. Under the combined effect of coastal currents and the wind component, the upwelling in surface layers commences late.

Further south, off Karwar, while the alongshore wind component is directed to equator during February to October, the onshore component is very strong during southwest monsoon season (Mathew, 1982). These also may be contributing to the delay in commencement of upwelling in surface layers and to its continued occurrence beyond southwest monsoon season.

It is interesting to note that while the upward movement continues beyond southwest monsoon season in layers close to surface,

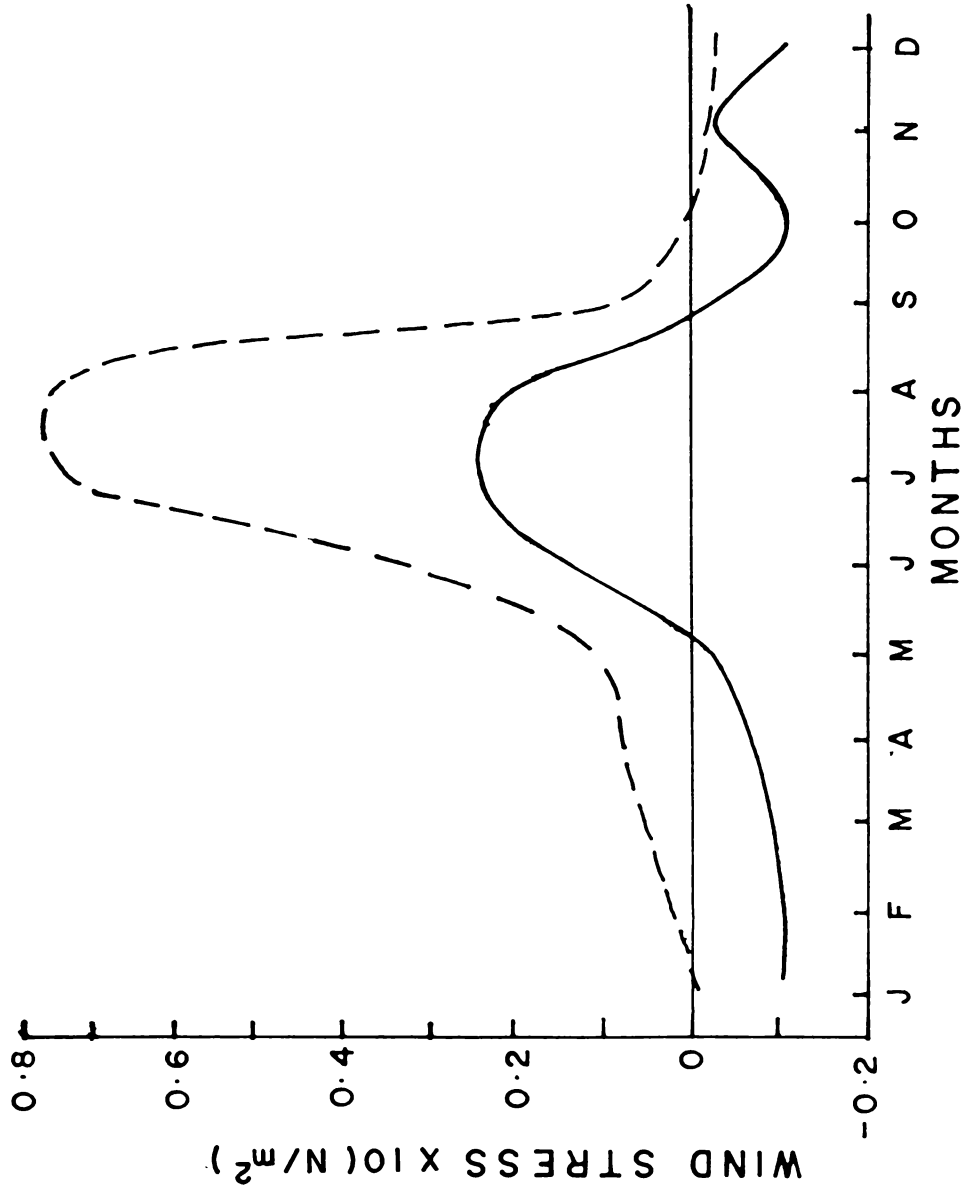


Fig.4.4 Monthly variation of mean wind stress components off Bombay. — parallel to coastline, (+) towards pole and (-) towards equator; ---- perpendicular to coastline, (+) onshore and (-) offshore. (From Mathew, 1982).

at the subsurface layers, the isotherms deepen after July. After slight upward tilt in September, sinking continues towards the end of the year in these subsurface layers. This indicates that in August, at subsurface layers, the current has turned towards north off the central west coast of India. This current direction off the west coast is favourable for sinking in northern hemisphere.

However, the upward movement continues in the upper regions of the thermocline even after southwest monsoon season. After the cessation of southwest monsoon, the water circulation in the surface layers weakens during the transition period between southerly currents of southwest monsoon season and the northerly currents of northeast monsoon season. During this period, wind component is towards south off Bombay (Fig. 4.4) and under the influence of the favourable winds, upwelling near the surface continues till October - November. The minimum depth of ML of about 15 m is observed during these months. By November, although the wind turns to be northeasterly, its speed is very low so that its effect is negligible. Hence, northerly currents of the northeast monsoon season contributes to sinking at all levels.

The longer duration of upwelling extending even to post-monsoon period, off the northern part of west coast of India has been observed in the studies by Pelagic Fisheries Project (Anon 1980). Some earlier observations off the northwest coast of India, although not conducted round the year, also have indicated the occurrence of upwelling even after the cessation of the southwest monsoon. Observation made off Bombay (from light house) by Gogate (1960) suggests that the top of thermocline has been found at about 10 m during middle of September through October in 1959. Edelman (1965) observed off Bombay in September 1962 the 25 °C

isotherm at about 20 m and the 23°C isotherm at about 50 m. Upsloping of isotherms, during post-monsoon or before the onset of northeast monsoon has been reported off northern part of west coast of India (Banse, 1968). He has indicated that during late September, off Bombay the discontinuity layer is at a depth of about 30 m.

On examining the oxygen and nutrient values in these regions, Banse (1968) found poorly oxygenated, low temperature waters which were rich in nutrients, in the continental shelf, during monsoon and post-monsoon months. Lowest oxygen values have been found during May, September and October in 1957, during October in 1958 and during July in 1959. Although year to year variations are observed, the oxygen minimum, in general, occurs over continental shelf, towards the end of southwest monsoon season or even during post-monsoon months. Summing up various data, Banse (1968) indicated the presence of cold rising waters north and possibly south of Bombay at shallow depths, at least until the northeast monsoon season. During this period, this is blanketed by warm surface water. This clearly agrees with the average thermal structure during post-monsoon, observed in the present study. The presence of 23°C isotherm between 35 - 50 m and sharp discontinuity at 30 - 50 m in early December 1960, on the outer shelf off Bombay, observed by Banse (1968) is also in agreement with the present results. He has suggested that continued occurrence of upwelling till November is due to the continued coastal currents in southerly direction. Although, the effect of these surface currents cannot be overlooked, wind also is favourable with an equatorward component during this period. Sinking is noticed at all levels during December.

Although current measurements in this area are highly scanty, Carruthers et al (1959) have found that bottom currents is directed towards equator off Bombay (at 43 m bottom depth), during early November 1958. This is favourable for upwelling. In present study also upwelling is found to extend till November. However, during this period, in still deeper layers sinking is noticed which indicates the presence of northerly currents at these levels. An interesting feature is the pronounced fluctuations of the isotherms between 60 - 110 m. Here, while the initial upwelling ceases by July, indicating a reversal of currents to northerly direction, upwelling is again noticed during September - October which is indicative of further southerly currents. Time series measurements of currents at different depths are essential to bring out these fluctuations very clearly. Banse (1968) noted "the main difficulty in interpreting the temperature and salinity observations off Bombay is the lack of simultaneous current measurements".

At subsurface, mild deepenings of isotherms are noticed in May (Fig. 4.2) after an initial upward tilt. Similar feature was noticed off Ratnagiri in 1973 (Fig. 4.3) and during certain years off Cochin, located further south along west coast of India (Anon, 1980). These appear to be related to changes in current directions. Before the establishment of steady flow towards south, as part of clockwise coastal circulation during southwest monsoon, current directions must be oscillatory. A temporary phase of northerly current would necessitate the presence of lighter water to the right of flow and hence would necessitate sinking. This may be the reason for the downward tilt of isotherms.

As noted earlier, similar fluctuations are noticed during post-monsoon also. At the subsurface, after the cessation of upwelling by

July, a secondary upward tilt of isotherms is noticed in September associated with unsteady direction of currents during the transition between the southerly and northerly directions of current. Mathew (1982) had also noticed a secondary upwelling off southwest coast of India but speculated it to be a localised feature generated by baroclinic waves.

4.3. HEAT CONTENT AND HEAT STORAGE

Heat content in different layers of 50 m thickness in upper ocean is presented in Fig. 4.5. In the upper 50 m column, heat content varies between $53 \times 10^8 \text{ J/m}^2$ and $61 \times 10^8 \text{ J/m}^2$ with the maximum occurring before the southwest monsoon and minimum during November. A secondary maximum is observed during winter season. Larger annual variations are encountered in the next 50 m layer (50 m - 100 m) where heat content varies between 42×10^8 and $56 \times 10^8 \text{ J/m}^2$. Higher values are observed before the southwest monsoon. After May, with the onset of the monsoon, a sudden decrease in heat content is observed which results from the early beginning of cooling due to upwelling at subsurface layers. Low values continue to prevail throughout the southwest monsoon season and minimum heat content occurs in September. Sinking at this subsurface level is manifested by a gradual increase in heat content after September.

In the 100 - 150 m layer, heat content ranges between 35×10^8 and $47 \times 10^8 \text{ J/m}^2$. In this layer, upwelling stops by July, when low values of heat content are encountered. After increasing slightly the heat content remains more or less constant till November. Afterwards, it increases as a result of sinking as indicated by the downward movement of isotherms. In the lowermost level considered (150 - 200 m), the variation is less (29×10^8 to $37 \times 10^8 \text{ J/m}^2$). In this layer also, after attaining maximum value in May, the heat content decreases till July.

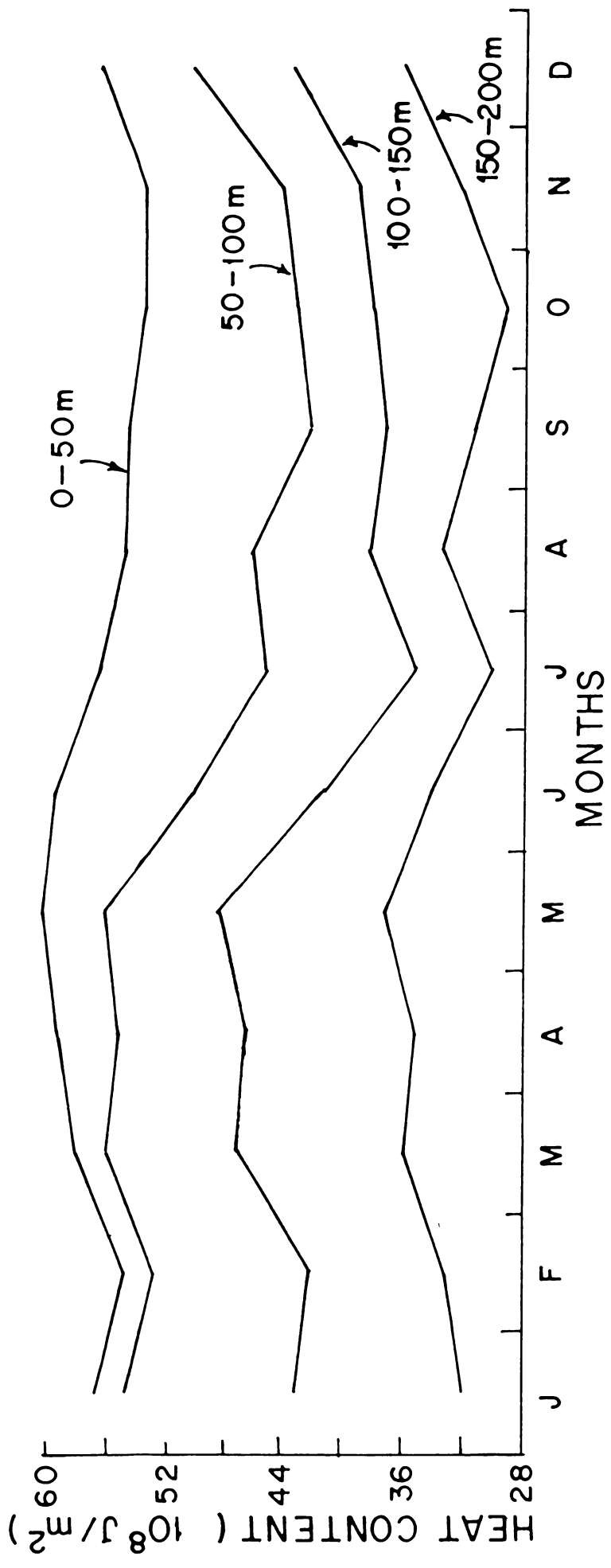


Fig.4.5 Average monthly variation of heat content in different layers, in Area II.

Between 150 - 200 m, there is an increase in August followed by decrease around October and subsequent increase.

The upper 200 m water column considered together, shows maximum heat content of $199 \times 10^8 \text{ J/m}^2$ before the southwest monsoon season (May). The heat content decreases during the southwest monsoon season to reach a low value of about $167 \times 10^8 \text{ J/m}^2$ in July. After increasing in August, the heat content decreases to attain the lowest value of $163 \times 10^8 \text{ J/m}^2$ in October and increases again in the following months. The annual range of heat content in this area is $36 \times 10^8 \text{ J/m}^2$ which is nearly equal to the amplitude in western north Pacific estimated by Bathen (1971).

The heat storage in different layers is presented in Fig. 4.6. In order to maintain similarity with data available in Area I, the presentation is confined to the upper 150 m. It can be seen that only the upper 50 m layer shows a nearly semi-annual cycle. This is in agreement with the findings in central Arabian Sea (Rao, 1988) but is different from the observations in western Arabian Sea (see Chapter 3). In this upper layer, the warming increases from about 15 W/m^2 in January to about 55 W/m^2 in March. Warming subsequently decreases leading to cooling during May. Maximum cooling of 70 W/m^2 seen during July, gradually changes by October to warming which again increases to about 45 W/m^2 in December.

In 50 - 100 m layer, warming of nearly 85 W/m^2 , seen in January, decreases to become a cooling by April. Cooling increases and reaches a maximum of about 145 W/m^2 in June. After June, the cooling gradually decreases till September and becomes warming in October. Warming increases suddenly in November and gradually thereafter to attain a value of about 155 W/m^2 by December. In this layer the range of the annual variation is about 290 W/m^2 . It can be seen that in this layer, the change over

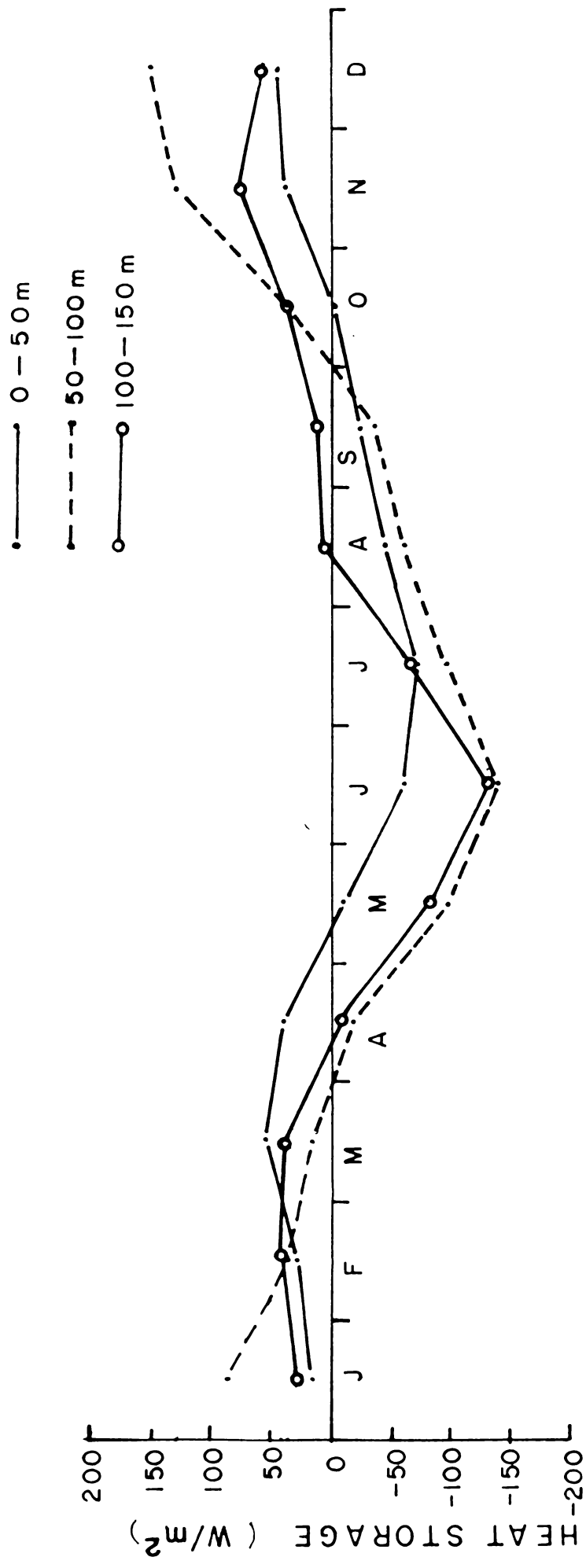


Fig.4.6 Average monthly variation of heat storage in different layers, in Area II.

from warming to cooling during pre-monsoon and from cooling to warming after the monsoon occur earlier by about $1\frac{1}{2}$ and $\frac{1}{2}$ months respectively compared to the layer above. This is the effect of earlier beginning and cessation of upwelling in this lower layer.

In the layer between 100 and 150 m, heat is stored from January to May ($\sim 50 \text{ W/m}^2$). This warming changes to cooling by April, almost coinciding with the layer just above. During summer monsoon, the cooling found in this layer is also similar to that in the layer above, reaching a maximum of 145 W/m^2 in June. However, in this layer, the warming commences even before the end of the monsoon season (August). This warming which is mild till September, increases towards the end of the year ($\sim 70 \text{ W/m}^2$).

Total heat storage in the upper 150 m (included in Fig. 4.8) shows an annual periodicity. Warming of about 100 W/m^2 is seen during January to March in this area. While in January, the warming is mainly contributed by the 50 - 100 m layer, in the following months all layers are found to contribute equally. In May, cooling is found to commence. This cooling before the southwest monsoon, is the effect of cooling in the 50 - 150 m. Cooling increases to the maximum of about 300 W/m^2 by June which is again largely contributed by the 50 - 150 m layer. Cooling decreases during the following months and changes to warming during October. The contribution of the 100 - 150 m layer to the cooling is negligible beyond August while the 0 - 50 m and 50 - 100 m layers contribute to the cooling equally from August to October. Warming steadily increases to reach a maximum of about 350 W/m^2 in December. Major contribution to this warming is provided by the 50 - 150 m layer.

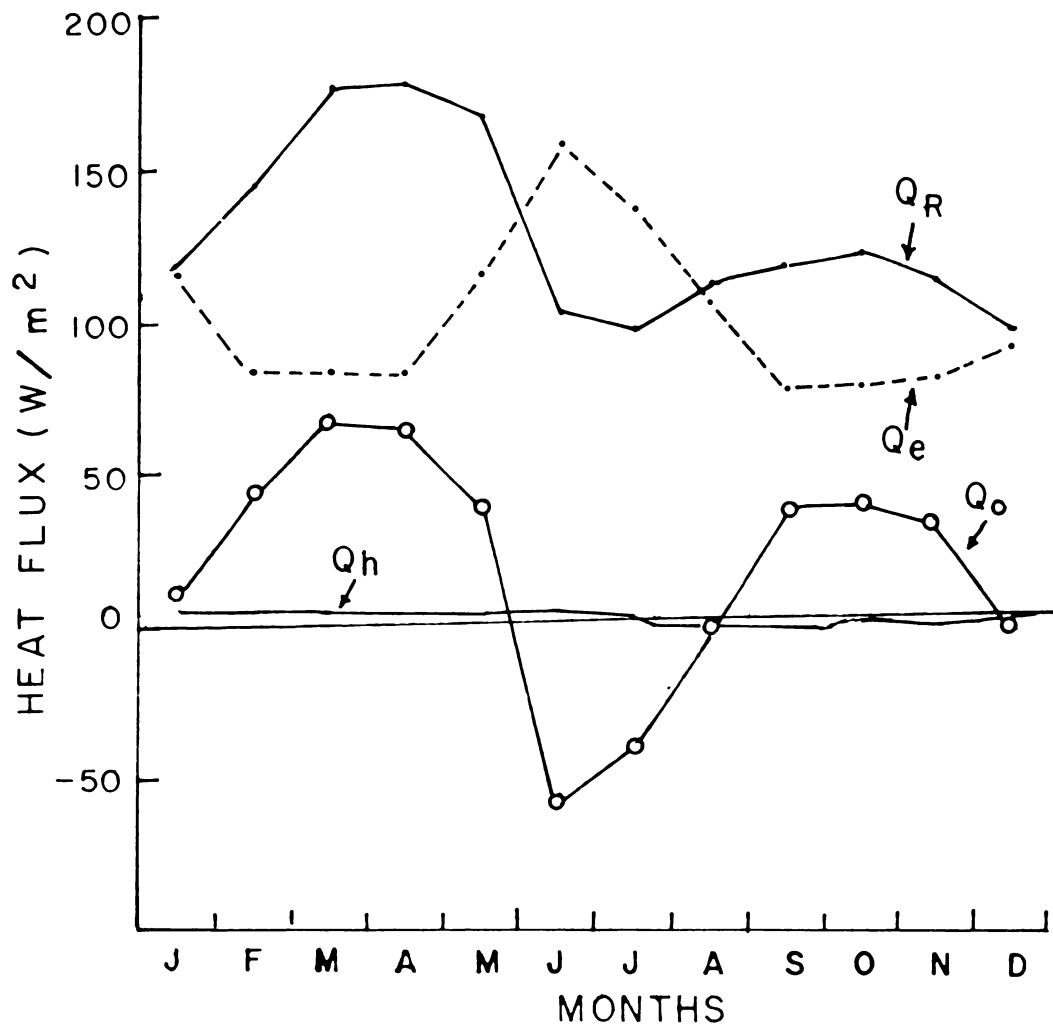


Fig.4.7 Average monthly variation of surface heat budget components, in Area II. Positive values of Q_o and Q_R indicate downward transfer and those of Q_e and Q_h indicate upward transfer.

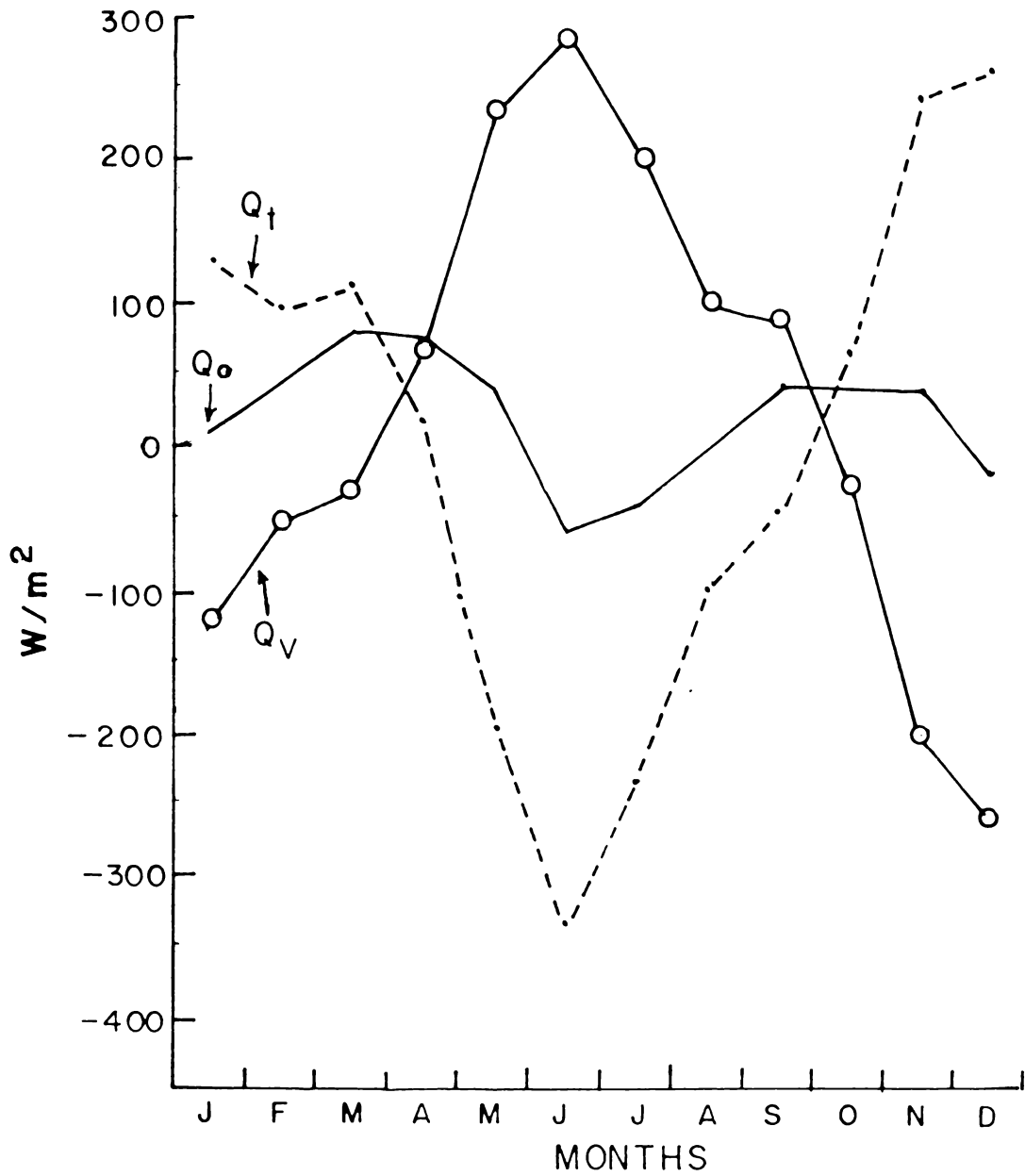


Fig.4.8 Average monthly variation of net surface heat exchange (Q_o), heat storage in upper ocean (Q_t) and heat advection (Q_v), in Area II. Heat advection out of the area (export) is positive.

4.4. HEAT EXCHANGE AT SEA SURFACE

Different components of the surface heat exchange in this area are presented in Fig.4.7. Values of individual components have been adapted from Hastenrath and Lamb (1979b). All the parameters exhibit semi-annual cycle. Net radiation varies from 100 to 185 W/m^2 . Radiation increases from about 120 W/m^2 in January to a maximum of about 185 W/m^2 during the southwest monsoon season. A drastic reduction after the onset of southwest monsoon is due to the increase in cloudiness. This is different from the observation in Area I where the reduction during southwest monsoon is very mild. Surface cooling in Area I due to intense upwelling reduces convection and hence also the cloudiness. Since upwelling is less intense off west coast of India, a similar effect is not found in Area II. During the post-monsoon months, slight increase in net radiation is noticed due to reduction in cloudiness. This is followed by a fall in net radiation during winter.

Heat loss due to evaporation varies between 75 W/m^2 and 155 W/m^2 . From values of about 110 W/m^2 during winter, evaporation decreases during the pre-monsoon period. This can be due to a fall in wind speed. Increase in evaporation during early summer monsoon is associated with the increase in wind speed, leading to maximum evaporation in June. This is similar to the findings in Area I also. The decrease of evaporation in Area II after June, is gradual as compared to Area I. This decrease can be due to a fall in SST which is associated with reduced insolation and also wind mixing. However, the absence of a sudden reduction in evaporation here, may be due to much less intense upwelling compared to Area I. Low wind speeds of post-monsoon also contributes to the continued low values during this period. Slight increase in

evaporation experienced subsequently, may be due to an increase in wind speed during the northeast monsoon season. Transfer of sensible heat to atmosphere is of very low magnitude throughout the year. During the latter part of southwest monsoon, this becomes almost zero.

The net heat gain at sea surface is largely a resultant of radiative and evaporative fluxes of heat. Net gain also shows a semi-annual cycle. However, unlike Area I, heat loss to atmosphere is noticed here during southwest monsoon season. From January onwards, the heat gain increases reaching a maximum of about 65 W/m^2 during March-April. After May, heat gain decreases as a result of increase in evaporation. Associated with the decrease in radiation and increase in evaporation, the heat is lost from sea surface during southwest monsoon and the loss reaches a maximum of about 65 W/m^2 in June. This is in contrast to Area I where the sea does not lose heat during the southwest monsoon season. During post-monsoon season, sea again gains heat to reach a secondary maximum of about 35 W/m^2 in September.

4.5. OCEANIC HEAT ADVECTION

Heat divergence through the upper 150 m, obtained as a residual of surface heat input and heat stored (Fig. 4.8) also indicates an annual signal and is, in general, a mirror image of heat storage indicating its predominant influence on heat advection. During January, heat import of about 110 W/m^2 to this area is seen. This import is utilized largely to warm the middle layer (50 - 100 m, see Fig. 4.6). During the following months, the import of heat gradually decreases to become export by the end of March. This reduction in import is a combined effect of an increase in surface heat input and fall in heat storage. Heat export in April-May is mainly due to negative heat storage. This export cools mainly

the 100 - 150 m layer (see Fig. 4.6). Export increases during the southwest monsoon season to reach a maximum of 275 W/m^2 in June. This export, inspite of slight heat loss to atmosphere, is due to upwelling and the associated cooling of the water column. Although all layers are found to cool during these months, the export cools the near surface layers (0 - 50 m) much less than the layers below. Export decreases after June. The export of heat, after July, cools the 0 - 100 m layer and does not cool the 100 - 150 m layer. From October onwards heat import is again noticed which reaches a maximum of 260 W/m^2 in December. This import warms the 100 - 150 m layer than the layers above (see Fig. 4.6).

The heat distribution during different heating and cooling seasons in Area II is examined. During pre-monsoon season (February - May), heat gain at sea surface of about $25 \times 10^8 \text{ J/m}^2$ is more than the warming ($13 \times 10^8 \text{ J/m}^2$) in the upper 50 m layer. However, heat is not transferred downwards as can be seen from the cooling of about $10 \times 10^8 \text{ J/m}^2$ in 50 - 150 m layer. This indicates that heat is exported from this area. This is different from Area I where heat import is seen below 100 m, during this period. During monsoon season (June - September), in Area II, 0 - 150 m layer cools by about $76 \times 10^8 \text{ J/m}^2$, nearly half of which is found to occur in 50 - 100 m layer. Considering the observed surface heat loss to atmosphere of about $6 \times 10^8 \text{ J/m}^2$, the export from this area is nearly $70 \times 10^8 \text{ J/m}^2$. It has been observed earlier that during this season, heat export from Area I (Chapter 3) is carried to the interior of ocean, elsewhere in the Somali Basin. Since studies on heat advection from eastern Arabian Sea has not been reported, it is not clear whether the heat export from Area II, during southwest monsoon, is transferred to the interior of the ocean near this locality or is carried laterally

to other localities. During October - December, surface heat gain of about $6 \times 10^8 \text{ J/m}^2$ equals the storage in upper 50 m layer. However, 50 - 150 m layer is warmed due to an import of nearly $40 \times 10^8 \text{ J/m}^2$. It may be noted that during this period, in Area I, heat import is seen below 100 m.

Annual cycle of the 20°C isotherm, which can be considered as indicative of the vertical movements of the middle of thermocline, also in general, shows an annual periodicity (Fig. 4.9). The 20°C isotherm attains a maximum depth of about 150 m during the pre-monsoon period. After May, this isotherm shoals to reach its minimum depth of 80 m. After this, the isotherm again starts deepening towards December. Mild upward movement is again observed in January - February. The pattern in this area is different from the much more complicated variations in Area I, where the effect of the subsurface dynamics associated with currents and eddies of the Somali Basin is of importance.

4.6 SIMULATION OF SEA SURFACE TEMPERATURE

Results of SST simulation is shown in Figs. 4.10a and b. Observed temperatures are also included in the figures. As pointed out in Chapter 1, horizontal advection is considered to be of lesser importance and is not included in these simulations. The r.m.s. differences between the observed and simulated series and correlation coefficients are given in Table 4.2.

Uncertainties in simulated SST due to uncertainties in different parameters of the processes considered (see Chapter 1) are presented in Table 4.1. The average values obtained for Area II which is utilised to estimate these errors are 22 W/m^2 , 48 m, $57.20 \times 10^{-7} \text{ m/s}$,

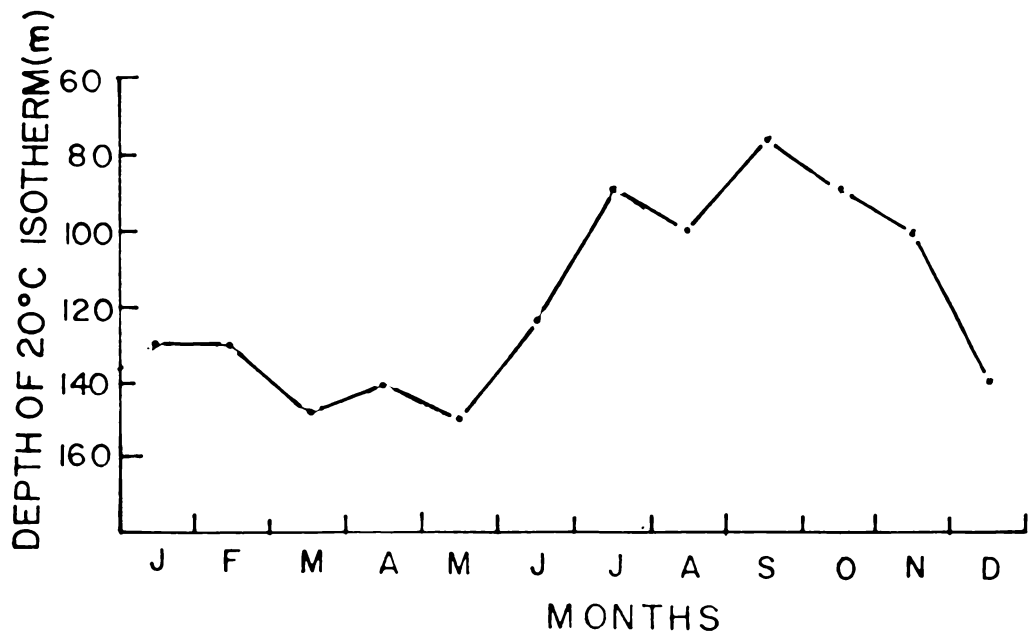


Fig.4.9 Average monthly variation of depth of 20°C isotherm, in Area II.

1.33×10^{-5} m/s for surface flux, MLD, entrainment velocity and vertical velocity respectively.

Surface heat flux (scheme 1) generates the observed semi-annual cycle of SST in this area (Fig. 4.10a). However, during southwest monsoon, the estimated temperatures are less than those observed and during winter these are higher. The r.m.s. difference between the observed and simulated series is 0.87°C and the correlation between the two is 0.5. Thus the variance of observed series, accounted by surface heat flux alone, is only 25%.

Table 4.1. Error in estimated SST due to uncertainties in different parameters, in Area II

Processes	Surface flux	Entrainment	Horizontal advection	Vertical advection
Error ($^{\circ}\text{C}$)	0.44	0.40	Process not considered	0.81

The inclusion of entrainment (scheme 2) shows some improvement after winter. However, during post-monsoon, excessive warming is noticed. As a result, the model has not improved the prediction on an annual basis. Correlation coefficient and r.m.s. difference do not show much change. The reason for increased warming could be the effect of the model as discussed in Chapter 3.

Since horizontal advection is not considered, scheme 3 is not worked out for Area II. Vertical advection is included and the results are presented as scheme 4 (Fig. 4.10b). Maximum upward velocity of 1.27×10^{-5} m/s is noticed in September and maximum downward speed of

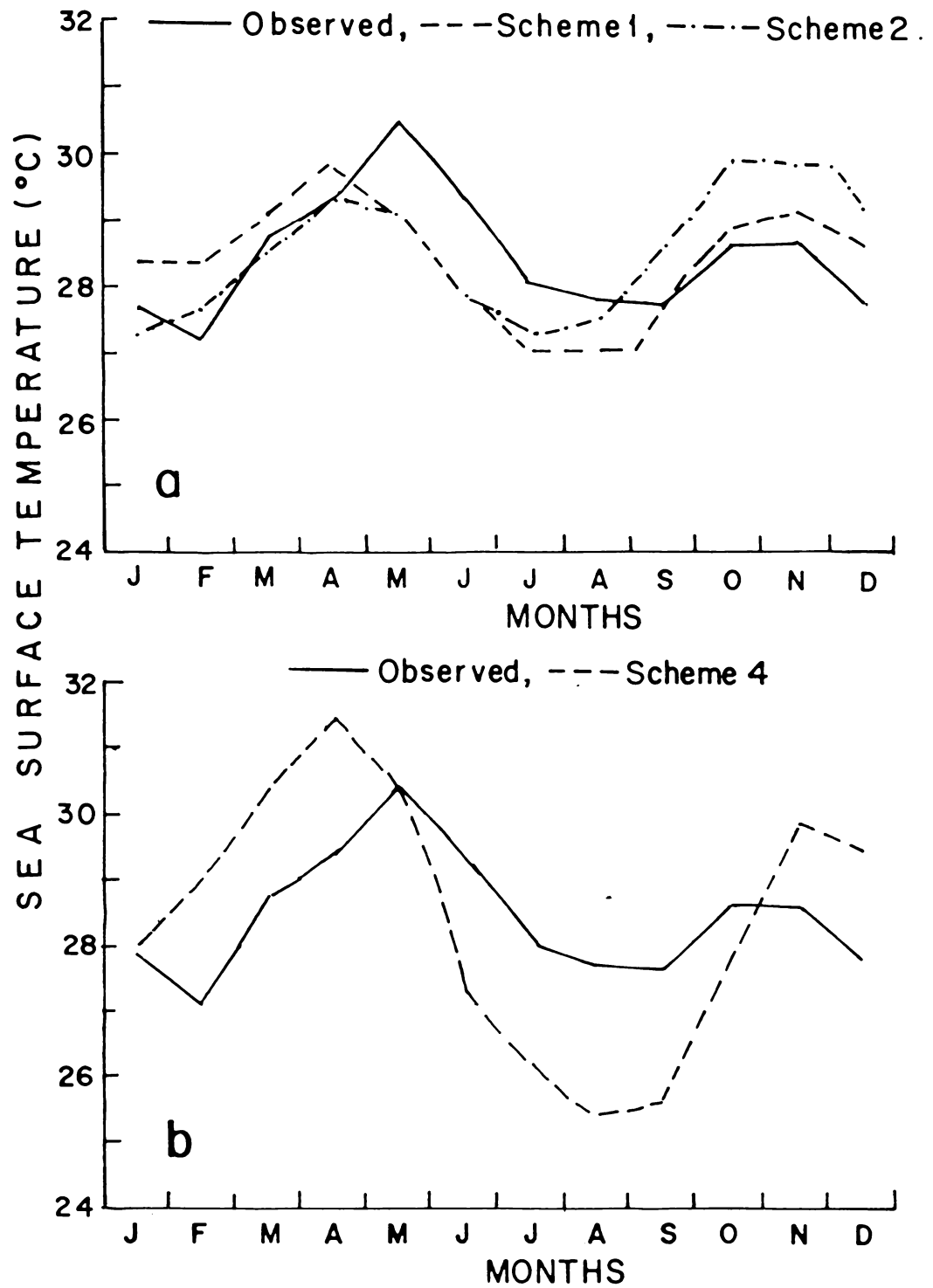


Fig.4.10 SST simulated by different schemes, in Area II. Observed SST is also included.

Table 4.2. r.m.s. difference and correlation coefficient
between observed and estimated monthly SST

Scheme No.	Process considered	r.m.s. difference (°C)	Correlation coefficient
1.	Surface heat flux	0.87	0.50
2.	Surface heat flux and Entrainment	0.86	0.54
3.	Surface heat flux Entrainment, Horizontal advection	Scheme 3 is not considered.	
4.	Surface heat flux Entrainment, Vertical advection (Horizontal advection not included)	1.68	0.50

1.54×10^{-5} m/s is noticed in December. The scheme degraded the results and the r.m.s. difference increased. This indicates that subsurface vertical movements do not influence the evolution of SST in Area II. Unlike Area I, here the upwelling associated with southwest monsoon is of lesser intensity and the thermocline is not found to outcrop sea surface and hence the oscillations of thermocline do not affect SST variations considerably. Emery (1976), Merle (1980) and McPhaden (1982) have indicated that subsurface processes normally do not affect SST variability. Studying upwelling off Indian coasts, Mathew (1982) opined that some times, upwelling occurs below surface layers off west coast of India, even when high SST continues to be present.

Thus, in Area II, surface flux and entrainment seem to be important during winter. Although comparatively high correlations have been noticed in this area during 1979 by Molinari et al (1986), they have also observed low correlations in certain parts of eastern Arabian Sea where variance of SST was found to be less than 0.5°C^2 . They have considered that the low signal to noise ratio could be the reason for the lower correlation coefficients. In the climatological data of present Area II also, SST variance is low ($\sim 0.4^{\circ}\text{C}^2$) and this may be a reason for low correlation in schemes 1 and 2, although r.m.s. differences between observed and simulated series are low.

CHAPTER 5

HEAT TRANSPORT IN THE NORTHERN INDIAN OCEAN

5.1. INTRODUCTION

While redistributing the heat received, the ocean currents transport heat from areas of excess heat towards deficit regions. The transport of heat by oceans is, at least on an annual basis, comparable to that by atmosphere (Vonder Haar and Oort, 1973). In their subsequent study, Oort and Vonder Haar (1976) have found that oceanic heat transport is of comparable order of magnitude as the heat input from atmosphere and that stored in the sea. It is observed that heat transport by the oceans, compared to that by atmosphere, is more prominent in low latitudes (Vonder Haar and Oort, 1973).

Of the various processes contributing to world climate, the heat advection by the oceans is the least understood. This is because of the difficulty in obtaining this component by direct method. In the direct method, temperature and velocity have to be measured simultaneously in the oceans on an annual basis. Such observations are very difficult to be carried out due to the vastness of oceanic areas. Also, the presence of eddies necessitates very high spatial and temporal resolution for getting representative average values of temperature and velocity. The study of oceanic heat flux by direct method is, therefore, practically impossible and prohibitively expensive. Hence, direct measurements available are limited to local areas.

As a result of the various difficulties, the heat transport in the oceans is obtained by indirect methods. One method is to compute the geostrophic current using density field and then to use the mean

temperature field to estimate the heat flux (Model, 1950; Jung, 1952; Bryan, 1962; Bennett, 1978; Wunch, 1980).

Alternatively, heat flux by ocean currents can be calculated as a residual of heat balance components of the ocean-atmosphere-earth system (Vonder Haar and Oort, 1973; Newell et al, 1974; Oort and Vonder Haar, 1976). However, this method does not resolve the heat transport separately for individual oceans. The more common method is to obtain advection from the heat balance of the oceans. Knowing the net heat exchange at sea surface and heat storage in the oceans, the residual (equation 1.19) gives the heat advection. This method has been employed for studying heat advection in Areas I and II (Chapters 3 and 4). This approach was followed by Lamb (1981) and Lamb and Bunker (1982) for north Atlantic, Merle (1980) for equatorial Atlantic, Etter (1983) for Gulf of Mexico, Hastenrath and Merle (1986) for tropical Atlantic, Bruce (1987) for Somali Basin and Rao (1988) for central Arabian Sea. In their studies on heat transport in world oceans, Hastenrath (1980) and Hsiung (1985) have considered that on a long-term basis, heat storage/depletion in the oceans vanishes.

The residual methods are also not without disadvantages. In the earth-atmosphere-ocean system, the balance is sought between large terms and hence the errors in the estimates can also be very large. In oceanic heat budget method, uncertainties are involved in estimating the components of heat flux at sea surface and also in evaluating the climatology of subsurface heat storage. The methods of estimation of various components of heat flux at sea surface are discussed in Chapter 1.

Utilizing a method of combining hydrographic data and wind stress for calculating heat transport, Bryan (1962) has found that heat transport in the vertical is also important. Hastenrath (1980) suggests that perhaps the direction of cross equatorial heat flux cannot be determined confidently due to large error limits. Hastenrath (1982) has updated his earlier estimates of heat transport and finds that different estimates from surface heat input as well as from hydrographic data agree closely. Etter (1983) obtained heat advection as residual of oceanic heat budget and also from a divergent heat budget equation given by Emery (1976). Wyrтки and Ulrich (1982) are of the view that the accuracy of heat advection as a residual is not sufficient for calculating the heat advection on a month to month basis, but can be utilized for the study on seasonal basis in the estimation of heat advection. Russel et al (1985) used a numerical model to generate global oceanic heat transport. Carton and Yoo (1987) suggested that the models should be used in conjunction with rich data sets for estimating seasonal heat transport. Studies on heat budget including oceanic and atmospheric heat transports have been reviewed by Hastenrath (1985).

Studies on heat advection as a residual of surface heat input and heat storage are available only at few selected areas in Indian Ocean (Bruce, 1987; Rao, 1988). In the estimate of heat advection by Hastenrath and Lamb (1980), heat storage in northern and southern parts of Indian Ocean was evaluated from annual range of SST between warm and cold seasons, assuming that the annual variation of temperature decreases linearly to zero at 150 m. The present study is based on the components of equation 1.19, available in literature.

5.2. ANNUAL CYCLE OF NET HEAT EXCHANGE AT SEA SURFACE

Net heat exchange values have been digitized from Hastenrath and Lamb (1980) for north Indian Ocean, at 5° latitude intervals from 2.5° S to 22.5° N. They used data for 60 years (1911-1970), compiled by 1° square areas for the study. The zonally averaged net heat exchange is presented in Fig. 5.1a. North Indian Ocean is, by and large, an area where heat gain from the atmosphere is noticed throughout the year. Heat loss is confined to north of 10° N during November-February. In the northern most latitudes of Indian Ocean, maximum loss noticed exceeds 50 W/m^2 during winter and maximum gain, exceeds 100 W/m^2 during pre-southwest monsoon. Between equator and about 10° N, throughout the year, heat gain varying between 25 and 80 W/m^2 is noticed. During summer monsoon season, sharp decrease in net heat gain is seen over large area. This is due to fall in radiation balance because of increase in cloudiness and an increase in evaporation due to strong southwesterly winds. A secondary maximum is reached after southwest monsoon season.

5.3. ANNUAL CYCLE OF HEAT STORAGE

As shown in Chapter 1, heat storage can be evaluated from vertical profiles of temperature using equation 1.17.

There are several difficulties associated with such evaluation. One difficulty is regarding the estimation of the depth upto which the annual variation of heat content extends. In most areas, the main influence is seen only upto 100 m, but in some isolated regions, it may extend upto 1000 m (Oort and Vonder Haar, 1976). Further, various individual temperature profiles terminate at different depths so that

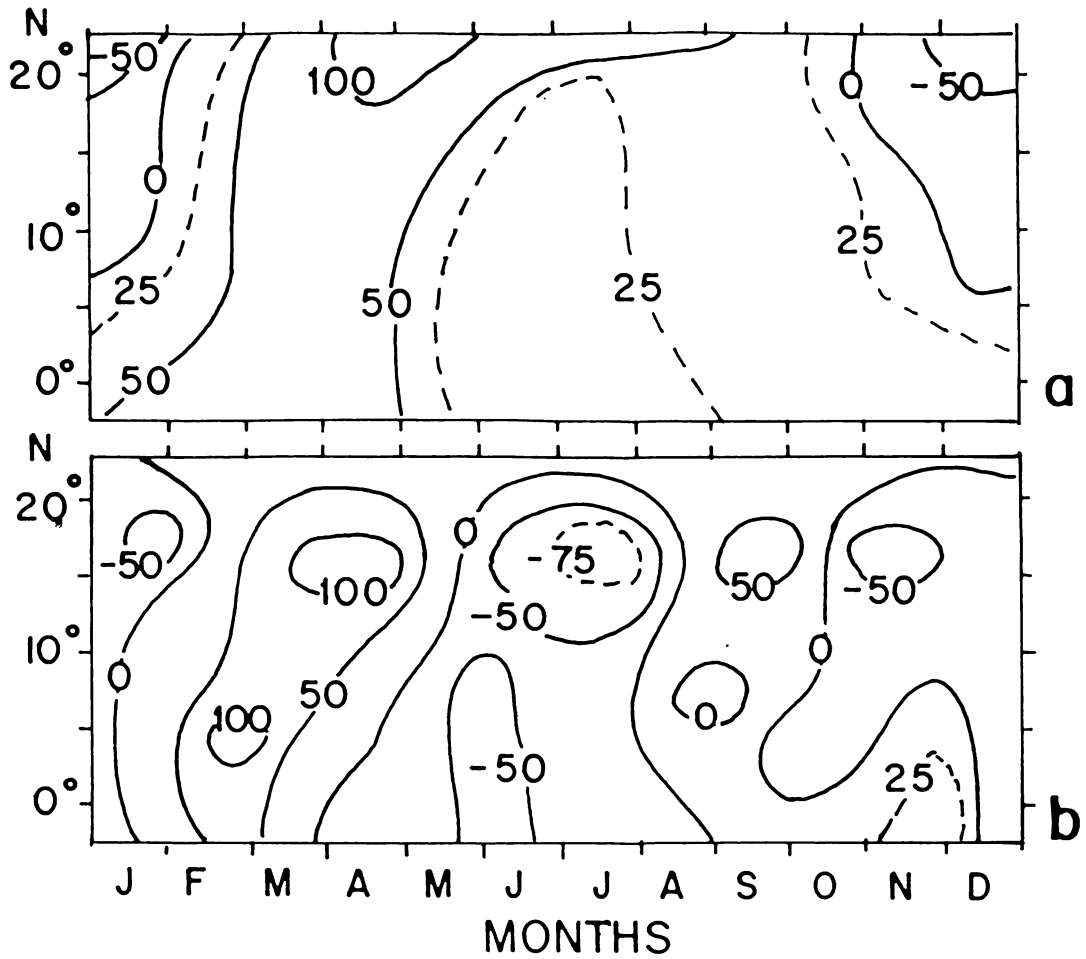


Fig.5.1 Zonally averaged (a) net surface heat gain (from Hastenrath and Lamb, 1980) and (b) parameterized heat storage (from Meehl, 1984), in northern Indian Ocean. Units are W/m^2 .

average profiles worked out will become less representative as depth increases. Different depth limits have been used by several authors for the estimation of heat storage in various oceanic regions (Bathen, 1971; Oort and Vonder Haar, 1976; Merle, 1980; Lamb, 1981; Lamb and Bunker, 1982; Bruce, 1987; Rao, 1988).

There can be data sparse regions, when large oceanic areas are considered and this may generate unrealistic climatology of heat storage. In regions of large interannual variability, the averaging of multiannual data in different grids for obtaining long-term average temperature profiles will not yield, in the true sense, the climatological averages. The averages may also be biased due to unequal data coverage. In areas of large horizontal gradients, as in coastal areas, compositing the data within selected grids will not produce homogenous average profiles.

Wyrtki and Ulrich (1982) examined the accuracy of heat storage computations and found that errors could also be introduced by combining the data obtained using different instrumentation and also due to the effect of station density. They have suggested that although it is difficult to study heat storage on a month to month basis, this can be attempted on the basis of heating and cooling seasons. Bretherton et al (1984) discussed the effectiveness of different sampling arrays with an aim to achieve an accuracy of $\pm 10 \text{ W/m}^2$ for heat storage which can be used for cost-effective optimal sampling scheme.

Studies have not been made on the annual cycle of heat storage in different latitudinal belts in the Indian Ocean based on monthly variation of average temperature profiles, obtained from historic data. Hastenrath and Lamb (1980) highlighted the need for such studies. Levitus

(1984) presented monthly heat storage in individual oceans using the departure of monthly mean temperature from the annual mean at selected levels.

Due to paucity of readily available heat storage data based on time differencing the heat content, in the present study, heat storage in north Indian Ocean has been adapted from Meehl (1984) who estimated heat storage using more easily available climatological average of SST and MLD, by developing a parameterization. These estimates are based on the assumption that temperature variations do not occur below the maximum MLD found during the year. Meehl (1984) calculated the northern hemispheric heat storage for individual oceans using mean SST from Alexander and Mobley (1976) and mean MLD from Robinson et al (1979). It has been found that estimates of parameterized zonally averaged heat storage, for global oceans in mid-latitudes are comparable in magnitude and phase with those obtained from actual data of Oort and Vonder Haar (1976). However, agreement is less for tropics. Further, better agreement is noticed in regions where temperature profile is controlled by entrainment at the base of ML, than in regions where MLD is forced by ocean dynamics.

Fig. 5.1b gives the annual cycle of zonally averaged heat storage in northern Indian Ocean digitized from Meehl (1984) at 5° latitude intervals from 2.5°S to 22.5°N . The heat storage exhibits a semi-annual signal in consonance with the occurrence of monsoons. Cooling is observed during winter and southwest monsoon seasons. Near the equator, maximum warming is noticed in February and heat is depleted during April to September. Using continuous data for $2\frac{1}{2}$ years, Mc Phaden (1982) noticed

heat depletion during this period, with interannual variation, in western Indian Ocean.

Further north, maximum warming of about 100 W/m^2 occurs in April-May. Negative storage is seen during May to August with maximum cooling of about 75 W/m^2 occurring during June-August. Warming is observed again during the post-monsoon months. A small pocket of heat storage of about 50 W/m^2 is seen around 17° N during September-October.

5.4. ANNUAL CYCLE OF HEAT ADVECTION

Annual and latitudinal variations of heat advection are presented in Fig. 5.2. In view of the inherent uncertainties in the estimation of different components of heat budget, absolute values in Fig. 5.2 may be considered with reservation. However, the major features are discernible. In the northern regions, heat is imported during winter and exported during summer in response to the surface heat exchange. Further south, the variations are more complex. By and large, heat export is noticed from this part, with comparatively low values during winter. Before southwest monsoon season, around 15° N , slight heat import is noticed which may be caused by the large heat storage during this time (Fig. 5.1b).

Subsequently, heat export increases to attain maximum values exceeding 100 W/m^2 during southwest monsoon season. This increase in export occurs, in spite of reduced heat gain from atmosphere (Fig. 5.1a). Hence, this export is the result of large negative heat storage. This could be a result of upwelling which cools the upper ocean. Off Somalia, intense upwelling takes place during this season (Chapter 3). The upwelled water spreads to extensive areas of Arabian Sea, contributing

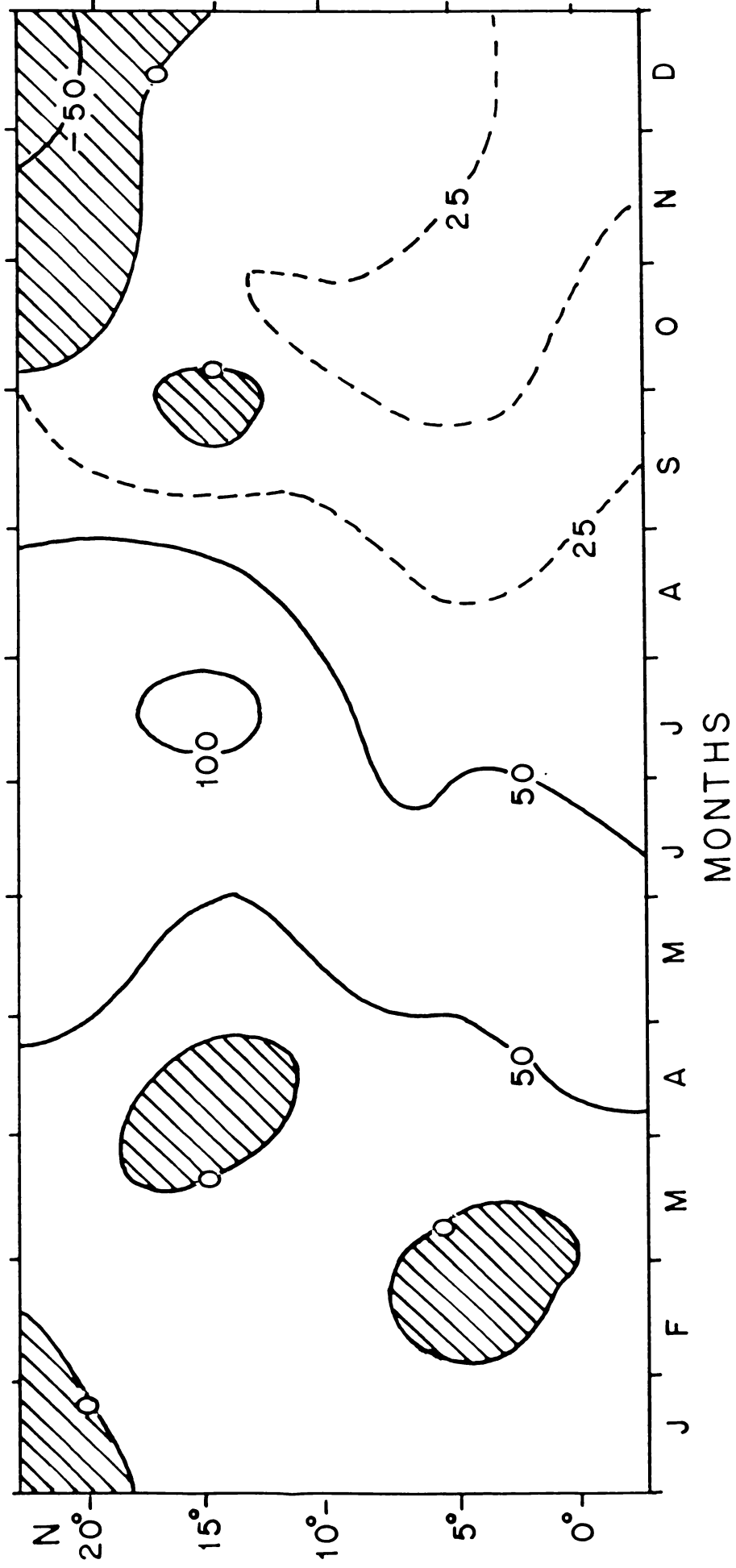


Fig.5.2 Zonally averaged heat advection in northern Indian Ocean. Units are W/m^2 . Hatched portions indicate heat import.

to the surface cooling. Similar effects are also caused by intense upwelling off Arabian coasts. During this season, upwelling occurs off the east and west coasts of India (Banse, 1959, 1968; Darbyshire, 1967; Murty and Varadachari, 1968; Sharma, 1968, 1978; Anon, 1980). Upwelling off central west coast of India is discussed in Chapter 4. Effect of upwelling in the summer cooling of Arabian Sea was pointed out by Rao et al (1976). Studies in the Andaman Sea (Ramesh Babu and Sastry, 1981) have also shown negative heat storage in a layer close to surface, during monsoon. Studying the heat budget of Arabian Sea during southwest monsoon season, Düing and Leetmaa (1980) have found that upwelling is the largest component and is hence responsible for the negative heat content of Arabian Sea during this season. This reduction in heat content during southwest monsoon season occurs, despite a mild heat gain from atmosphere and results in observed heat export during this period.

Towards the end of southwest monsoon season, by September, the heat export decreases rapidly as a consequence of cessation of upwelling and the associated cooling. From September onwards, there is no evidence of upwelling (Düing and Leetmaa 1980). This results in heat storage and since there is not much change in heat gain at sea surface, the heat export decreases. A small pocket of heat import is seen centred around 17° N. In these latitudes, export of heat continues during October–November, consequent to the negative heat storage during these months (see Fig.5.1b). Ramesh Babu and Sastry (1981) noticed positive heat storage in October and negative storage in November in the upper 20 m, in Andaman Sea. Perhaps, the prevalence of cyclones in Arabian Sea and Bay of Bengal may have an influence in this heat depletion. These months are characterized by depressions in Arabian Sea and Bay of Bengal, several of which turn

into severe cyclones. It can be seen from the data on cyclones presented by Mooley and Mohite (1984) that maximum number of cyclones occur during May-June and October-November. The mixing due to intermittent occurrence of cyclones will result in a depletion of heat from surface layers.

In the equatorial regions, by and large, heat export is observed. Maximum export of about 65 W/m^2 occurs during pre-monsoon and early southwest monsoon seasons. After southwest monsoon season, export of about 25 W/m^2 is noticed till the end of the year.

Lamb and Bunker (1982) presented heat advection in north Atlantic Ocean, using heat storage upto 300 m as well as upto 500 m. Since the present study is based on parameterized heat storage, a close comparison may not be possible with the results in North Atlantic and also with global oceanic heat advection studies by Oort and Vonder Haar (1976).

It can be noted that, between equator and 30°N , in the Atlantic Ocean, there is a predominance of heat export. There are long durations and large latitudinal extents for which export is more than 50 W/m^2 and very often values reach 150 W/m^2 . Compared to this, in north Indian Ocean, maximum export of about 100 W/m^2 is seen only during peak monsoon at about 15°N . Another striking difference is that while in north Indian Ocean heat import is not observed between equator and 15°N , high values of heat import and export are seen in these latitudes in the Atlantic during the course of the year. In the global ocean, between $0-15^\circ \text{N}$, maximum export of about 150 W/m^2 has been found during summer, with a secondary maximum during winter. Between 15° and 25°N , mild import is seen in global ocean.

Oort and Vonder Haar (1976) further noticed around $45^\circ-60^\circ \text{N}$, heat import during winter. This was attributed to western oceans, where dry continental air extracts heat from sea surface. However, in western

Indian Ocean upwelling during southwest monsoon causes large heat export, the reasons for which are two fold. Firstly, monsoon air being moist laden, heat extraction from sea surface is reduced. Secondly, off the east African coast and Arabian coast, due to intense upwelling during southwest monsoon season, net radiation is increased by clear skys, evaporation is suppressed by cold surface waters and ocean experiences large net surface heat gain.

Latitudinal variation of monthly heat advection averaged from the annual cycle is presented in Fig. 5.3. Heat advection increases from north ($\sim 20 \text{ W/m}^2$) to about 30 W/m^2 around 15°N . Advection shows a decrease around 7°N and increases slightly near equator. The meridional profile adapted from Hastenrath and Lamb (1980) is also shown in Fig.5.3 for comparison. Although the estimates of Hastenrath and Lamb (1980) do not take into consideration the oceanic heat storage, the values show a general agreement with the present results.

5.6. INTEGRATED HEAT TRANSPORT

Total heat transport during every month, in each of the 5° latitudinal belts has been evaluated by multiplying the zonally averaged heat advection (Fig. 5.2) by the oceanic area in the respective belts. The longitudinal limits have been taken as 30°E and 120°E (Hastenrath and Lamb, 1980). Total heat transport in each 5° latitude belt for every month, is progressively added from north to south to get integrated transport. The necessary boundary condition for this integration is provided by the presence of land mass in the north. The condition is that no northward oceanic heat transport occurs across 25°N latitude belt. The progressive integration provides meridional heat transport across

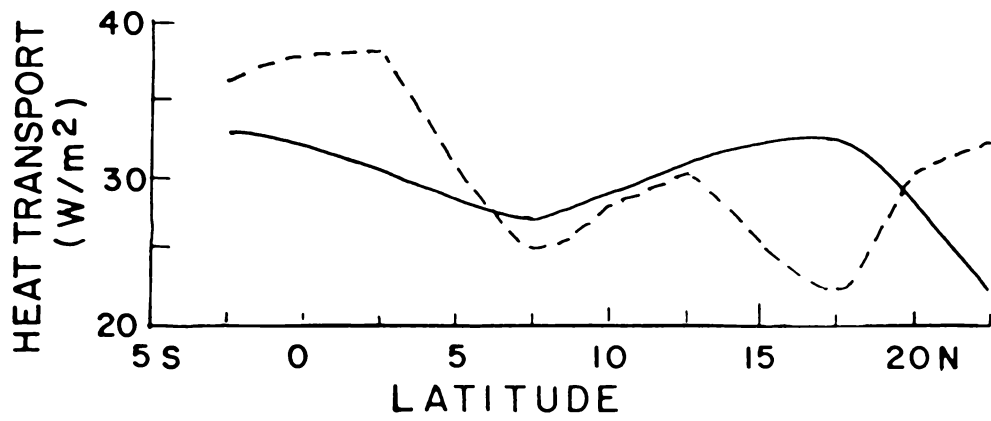


Fig.5.3 Latitudinal variation of annual average of heat transport in northern Indian Ocean (————). Variation presented by Hastenrath and Lamb (1980) is also included (-----).

latitudes at 5° intervals from 20° N to the equator. This transport was earlier termed as 'VZINMHT' (Vertically and Zonally Integrated Net Meridional Heat Transport) by Lamb (1981) and Lamb and Bunker (1982). As pointed out earlier, the advection in the surface layers alone is obtained.

Annual cycle of integrated transport across different latitudinal bands is presented in Table 5.1. During winter months, slight northerly transport is noticed which is more pronounced during December, when maximum northward flux of about $10 \times 10^{13} \text{W}$ is noticed across several latitudes. During southwest monsoon season, heat flux increases and becomes southerly in the entire north Indian Ocean. Maximum fluxes are noticed during June and July, when cross equatorial southerly flux of about $100 \times 10^{13} \text{W}$ is noticed. This cross equatorial flux decreases in September and increases again in October to about $40 \times 10^{13} \text{W}$.

It is interesting to note that throughout the year, the heat flux is from the north to the south Indian Ocean. The north Indian Ocean is largely an area of net heat gain from atmosphere throughout the year. This southerly transport is due to excess heat gain in Arabian Sea which is exported across the equator through surface layers necessitating a northward transport at intermediate depths. It has earlier been pointed out that the north Indian Ocean is a region of substantial heat export, (Hastenrath and Lamb, 1980; Düing and Leetmaa, 1980).

The present result is different from that in Atlantic Ocean where annual average flux is northerly, across all latitudes (Lamb, 1981). Further, in Atlantic Ocean, the maximum equatorial flux exceeding $200-250 \times 10^{13} \text{W}$ is directed northwards during September-October. Minimum

Table 5.1. Latitudinal and monthly variation of heat transport (10^{13} W) across latitudinal belts
 +ve values indicate southward transport

Latitude	MONTHS												AVERAGE
	JAN	FEB	MAR	APR	MAY	JUN	JUL	AUG	SEP	OCT	NOV	DEC	
20 N	- 6.2	+ 1.5	+ 4.3	+11.3	+11.3	+ 7.4	+ 6.4	+ 6.8	+ 3.7	- 0.6	- 6.2	- 7.2	+ 2.7
15 N	+ 2.9	+10.3	+ 4.3	+ 8.5	+20.9	+30.8	+34.7	+29.6	- 0.4	+ 4.9	+ 2.0	- 9.6	+11.6
10 N	+ 1.8	+12.1	+12.4	+ 8.5	+35.6	+56.6	+70.8	+59.0	- 0.4	+14.8	+10.1	- 7.8	+22.8
5 N	+11.7	+12.1	+18.3	+18.4	+64.4	+78.3	+83.4	+68.9	+ 8.7	+25.9	+18.0	- 7.8	+33.4
0	+24.1	+ 3.5	+16.4	+41.0	+88.8	+100.9	+98.4	+78.3	+17.0	+39.1	+28.2	+ 2.7	+44.9

northward flux in Atlantic occurs during May-June and southerly transport occurs during December only. Average cross equatorial transport of about $113 \times 10^{13} \text{W}$ in Atlantic Ocean is northerly (Lamb and Bunker, 1982). Present study indicates that average cross equatorial transport of $45 \times 10^{13} \text{W}$ is directed southwards in Indian Ocean.

For global oceans, strongest northerly transport occurs at $10^\circ - 20^\circ \text{N}$ during spring and fall (Oort and Vonder Haar, 1976). During this period, the transport is less in equatorial areas. Maximum transport across the equator is southerly and is observed in August. Unlike the Indian Ocean, for global Ocean the cross equatorial flux changes direction during the year in such a way that, in general, it is from summer to winter hemisphere.

Meridional profiles of integrated transport averaged for the whole year, for southwest monsoon season (May to September) and for non-monsoon season (October to April) are shown in Fig. 5.4. For the year as a whole, the southerly transport increases from about $3 \times 10^{13} \text{W}$ at the northern part to about $45 \times 10^{13} \text{W}$ across the equator. The cross equatorial flux, in Atlantic Ocean is northerly and is about $100 \times 10^{13} \text{W}$ (Lamb, 1981; Lamb and Bunker, 1982). Further, Lamb and Bunker (1982) found differences in this transport when different data sets were used for surface heat input. The cross equatorial flux in the present study is less than that by Hsiung (1985) who had assumed that oceanic heat storage vanished on a long-term basis.

At all latitudes, the southward heat transport is more during southwest monsoon season (Fig. 5.4). Cross equatorial southerly fluxes are about $75 \times 10^{13} \text{W}$ and $20 \times 10^{13} \text{W}$ during monsoon and non-monsoon months

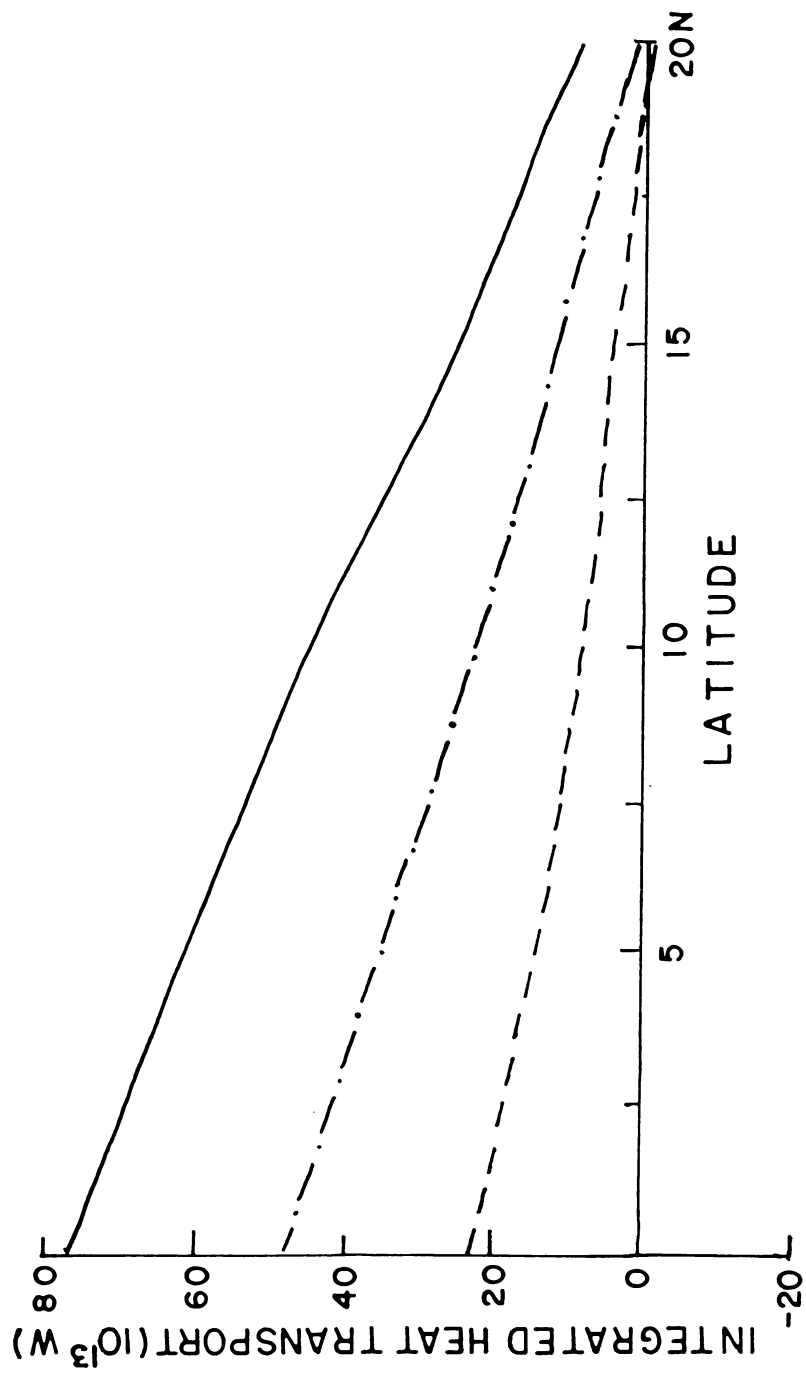


Fig.5.4 Latitudinal variation of integrated heat transport in northern Indian Ocean. ——— annual average, -·-·-·- average of south west monsoon months and - - - - - average of non-monsoon months.

respectively. These compare well with the southerly flux across the equator, estimated to be $83 \times 10^{13} \text{ W}$ during summer half year and $14 \times 10^{13} \text{ W}$ during winter half year by Hastenrath and Lamb (1980). However, it may be noted that they used heat storage obtained from the difference in mean SST during half yearly periods, under the assumption that this variation decreases uniformly to become zero at 150 m.

On comparing with the other estimates of heat transport across the latitudes (Table 5.2) which assume that on a long-term basis, the oceanic heat storage vanished, it is found that the present results, are, in general, comparable with those of Hastenrath (1980) and Hastenrath and Lamb (1980) and are lesser than those of Hsiung (1985). Meridional heat flux due to Ekman transport (Levitus, 1987b) is also included in Table 5.2. The pattern qualitatively agrees with the present results obtained from heat balance components. The dominance of southerly flux was attributed to the southwest monsoon when the winds are favourable for southerly Ekman transport.

From present study, it is seen that about 75% of southward transport in the north Indian Ocean occurs during the southwest monsoon season. Studies of SST variation using numerical models also suggest that advection during southwest monsoon removes major part of heat gained at sea surface during the course of the year (Shetye, 1986). As noted earlier, upwelling occurring during the southwest monsoon season, may be one of the factors that contribute to the negative heat storage and the heat depletion from north Indian Ocean. A good monsoon will trigger intense upwelling and hence export more heat from north Indian Ocean.

Table 5.2. Comparison of various estimates of meridional southerly heat flux (10^{13} W) in northern Indian Ocean

Latitude	Present study	Hastenrath (1980)	Hsiung (1985)	Hastenrath and Lamb 1980	Ekman heat flux (Levitus, 1987)
20 N	3	5.0	5.1	5.0	120
15 N	12	10.0	19.2	12.0	35
10 N	23	15.0	36.5	22.0	54
5 N	33	30.0	56.3	30.0	115
0	45	49.0	83.0	52.0	-

Results of some studies on SST and rainfall by Joseph and Pillai (1984) also give an indication that such a process is possible. They found that SST in Arabian Sea and Bay of Bengal during post-monsoon months is negatively correlated with rainfall. This may be because a good monsoon induces intense upwelling and hence exports more heat from north Indian Ocean which in turn results in lower SST during post-monsoon months.

Joseph (1981) considered that large scale monsoon failure during 1965-66 caused an increase in SST of Arabian Sea and Bay of Bengal and the resulting warm sea was responsible for good monsoon in 1967 which cooled the sea and the cycle was repeated.

Thus it appears that the heat exported from the north Indian Ocean may have a bearing on the monsoon activity. It must, however, be noted that rainfall anomalies are dependent also on various circulation parameters. The verification of relationship, if any, between monsoon activity and heat transport, as suggested above, requires good quality data on surface heat flux and subsurface temperature profiles during individual years.

CHAPTER 6

SUMMARY AND CONCLUSIONS

The exchange of energy at the naviface plays a paramount role in various atmospheric and oceanic processes such as atmospheric circulation, ocean currents, heat storage and advection, mixing in atmosphere and sea, upwelling and sinking of ocean water etc. The upper ocean thermal structure which modulates the climate is, to a great extent, influenced by the air-sea interaction processes.

Northern Indian Ocean is an area which comes under the influence of seasonally reversing monsoons. Results of studies on the air-sea interaction processes, upper ocean thermal structure, variations in heat content, heat storage and advection and the factors that affect them, on short-term and on climatological scales, at selected regions in Arabian Sea have been presented in the preceding chapters. The annual cycle of heat advection in northern Indian Ocean has also been studied.

Variations on a day to day basis of different energy exchange components and the upper ocean thermal characteristics at two fixed stations in east central Arabian Sea, during pre-onset and after the onset of southwest monsoon are studied using data collected during MONEX-79. Radiation balance is estimated using empirical formulae. Fluxes of momentum, latent heat and sensible heat are evaluated by bulk aerodynamic method using coefficients that vary with wind speed and stability of atmosphere (Bunker, 1976).

The long-term subsurface data at two areas, situated in western and eastern Arabian Sea, are used for studying the climatology of the

upper ocean thermal structure. These data have been subjected to quality control scheme. The annual cycle of surface heat budget in these areas is also examined using the heat exchange parameters adapted from Hastenrath and Lamb (1979b). In order to understand the relative importance of different processes in the evolution of SST, a model suggested by Mc Phaden (1982) is made use of.

Zonally averaged net surface heat gain at 5° latitude intervals, between 2.5° S and 22.5° N, adapted from Hastenrath and Lamb (1980) and the zonally averaged heat storage, estimated by parameterization, (Meehl, 1984) have been utilized to study the monthly variation of heat advection. Integrated heat transports across different 5° latitude belts have also been evaluated.

Studies on short-term variations show that the fluxes of heat and momentum in eastern Arabian Sea increase under the influence of a storm that occurred over Bay of Bengal, before the onset of southwest monsoon. In the upper ocean, convective mixing and downward flux of heat are noticed under the influence of the storm. After the onset of southwest monsoon, the fluxes show considerable increase. The momentum flux, on an average, increases by 0.5 N/m^2 and the net heat transfer changes from a gain of 80 W/m^2 to a loss of 150 W/m^2 .

Of the two stations studied, the northern station registers larger fluxes after the onset vortex, either due to a differential interaction of the monsoon onset vortex or as a feature of the monsoon flow. This station shows an increase in heat content at subsurface layers just before the onset, possibly due heat advection, suggesting some readjustments.

Although both the stations show upwelling under the influence of onset vortex, more intense upward movement has been noticed at the southern station near which the storm remained for a longer period during its formative stages. On examining the relative importance of the different terms of heat budget of the upper layer at the northern station during the onset vortex, it has been found that surface heat flux is of greater importance compared to entrainment and heat advection.

Convective turbulence is noticed in the upper layers of east central Arabian Sea when the area comes under the influence of storm in Bay of Bengal during pre-onset and also after the onset of southwest monsoon. Investigations on stability parameter h/L , where h is MLD and L is Monin-Obukhov length, show that under the influence of the storm which occurred in Bay of Bengal during pre-onset, the mixing in upper ocean is dominated by buoyancy flux while after the onset, mixing is influenced by buoyancy and wind.

Climatological studies of upper ocean thermal structure and surface energy exchange in the western and eastern parts of Arabian Sea bring out the similarities/differences and the causative factors for the observed features. SST shows bimodal fluctuations in Area I (northern part of Somali current region; western Arabian Sea) and Area II (off central west coast of India; eastern Arabian Sea) with the maxima occurring during pre and post-southwest monsoon seasons and the minima during southwest monsoon and winter seasons. However, very low SST is observed during August in Area I where the annual amplitude of variations is about 7°C . Lower annual range of about 3.3°C is seen in Area II. This difference is caused by very intense upwelling occurring in Area I during the summer monsoon.

In Area I, upper ocean thermal characteristics show predominantly semi-annual periodicity. Maximum MLD is observed in June and minimum in August. Thermal structure variations in Area I is related to the complex dynamics encountered in Somali Basin and equatorial regions. Upwelling in Somali Basin occurs at the 'turning offshore' regions of the twin eddies that spin up in response to the southwest monsoon. Upwelling in Area I is related to the northern eddy.

In the surface layers, the southern eddy translates northwards into Area I in August and under the combined effect of the northern and southern eddies, intense upwelling occurs in the northern part of Somali current region. By September, these two eddies coalesce into a single large eddy which moves further north of Area I. Since the upwelling region also shifts northwards, upwelling ceases in Area I followed by sinking in September. In the lower layers, in this area, upwelling starts by early June which may be due to the occurrence of a subsurface eddy which appears to have been generated near the equator and translated northwards. Sinking occurs at subsurface in August itself, possibly due to earlier translation of the subsurface eddy further north of Area I.

Below the surface layers, the upward tendency of thermocline seen before southwest monsoon and in November-December, is associated with equatorial easterly jet which occurs in the transition periods between the two monsoons and is fed from the western Indian Ocean.

Heat content in the different layers in Area I, varies with a semi-annual periodicity. Maximum occurs before and after the southwest monsoon season. The minimum which occurs in August in the upper layers is advanced by one month, below 100 m.

Half-yearly periodicity is seen in the annual variation of heat storage also. Warming takes place during pre-southwest monsoon period and towards the latter part of southwest monsoon season while cooling occurs during winter and southwest monsoon seasons. In the top 150 m, maximum warming (530 W/m^2) and cooling (400 W/m^2) occur during September and June-July respectively.

In Area I, the net radiation does not show any drastic reduction during southwest monsoon season. Further, after the establishment of monsoon, evaporation decreases. These are the effects of very low SST caused by intense upwelling during this period. The annual variation of net heat exchange shows two maxima during pre-and post-southwest monsoon seasons. Although there is substantial reduction in the net heat gain, during the early part of southwest monsoon season, the sea does not lose heat.

Heat advection also shows semi-annual periodicity in Area I. Annual range of heat advection is about 800 W/m^2 which is nearly 8 times the net surface heat exchange. Maximum export of about 450 W/m^2 is seen during June-July and maximum import of about 375 W/m^2 is seen in September.

Large import of heat to Area I occurs below 100 m before southwest monsoon (February-May). The heat budget of upper ocean, during southwest monsoon is related to the eddies and the associated vertical movements of thermocline, in the Somali Basin. During this period, although large amount of heat is transported horizontally from Area I, vertical transport of heat from 0 - 100 m layer to deeper layers is also seen. After southwest monsoon, during October-December, advection of heat out of this

area is seen below 100 m.

Model studies on the evolution of SST in Area I, by incorporating surface heat flux, entrainment, horizontal and vertical advectons have enabled to identify the processes which are important during different seasons. The inclusion of horizontal advection improves the results substantially throughout the year. However, during southwest monsoon season, vertical advection contributes considerably to the observed monsoonal cooling.

In the eastern Arabian Sea (Area II), annual periodicity is predominant in the thermal characteristics. Maximum MLD is noticed during January and February (~ 80 m) and the minimum depth of about 15 m is seen during October and November.

In this area, below 100 m, the upward tilt of isotherms commences in May and reaches the minimum depth in July. This is followed by sinking. These are due to southerly coastal current during southwest monsoon season and its reversal subsequently. In the upper layers, the upwelling commences late and continues till October-November when the minimum depth of ML is attained. During the early part of southwest monsoon season, although the southerly coastal current is favourable for upwelling, the southwesterly wind is not favourable. This causes the delay in the commencement of upward movement in surface layers. The wind becomes favourable for upwelling during the post-monsoon months.

During the post-monsoon, a secondary upwelling is noticed at subsurface layers in this area, indicating that the current has again temporarily turned southerly during the transition period, before setting in the steady northerly direction. Conversely⁴ the transition between

northeast and southwest monsoons is characterized by a temporary phase of sinking.

In the eastern Arabian Sea, annual periodicity is predominant in the variation of heat content. In all layers the maximum heat content is seen in May. While the upper 50 m exhibits mild gradual decrease till November, in the layers below, rapid decrease is noticed, till July.

Excepting the upper 50 m, the heat storage shows clear annual periodicity. Heat depletion is seen at all levels during the southwest monsoon season. For the entire 150 m, maximum warming of about 300 W/m^2 occurs in December and maximum cooling of about 325 W/m^2 occurs in June.

All components of surface heat exchange exhibit semi-annual fluctuations in the eastern Arabian Sea also. Sharp decrease in radiational flux and increase in evaporation are noticed during southwest monsoon season. Net heat gain is nearly zero during winter and maximum during pre-monsoon. Maximum heat loss of about 50 W/m^2 is seen during southwest monsoon season.

Heat advection also has an annual periodicity with heat export occurring during southwest monsoon and import during the remaining period. Annual range of advection of 550 W/m^2 is roughly four times the net heat gain. Maximum export of about 300 W/m^2 is seen in June and maximum import of about 250 W/m^2 occurs in December. It can be seen that the annual range of heat advection as well as its ratio to the surface heat input are comparatively less in the eastern Arabian Sea.

In eastern Arabian Sea, during southwest monsoon, large heat export is seen in upper 150 m and vertical transfer of heat is not noticed

in these layers. Before southwest monsoon (February-April), heat export of lesser magnitude is seen while after southwest monsoon (October-December) heat import is seen below 50 m.

The model incorporating surface heat exchange simulates, in Area II, the observed pattern with semi-annual periodicity, although with lesser amplitude of pre-monsoonal warming and winter cooling. The warming after winter is better reproduced by the inclusion of entrainment. Horizontal and vertical advections do not appear to be important in this area. The model does not appear to be suitable for the simulation of SST in eastern Arabian Sea, possibly due to low value of signal to noise ratio.

Annual variation of zonally averaged heat advection in north Indian Ocean shows that maximum export of about 100 W/m^2 occurs around 15°N during southwest monsoon season. This is due to large negative heat storage caused by intense upwelling in several parts of northern Indian Ocean. By and large, northern Indian Ocean is an area of heat export.

Vertically (limited to ML) and zonally integrated net meridional heat transport is mostly southerly. It is seen that, on an average, a monthly cross equatorial flux of $45 \times 10^{13} \text{ W}$ takes place from north to south. Maximum cross equatorial heat transport of $100 \times 10^{13} \text{ W}$ occurs in June and July. Average monthly flux from the north to the south Indian Ocean during southwest monsoon season is about four times than that during the non-southwest monsoon months.

The possibility of some relationship between the intensity of southwest monsoon and the heat advected out of north Indian Ocean during the previous year is indicated. This must, however, be tested with large data base with sufficient spatial resolution, for obtaining net surface heat gain and oceanic heat storage during individual years.

REFERENCES

- *Albereeht, F.A.W., 1958. Untersuchungen über den Wärmehaushalt an der Meeresoberfläche und die Meeresströmungen im Indischen Ozean. *Geophys. Pura. Appl.*, 39: 194-215.
- Aleem, A.A., 1967. Concepts of currents, tides and winds among medieval Arab geographers in Indian Ocean. *Deep Sea Res.*, 14: 459-463.
- Aleem, A.A., 1973. History of Arab navigation in Indian Ocean. *J. Mar. Biol. Assn. India Suppl.* dedicated to Dr. N.K. Panikkar, 254-270.
- Alexander, R.C. and R.L. Mobley, 1976. Monthly average sea surface temperatures and ice pack limits on a 1° global grid. *Mon. Weath. Rev.*, 104: 143-168.
- Anderson, D.L.T. and P.B. Rowlands, 1976. The Somali current response to southwest monsoon. The relative importance of local and remote forcing. *J. Mar. Res.*, 34: 395-417.
- Anjaneyulu, T.S.S., 1980. A study of air and sea surface temperature over the Indian Ocean. *Mausam*, 31: 551-560.
- *Anon., 1950. Atlas of ocean currents-Indian Ocean. U.S. Navy Hydro. Office Publ.
- Anon., 1952. Indische Ocean Oceanographische en Meteorologische gegevens. 2nd Edition. Koninklijk Nederlands Meteorologisch Instituut, Publ. No. 135, 1: Text 31 pp. and 2: 24 charts.
- Anon., 1960. Summary of oceanographic conditions in Indian Ocean. U.S. Navy Hydro. Office, - SP - 53: 142 pp.
- Anon., 1980. Oceanographic investigations along the southwest coast of India (1976-78). A report for the pelagic fishery investigations on southwest coast-phase II-Project. FAO. Rome, 51 pp.
- Anon., 1986. World Ocean circulation experiment. WOCE Discussions on physical processes. Reports of subject meetings on interbasin exchanges, gyre interactions, deep circulation and its relation to topography and oceanic heat flux. U.S. WOCE. planning report No. 5: 143 pp.
- Anto., A.F., Rao, L.V.G. and Y.K. Somayajulu, 1982. Surface layer conditions of the atmosphere over western Bay of Bengal during MONEX. *Indian J. Mar. Sci.*, 11: 15-20.
- *Ashbal, P. 1961. New world maps of global solar radiation during IGY 1957-58. Hebrew University, Dept. Climatology and Meteorology, Jerusalem, Israel.
- Banse, K. 1959. On upwelling and bottom trawling off the southwest coast of India. *J. Mar. Biol. Assn. India*, 1: 33-39.

- *Banse, K., 1960. Bemerkungen Zu meerezkundiichen Beobachtunglu von der Ostkuste von Indian Kieler Meeresforch, 16: 214-220.
- Banse, K., 1968. Hydrography of the Arabian Sea shelf of India and Pakistan and effects on demersal fisheries. Deep Sea Res., 15: 45-79.
- Banse, K., 1972. Upsloping of isotherms on the continental shelf off Goa and Bombay in June 1967. J. Mar. Biol. Assn. India, 14: 344-356.
- Bathen, K.H., 1971. Heat storage and advection in the north Pacific Ocean. J. Geophys. Res., 76: 676-687.
- Bennet, A.F., 1978. Poleward heat flux in southern hemispheric ocean. J. Phys. Oceanogr., 8: 785-798.
- *Berliand, T.G., 1960. Methods of climatological computations of total incoming solar radiation. Meteorol. Gidrol, No.6, 9-12, MGA 12: 1486.
- Bhumralkar, C.M., 1978. Relation between evaporation over Arabian Sea and rainfall at the west coast of India during monsoon. Indian J. Meteorol. Hydrol. Geophys., 29: 150-161.
- *Black, J.N., 1956. The distribution of solar radiation over earth's surface. Arch. Meteorol. Geophys., (B) 7: 166-189.
- Bretherton, F.P., Mc Phaden, M.J. and E.B. Kraus, 1984. Design studies for climatological measurements of heat storage. J. Phys. Oceanogr., 14: 318-337.
- Brocks, K. and L. Krugermeyer, 1972. Hydrodynamic roughness of sea surface. In: Studies in Physical Oceanography (Ed. Gordon, E.L.) Gordon and Breach Science Publishers, Inc., N.Y., 1: 75-92.
- Brown, O.B., Bruce, J.G. and R.H. Evans, 1980. Sea Surface temperature evolution in the Somali Basin during southwest monsoon 1979. Science., 209: 595-597.
- Bruce, J.G., 1968. Comparison of near surface topography during two monsoons in the western Indian Ocean. Deep Sea Res., 15: 665-678.
- Bruce, J.G., 1973. Large scale variation in Somali current during southwest monsoon 1970. Deep Sea Res., 20: 837-846.
- Bruce, J.G., 1974. Some details of upwelling off Somalia and Arabian coasts. J. Mar. Res., 32: 415-423.
- Bruce, J.G., 1979. Eddies off Somali coast during southwest monsoon. J. Geophys. Res., 84: 7742-7748.
- Bruce, J.G., 1987. Seasonal heat content variations in the northwestern Indian Ocean. Oceanologia Acta, Sp No., 77-83.

- Bruce, J.G. and G.H. Volkman, 1960. Some measurements of current off Somali coast during northeast monsoon. *J. Geophys. Res.*, 74: 1958-1967.
- Bruce, J.G. and W. Beatty, 1985. Some observations on coalescing of Somali eddies and a description of the Socotra eddy. *Oceanologia Acta*, 8: 207-213.
- Bryan, K., 1962. Measurement of meridional heat transport by ocean currents. *J. Geophys. Res.* 67: 3403-3414.
- Budyko, M.I., 1956. Heat balance of the earth's surface. (Translated from Russian)., *U.S. Weather. Beaur.*, Washington D.C., 259. pp.
- Budyko, M.I., 1974. *Climate and Life*. Academic Press, 508 pp.
- Bunker, A.F., 1976. Computations of surface energy flux and annual air-sea interaction cycles of north Atlantic Ocean. *Mon. Weath. Rev.*, 104: 1122-1140.
- Camp, N.T. and R.L. Elsberry, 1978. Oceanic thermal response to strong atmospheric forcing. II. Role of one dimensional processes. *J. Phys. Oceanogr.*, 8: 215-224.
- Cane, M.A., 1980. On the dynamics of equatorial currents with application to Indian Ocean. *Deep Sea Res.*, 27: 525-544.
- Carruthers, O.N., Gogate, S.S., Naidu, J.R. and T. Leavastu, 1959. Shoreward upslope of the layer of minimum oxygen off Bombay: its influence on marine biology, especially fisheries. *Nature*, 183: 1084-1087.
- Carton, J. and J.M. Yoo, 1987. Determining seasonal heat transport in the Atlantic Ocean. *Tropical Ocean Atmos. Newsletter*, No. 41: 15-16.
- Chang, S.W. and R.A. Anthes, 1978. Numerical simulations of ocean's nonlinear, baroclinic response to translating hurricanes. *J. Phys. Oceanogr.*, 8: 468-480.
- Charnock, H., 1955. Wind stress on water surface. *Quart. J. Roy. Meteorol. Soc.*, 81: 639-640.
- Colborn, J.G., 1975. Thermal structure of the Indian Ocean. *IIOE Oceanogr. Monograph 2*. East West Center Press. (Honolulu), 173 pp.
- Colon, J.A., 1964. On interactions between the southwest monsoon and the sea surface over the Arabian Sea. *Indian J. Meteorol. Geophys.*, 15: 183-200.
- Cox, M.D., 1970. A theoretical model of Indian Ocean. *Deep Sea Res.*, 17: 47-75.
- Darbyshire, M., 1967. The surface waters of the coast of Kerala, South India. *Deep Sea Res.*, 14: 295-320.

- Das, P.K., Dube, S.K. and G.S. Rao, 1987. A steady state model of the Somali current. *Proc. Indian Acad. Sci. (Earth & Planet. Sci.)*, 96: 279-290.
- Das, V.K., Gouveia, A.D. and K.K. Varma, 1980. Circulation and water characteristics on isanosteric surfaces in the northern Arabian Sea during February-April. *Indian J. Mar. Sci.*, 9: 156-165.
- Deacon, E.L., 1962. Aerodynamic roughness of the sea. *J. Geophys. Res.*, 67: 3167-3112.
- Deacon, E.L. and K.E. Webb, 1962. Small scale interactions. In: *The Sea, I*: (Ed. Hill, M.N.), Wiley and Sons, 43-87.
- Defant, A., 1961. *Physical Oceanography, I* : Pergamon Press, 729 pp.
- de Szocke, R.A. and C.A. Paulson, 1987. The ocean surface layer: a global sampling strategy, U.S. WOCE Planning Report, No.6, U.S. WOCE Planning Office, 49 pp.
- Düing, W., 1970. The monsoon regime of the currents in the Indian Ocean. *IIOE Oceanogr. Monograph 1*, East-west Center Press (Honolulu), 68pp.
- Düing, W. and F. Schott, 1978. Measurements in the source region of the Somali current during the monsoon reversal. *J. Phys. Oceanogr.* 8: 278-289.
- Düing W. and A. Leetmaa, 1980. Arabian sea cooling. A preliminary heat budget. *J. Phys. Oceanogr.* 10: 307-312.
- Dunckel, M., Hasse, L., Krugermeyer, L., Schriever, D. and J. Wucknits, 1974. Turbulent fluxes of momentum heat and water vapour in atmospheric surface layer at sea during ATEX. *Boundary Layer Meteorol.*, 6: 81-106.
- *Edelman, H.S., 1965. Brief characteristics of the water masses in the Gulf of Aden and north Arabian Sea (Data of 2nd Indian Ocean Expedition of AZOV-Black Sea Institute of Marine Fisheries and Oceanography) In Russian, *Trudy Vess. Nauch-Isslet. Inst. Morsk. Rib. Choz. Okeanogr. (VW IRO)*, 57: 93-107.
- Elizarov, A.A., 1973. Oceanographic investigations on the shelf and slope off western India, In: *Soviet Fisheries Investigations in the Indian Ocean* (Ed. Bogdnov, A.S.), Israel Program for Scientific Translations, 29-41.
- *Ellis, R.S., 1952. Preliminary study of the relation between sea surface temperature of north Indian Ocean and precipitation over India. M.S. Thesis. Dept. Meteorol., Florida State University.
- Elsberry, R.L. and N.T. Camp, 1978. Oceanic thermal response to strong atmospheric forcing. I. Characteristics of forcing events. *J. Phys. Oceanogr.*, 8: 206-214.

- Elsberry, R.L. and R.W. Garwood, 1980. Numerical ocean prediction models. Goals for 1980s. *Bull. American Meteorol. Soc.*, 61: 1556-1566.
- Emery, W.J., 1976. Role of vertical motion in the heat budget of the upper north eastern Pacific Ocean. *J. Phys. Oceanogr.*, 6: 299-305.
- Emery, W.J. and J.S. Dewar, 1982. Mean temperature-salinity, salinity-depth and temperature-depth curves for the north Atlantic and north Pacific. *Progr. Oceanogr.*, 11: 219-305.
- Etter, P.C., 1983. Heat and freshwater budget of Gulf of Mexico. *J. Phys. Oceanogr.*, 13: 2058-2069.
- Evans, R.H. and O.B. Brown, 1981. Propagation of thermal fronts in the Somali current system. *Deep Sea Res.*, 28: 521-527.
- Fieux, M. and H. Stommel, 1977. Onset of southwest monsoon over Arabian Sea from marine reports of surface winds. *Mon. Weath. Rev.*, 105: 231-236.
- *Findley, A.G., 1866. A directory for navigation in Indian Ocean. Richard Holmes Lomrie, 1062 pp.
- Fissel, D.B., Pond, S. and M. Miyake, 1977. Computation of surface fluxes from climatological and synoptic data. *Mon. Weath. Rev.*, 105: 26-36.
- Frieche, R.L. and K.F. Schmitt, 1976. Parameterization of air-sea interface fluxes of sensible heat and moisture by bulk aerodynamic formulas. *J. Phys. Oceanogr.*, 6: 801-809.
- *Fuglister, F.C., 1960. Atlantic ocean atlas of temperature and salinity profiles and data from international geophysical year of 1957 and 58. Woods Hole Oceanographic Institution, Atlas Series. 1. 209 pp.
- *Galle, P.H., 1924. Climatology of Indian Ocean.
- Garratt, J.R., 1977. Review of drag coefficients over oceans and continents. *Mon. Weath. Rev.*, 105: 915-929.
- Garwood, R.W., 1979. Air-Sea interaction and dynamics of the surface mixed layer. *Rev. Geophys. Space Phys.*, 17: 1507-1524.
- *Gogate, S.S., 1960. Some aspects of hydrobiology of Bombay waters. M.S. Thesis. University of Bombay, 111 pp.
- Gopalakrishna, V.V., Sarma, M.S.S., Sadhuram, Y. and V. Ramesh Babu, 1987. Heat content variations in the north eastern Arabian Sea during a weak spell of 1986 summer monsoon. *Proc. Sym. Short-Term Variability of Physical Oceanographic Features in the Indian Waters. 19-27 Feb. 1987. Cochin*, 5-9.
- Gorshkov, S.G., 1978. World atlas Vol.2, Atlantic and Indian Oceans. Pergamon Press (In Russian), 306 charts.

- Hastenrath, S., 1980. Heat budget of tropical ocean and atmosphere. *J. Phys. Oceanogr.*, 10: 157-170.
- Hastenrath, S., 1982. On meridional heat transport in world oceans. *J. Phys. Oceanogr.*, 12: 923-927.
- Hastenrath, S., 1985. Climate and circulation of the tropics. D. Reidel Publishing Company, 455 pp.
- Hastenrath, S. and P.J. Lamb, 1979a. Climatic atlas of the Indian Ocean. Part I. Surface climate and atmospheric circulation. University of Wisconsin Press, 116pp.
- Hastenrath, S. and P.J. Lamb, 1979b. Climatic atlas of the Indian Ocean. Part II. The oceanic heat budget. University of Wisconsin Press, 110 pp.
- Hastenrath, S. and P.J. Lamb, 1980. On heat budget of hydrosphere and atmosphere in the Indian ocean. *J. Phys. Oceanogr.*, 10: 694-708.
- Hastenrath, S. and J. Merle, 1986. Annual march of heat storage and export in the tropical Atlantic Ocean. *J. Phys. Oceanogr.*, 16: 694-708.
- Hellerman, S. and M. Rosenstein, 1983. Normal monthly wind stress over the ocean with error estimates. *J. Phys. Oceanogr.*, 13: 1093-1104.
- Hicks, B.B., 1972. Some evaluation of drag and bulk transfer coefficients over water bodies of different sizes. *Boundary Layer Meteorol.*, 3: 201-213.
- Holland, W.R., 1977. The role of upper ocean as a boundary layer in models of oceanic general circulation. In: *Modelling and Prediction of the Upper Layers of the Ocean* (Ed. Kraus, E.B.), Pergamon Press, 7-30.
- Holt, T. and Sethuraman, 1987. A comparison of the significant features of the marine boundary layers over the east central Arabian Sea and north central Bay of Bengal during MONEX-79. *Mausam*, 38: 171-176.
- Hsiung, J., 1985. Estimates of global oceanic meridional heat transport. *J. Phys. Oceanogr.*, 15: 1405-1413.
- *Jacobs, W., 1942. On the energy exchange between ocean and atmosphere. *J. Mar. Res.*, 5: 37-60.
- Jambunathan, R. and K. Ramamurthy. 1975. Sea and air temperature distribution over Arabian Sea. *Indian J. Meteorol. Geophys.*, 26: 465-478.
- Jayaraman, R. and S.S. Gogate, 1957. Salinity and temperature variations in the surface waters of Arabian Sea off Bombay and Sourashtra coasts. *Proc. Indian Acad. Sci.*, 45B: 151-164.

- Joseph, P.V. 1981. Ocean-atmosphere interaction on a seasonal scale over north Indian Ocean and Indian summer monsoon rainfall and cyclone tracks. *Mausam*, 32: 237-246.
- Joseph, P.V. and P.V. Pillai, 1984. Air-sea interaction on a seasonal scale over north Indian Ocean-Part I - International variation of SST and Indian summer monsoon rainfall. *Mausam*, 35: 323-330.
- Joseph, P.V. and P.V. Pillai, 1986. Air-sea interaction on a seasonal scale over north Indian Ocean-Part II - Monthly mean atmospheric and oceanic parameters during 1972-1973. *Mausam*, 37: 159-168.
- *Jung, G.H., 1952. Note on meridional transport of energy by oceans. *J. Mar. Res.*, 11: 39-146.
- Kesavamurthy, R.N., 1981. The southern oscillation and summer monsoon variability. Internatl. Conf. Early Results of FGGE and Large Scale Aspects of its Monsoon Expts. April 1981 WMO, Geneva, (7)20-(7)23.
- *Kimball, H.H., 1926. Amount of solar radiation that reaches the surface of earth on land and sea. *Mon. Weath. Rev.*, 56: 383-389.
- Kondo, J., 1975. Air-sea bulk transfer coefficients in diabatic conditions. *Boundary Layer Meteorol.*, 9: 91-112.
- Kraus, E.B., 1972. Atmosphere-ocean interaction. Clarendon Press (Oxford), 275 pp.
- Kraus, E.B., 1977. Introduction. Chapter 1. In: Modelling and Prediction of the Upper Layers of the Ocean (Ed. Kraus, E.B), Pergamon Press, 1-3.
- *Krishnamurti, T.N., 1981. Cooling of Arabian Sea and onset vortex during 1979. Recent progress in equatorial oceanography. A report of final meeting of SCOR working group 47, Venice. Italy.
- Lamb, P.J., 1981. Estimate of annual variation of Atlantic Ocean heat transport. *Nature*, 290: 766-768.
- Lamb, P.J., 1984. On the mixed layer climatology of the north and tropical Atlantic. *Tellus*, 36a: 292-305.
- Lamb, P.J. and A.F. Bunker, 1982. The annual march of the heat budget of the north Atlantic Oceans. *J. Phys. Oceanogr.*, 12: 1388-1410.
- *Landsberg, H.E., Idppmann, K., Paffen, H. and C. Troll, 1963. *Weltkorten sur Klimakunde*. Springer-Verlog. Berlin.
- Large, W.F. and S. Pond, 1981. Open ocean measurements of flux in moderate to strong winds. *J. Phys. Oceanogr.*, 11: 324-336.
- Launiainen, J., 1979. Studies of energy exchange between the air and the sea surface on the coastal area of the Gulf of Finland. *Finnish Mar. Res.*, 246: 3-110.

- Leetmaa, A., 1972. The response of Somali current to southwest monsoon of 1970. *Deep Sea Res.*, 19: 319-325.
- Leetmaa, A., 1973. The response of the Somali current at 2° S to the southwest monsoon. *Deep Sea Res.*, 20: 397-400.
- Leetmaa, A., Quadfasel, D.R. and D. Wilson, 1982. Development of the flow field during the onset of the Somali current, 1979. *J. Phys. Oceanogr.*, 12: 1325-1332.
- Leipper, D.F., 1967. Observed ocean conditions and hurricane Hilda 1964. *J. Atmos. Sci.*, 24: 182-196.
- Levitus, S., 1984. Annual cycle of temperature and heat storage in world oceans. *J. Phys. Oceanogr.*, 14: 727-746.
- Levitus, S., 1987a. Rate of change of heat storage of the world oceans. *J. Phys. Oceanogr.*, 17: 518-528.
- Levitus, S., 1987b. Meridional Ekman heat fluxes for the world oceans and individual ocean basins. *J. Phys. oceanogr.* 17: 1484-1492.
- Levitus, S. and A.H. Oort, 1977. Global analysis of oceanographic data. *Bull. American Meteorol. Soc.*, 58: 1270-1284.
- Lighthill, M.J., 1969. Dynamic response of the Indian Ocean to onset of southwest monsoon. *Phil. Trans. Roy. Soc. A.*, 265: 45-92.
- Luther, M.E. and J.J. O'Brien, 1985. A model of the seasonal circulation in Arabian Sea forced by observed winds. *Prog. Oceanogr.*, 14: 353-385.
- Malkus, J.S., 1962. Large Scale interactions. In: *The Sea I* (Ed. Hill, M.N.), Inter Science Publications, New York, 88-285.
- Mani, A., Chacko, O., Krishnamurthy, V. and V. Desikan, 1965. Radiation balance of Indian Ocean. *Proc. Sym. Meteorol. Results of II OE, Bombay* (Ed. Pisharoty, P.R.), 165-167.
- Mathew, B., 1982. Studies on upwelling and sinking in the seas around India. Ph.D. Thesis, University of Cochin, 159 pp.
- Mc Phaden, M.J., 1982. Variability in the central equatorial Indian Ocean. Part II: Oceanic heat and turbulent energy balances. *J. Mar. Res.*, 40: 403-419.
- Meehl, G.A., 1984. A calculation of ocean heat storage and effective ocean surface layer depths for the northern hemisphere. *J. Phys. Oceanogr.*, 14: 1747-1761.
- Meehl, G.A. and W.M. Washington, 1985. Sea surface temperature computed by simple ocean mixed layer copuled to an atmospheric G.C.M. *J. Phys. Oceanogr.*, 15: 92-104.

- Melville, W.K., 1977. Wind stress and roughness length over breaking waves. *J. Phys. Oceanogr.*, 7: 702-710.
- Merle, J., 1980. Seasonal heat budget in the equatorial Atlantic Ocean. *J. Phys. Oceanogr.*, 10: 464-469.
- Miller, P.R., Sivaramakrishnan, M.V. and R. Suryanarayana, 1963. Preliminary results and future plans of IIOE meteorology Programmes - computer plans. Proc. Seminar Jointly Sponsored by NSF (USA), IMD and USIS, 30-41.
- *Model F., 1950. Warmwasserheizung Europe. *Ber. Deut. Welterdienstes* 12: 51-60. (In German).
- Molinari, R.L., Festa, J.F. and E. Marmolijo, 1985. Evolution of sea surface temperature in the tropical Atlantic Ocean during FGGE, 1979. II Oceanographic fields and heat balance of the mixed layer. *J. Mar. Res.*, 43: 67-81.
- Molinari, R.L., Swallow, J.C., and J.F. Festa, 1986. Evolution of the near surface thermal structure in the western Indian Ocean during FGGE, 1979. *J. Mar. Res.*, 44: 739-762.
- Moley, D.A. and C.M. Mohite, 1984. Cyclonic storms of Arabian Sea 1877-1980. *Mausam*, 35: 127-134.
- Mukherjee, A.K. and D.K. Paul, 1980. Influence of Arabian Sea cyclonic systems on the onset of monsoon. Results of summer MONEX field phase. Research. Part A. FGGE Operations Report, 9: WMO, Geneva, 52-67.
- Murty, C.S. and V.V.R. Varadachari, 1968. Upwelling along the east coast of India. *Bull. Natl. Inst. Sci. India*, No: 38, 80-86.
- Murthy, P.G.K. and P. Madhusoodanan, 1987. Diurnal variability of hydrographic conditions in the surface layer off calicut in February 1985. Proc. Sym. Short-term Variability of Physical Oceanographic Features in the Indian Waters. 19-20 Feb. 1987, Cochin, 67-71.
- Murty, V.S.N., Rao D.P. and J.S. Sastry, 1983. The lowering of sea surface temperature in the east central Arabian Sea associated with a cyclone. *Mahasagar*, 16: 67-71.
- *Newell, R.E., Kidson, J.W., Vincent, D.G. and G.J. Boer, 1974. The general circulation of the tropical atmosphere and interactions with extratropical latitude. Vol. II. M.I.T. Press. U.S.A., 371 pp.
- Nicholls, S. and C.J. Readings, 1979. Aircraft observations of the structure of the lower boundary layer over the ocean. *Quart. J. Roy. Meteorol. Soc.*, 105: 785-802.
- Niiler, P.P. and E.B. Kraus, 1977. One dimensional models of the upper ocean. In: *Modelling and prediction of the upper layers of the ocean* (Ed. Kraus, E.B.), Pergamon Press, 143-172.

- Noble, A., 1968. Studies of sea water off north Canara Coast. *J. Mar. Biol. Assn. India*, 10: 197-223.
- Nyenzi, B.S., 1980. Influence of low tropospheric flow on onset of summer monsoon flow over India in June 1979. Results of Summer MONEX field phase. Research. Part A. FGGE Operation Report, 9:WMO, Geneva, 68-80.
- Oort, A.H. and T.H. Vonder Haar, 1976. On the observed annual cycle of the ocean atmosphere heat balance over the northern hemisphere. *J. Phys. Oceanogr.*, 6: 781-800.
- Padmini, R., 1981. Studies on energy exchange between sea and atmosphere from the Indian Ocean with special reference to Arabian Sea and Bay of Bengal. Ph.D. Thesis. University of Cochin, 198 pp.
- Pant, M.C., 1977. Wind stress and fluxes of sensible heat and latent heat over Arabian Sea during ISMEX 1973. *Indian J. Meteorol. Hydrol. Geophys.*, 28: 189-196.
- Patil, M.R., Ramamritham, C.P., Varma, P.U., Nair, C.P. and P. Myrland, 1964. Hydrography of the west coast of India during the pre-monsoon period of the year 1962. Part I - shelf water of Maharashtra and southwest Saurashtra coasts. *J. Mar. Biol. Assn. India*, 6: 151-166.
- Payne, R.E., 1972. Albedo of sea surface. *J. Atmos. Sci.*, 29: 959-970.
- Perry, A.H. and J.M. Walker, 1977. Ocean atmosphere system. Longman Inc., New York. 160 pp.
- Pisharoty, P.R., 1965. Evaporation from the Arabian Sea and the Indian southwest monsoon. Proc. Sym. Meteorol. Results of IIOE, Bombay. (Ed. Pisharoty, P.R.), 43-54.
- Pisharoty, P.R., 1981a. The Asiatic summer monsoon - A new theory. Intern. Conf. Early Results of FGGE and Large Scale Aspects of its Monsoon Expts, April 1981, W.M.O. Geneva., (5)43-(5)47.
- Pisharoty, P.R., 1981b. Sea surface temperature and monsoon. Monsoon dynamics (Ed. Lighthill, M.J. and R.P. Pearce), Cambridge University Press, London., 238-251.
- Pond, S., Fissel, D.B. and C.A. Paulson, 1974. A note on bulk aerodynamic coefficients for sensible heat and moisture fluxes. *Boundary Layer Meteorol.*, 6: 333-339.
- Portman, D.J. and E. Ryznar, 1971. An investigation of heat exchange. IIOE Meteorological Monograph 5, East-West Center Press (Honolulu), 78 pp.
- Price, J.F., Moores, C.N.K. and J.C. Van Leer, 1978. Observation and simulations of storm induced mixed layer deepening *J. Phys. Oceanogr.*, 8: 582-599.

- *Privett, D.W. 1959. Monthly charts of evaporation from north Indian Ocean (including Red sea and Persian Gulf). *Quart. J. Roy. Meteorol. Soc.*, 85: 424-428.
- *Puttulo, J.G., 1957. Seasonal heat budget of the oceans. D.Sc. Thesis. University of California, 104 pp.
- Quadfasel, D.R., 1982. Low frequency variability of 20 °C isotherm topography in the western equatorial Indian Ocean. *J. Geophys. Res.*, 87: 1990-1996.
- Quadfasel, D.R. and F. Schott, 1982. Watermass distribution at the intermediate layers off Somali coast during the onset of southwest monsoon 1979. *J. Phys. Oceanogr.*, 12: 1358-1372.
- Ramage, C.S., 1972. Interaction between tropical cyclones and China Sea. *Weather*, 27: 484-490.
- Ramage, C.S., Miller, F.R. and C. Jeffries, 1972. Meteorological atlas of International Indian Ocean Expedition. Vol I, The surface climate of 1963 and 1964. Natl. Sci. Foundation, Washington D.C., 157 p.
- Ramam, K.V.S., Murthy, P.G.K. and C.K.B. Kurup, 1979. Thermal structure variation in Arabian Sea in May- July 1973. *Mausam*, 30: 105-112.
- Ramamrithm, C.P. and R. Jayaraman, 1960. Hydrographic features of the continental shelf waters off Cochin during the years 1958-59. *J. Mar. Biol. Assn. India*, 2: 155-168.
- Ramamrithm, C.P. and M.R. Patil, 1965: Hydrography of the west coast of India during the pre-monsoon period of the year 1962, Part 2; in and offshore waters of Konkan and Malabar coasts. *J. Mar. Biol. Assn. India*, 7: 150-168.
- Ramanadham, R., Rao, G.R.L. and D.P. Rao, 1968. Seasonal variation in heat flux from the sea surface over Bay of Bengal. *Bull. Natl. Inst. Sci. India Part II*, 38: 1004-1010.
- Ramanadham, R., Somanadham, S.V.S. and R.R. Rao, 1981. Heat budget of the north Indian oceanic surface during MONSOON 77. *Monsoon Dynamics* (Ed. Lighthill, M.J. and R.P. Pearce), Cambridge University Press, London, 491-507.
- Ramasastri, A.A. and P. Myrland, 1959. Distribution of sea temperature, salinity and density in the Arabian Sea along the south Malabar coast (South India) during post monsoon season. *Indian J. Fish.*, 6: 223-255.
- Ramesh Babu, V., Rao, L.V.G., Varkey, M.J. and P.U. Varma, 1976. Temperature distribution in the upper layers of the northern and eastern Arabian Sea during Indo-Soviet Monsoon Experiment. *Indian J. Hydrol. Geophys.*, 27: 291-293.

- Ramesh Babu, V., Varkey, M.J., Kesava Das, V. and A.D. Gouveia, 1980. Watermass and general hydrography along the west coast of India during early March. *Indian J. Mar. Sci.*, 9: 82-89.
- Ramesh Babu, V. and J.S. Sastry, 1981. Heat storage in the Andaman Sea. *Mausam*, 32: 145-150.
- Ramesh Babu, V. and J.S. Sastry, 1984. Summer cooling in the east central Arabian Sea - A process of dynamic response to the southwest monsoon. *Mausam*, 35: 17-26.
- Rao, D.P., Sarma, R.V.N., Sastry, J.S. and K. Premchand, 1976. On the lowering of surface temperature in the Arabian Sea with the advance of southwest monsoon. *Proc. Sym. Tropical Monsoons.*, Pune, 106-115.
- Rao, D.S., 1987. Short-term variability in the thermal structure of the upper central Arabian Sea during MONEX - 79. *Proc. Sym. Short-Term Variability of Physical Oceanographic Features in the Indian Seas.*, 19-20 Feb. 1987, Cochin, 23-34.
- Rao, G.R.L. and V.S. Naidu, 1987. Ekman pumping velocity in the Arabian Sea during MONEX - 79. *Indian J. Mar. Sci.*, 16: 126-128.
- Rao, L.V.G., Cherian, T., Varma, K.K. and V.V.R. Varadachari, 1974. Hydrographical features of inner shelf waters along the central west coast of India. *Mahasagar*, 7: 15-26.
- Rao, R.R., 1984. A case study on the influence of summer monsoonal vortex on the thermal structure of upper central Arabian Sea during onset phase of MONEX-79. *Deep Sea Res.*, 31: 1511-1521.
- Rao, R.R., 1986. On the thermal response of upper eastern Arabian Sea to the summer monsoonal forcing during monsoon - 77. *Mausam.*, 37: 77-84.
- Rao, R.R., 1987a. The observed variability of the cooling and deepening of the mixed layer in the central Arabian Sea during MONSOON-77. *Mausam*. 38: 43-48.
- Rao, R.R., 1987b. On the thermal response of the upper central Arabian Sea to the summer monsoonal forcing during MONSOON-77. *Mausam*, 38: 293-302.
- Rao, R.R., 1988. Seasonal heat budget estimates of the upper layers in the central Arabian Sea. *Mausam*, 39: 241-248.
- Rao, R.R., Somanadham, S.V.S. and S. Nizamuddin, 1978. Study of the influence of energy budget of the north Indian Ocean on the behaviour of Indian summer monsoon. *Indian J. Meteorol. Hydrol. Geophys.* 29: 253-258.

- Rao, R.R., Ramam, K.V.S. and R. Santha Devi, 1981a. The energy budget at selected stations over the north Indian Ocean during MONSOON - 77. Monsoon dynamics (Ed. Lighthill, M.J. and R.P. Pearce), Cambridge University Press, 509-521.
- Rao, R.R. Murthy, P.G.K., Joseph, M.G. and K.V.S. Ramam, 1981b. On the space time variability of ocean surface mixed layer characteristics of central and eastern Arabian Sea during Monsoon-77. Internatl. Conf. Early Results of FGGE and Large Scale Aspects of its Monsoon Expts. April 1981. WMO, Geneva, (9) 20- (9)27.
- Rao, R.R., Rao, D.S., Murthy, P.G.K. and M.X. Joseph, 1983. A preliminary investigation on summer monsoonal forcing on the thermal structure of upper Bay of Bengal during MONEX-79. Mausam, 34: 239-250.
- Rao, R.R., Ramam, K.V.S., Rao, D.S. and M.X. Joseph, 1985. Surface heat budget estimates at selected areas of north Indian Ocean during MONSOON-77. Mausam, 36: 21-32.
- Reed. R.K., 1976. On estimation of net long wave radiation from oceans. J. Geophys. Res., 81: 5793-5794.
- Reed. R.K., 1977. On estimating insolation over sea surface. J. Phy. Oceanogr., 7: 482-485.
- Reddy, K.G., Rao, M.V., Prasad, P.H. and G.R.L. Rao, 1984a. Net energy exchange at sea surface over the Arabian Sea during the summer monsoon. Mausam, 35: 134-135.
- Reddy, K.G., Rao, M.V., Prasad, P.H. and G.R.L. Rao, 1984b. Fluxes of sensible and latent heat over the Arabian Sea during MONEX-79. Indian J. Mar. Sci. 13: 134-135.
- Reverdin. G. and M. Fieux, 1987. Sections in the western Indian Ocean-Variability in the temperature structure. Deep Sea Res., 34: 601-626.
- *Reynolds, R.W., 1983. A Comparison of sea surface temperature anomalies. J. Cli. Appl. Meteorl., 22: 447-459.
- Robinson, M.K., Bauer, R.A. and E.A. Schroeder, 1979. Atlas of north Atlantic - Indian Ocean monthly mean temperatures and mean salinities of surface layer. Naval Oceanographic Office, Pub. 18, Washington D.C., 213 pp.
- Roden, G.I., 1959. On the heat and salt balance of California current region. J. Mar. Res., 18: 36-61.
- Roll, H.U., 1965. Physics of marine atmosphere. Academic Press, 426 pp.
- Roll, H.U., 1972. Problem areas in air-sea interaction. In: Studies in physical oceanography (Ed. Gordon, E.L.), Gordon and Breach Science Publishers Inc. N.Y., 1: 63-73.

- Russel, G.L., Tsang, L.C. and J.R. Miller, 1985. Seasonal ocean heat transports computed from an atmospheric model. *Dynamics Atmos. Oceans*, 9: 253-272.
- Saha, K.R., 1970a. Zonal anomaly of sea surface temperature in equatorial Indian Ocean and its possible effect on monsoon. *Tellus*, 22: 403-409.
- Saha, K.R., 1970b. Air and water vapour transport across the equator in western Indian Ocean during northern summer. *Tellus*, 22: 681-687.
- Saha, K.R. and R. Suryanarayana, 1972. Mean monthly fluxes of sensible and latent heat from the surface of Indian Ocean. *J. Mar. Biol. Assn. India*, 14: 663-670.
- Sastry, J.S. and R.S. D'Zouza, 1970. Oceanography of the Arabian Sea during south west monsoon - Part I: Thermal structure. *Indian J. Meteorol. Geophys.*, 21: 367-382.
- Sastry, J.S. and R.S. D'Zouza, 1971. Oceanography of the Arabian Sea during southwest monsoon - Part II: Stratification and circulation. *Indian J. Meteorol. Geophys.*, 22: 23-34.
- Sastry, J.S. and R.S. D'Zouza, 1972. Oceanography of the Arabian Sea during southwest monsoon - Part III: Salinity. *Indian J. Meteorol. Geophys.*, 23: 479-490.
- Sastry, J.S. and R.S. D'Zouza, 1973. Oceanography of the Arabian Sea during southwest monsoon - Part IV: Dissolved oxygen. *J. Mar. Biol. Assn. India*, 15: 46-60.
- Sastry, J.S. and V. Ramesh Babu, 1985. Summer Cooling of Arabian Sea - A review. *Proc. Indian Acad. Sci. (Earth & Planet. Sci.)*, 94: 117-128.
- Schott, F. and D.R. Quadfasel. 1982. Variability of Somali current system during the onset of southwest monsoon, 1979. *J. Phys. Oceanogr.*, 12: 1343-1357.
- *Scott, G, 1902. Oceanographic and maritime meteorology. *Wissenschaftliche Ergebnisse der Deutschen Tiefsee - Expedition auf dem Dampfer Valdivia, 1889-1902.*
- *Seckel, G.R., and F.H. Beaudry, 1973. The radiation from sun and sky over the north Pacific Ocean (abstract). *Trans. American Geophys. Union*, 54: 1114.
- Seetharamayya, P. and A. Master, 1984. Observed air-sea interface conditions and a monsoon depression during MONEX-79. *Arch. Meteorol. Geophys. Biocl. Ser. A.*, 3: 61-67.

- Seetharamayya, P. and A.H. Mullan, 1987. Storm induced vertical thermal variations (warming and cooling) in eastern Arabian Sea during MONEX-79. Proc. Sym. Short-term Variability of Physical Oceanographic Features in Indian Waters. 19-20 Feb. 1987, Cochin, (supplement).
- Senguin, W.R. and K.B. Kidwell, 1980. Influence of synoptic scale disturbances on surface fluxes of latent and sensible heat. Supplement I to Deep Sea Res., 26: 51-64.
- Sikka, D.R. 1980. Some aspects of large scale fluctuations of summer monsoon rainfall over India in relation to fluctuations in the planetary and regional scale circulation parameters. Proc. Indian Acad. Sci. (Earth & Planet. Sci.), 89: 179-195.
- Sikka, D.R. and B. Grossman, 1980. Summer MONEX weather summary. In: Summer MONEX field phase report. FGGE Operations Report, 8:(A2)1-(A2)49.
- Simon, B., 1987. Variability of surface heat exchanges in the seas adjoining India using satellite data. Proc. Sym. Short-term Variability of Physical Oceanographic Features in the Indian Waters. 19-20 Feb. 1987, Cochin, 143-147.
- Simpson, J.J. and C.A. Paulson, 1979. Mid-ocean observations of atmospheric radiation. Quart. J. Roy. Meteorol. Soc., 105: 487-502.
- Shajahan, Shah Md., 1980. An evaluation of near surface fluxes of momentum, sensible and latent heat in the Arabian Sea during the onset phase of monsoon. Results of MONEX Field Phase. Research. Part A. FGGE Operations Report, 9: 187-206.
- Sharma, G.S., 1966. Thermocline as an indicator of upwelling. J. Mar. Biol. Assn. India, 8: 8-19.
- Sharma, G.S., 1968. Seasonal variations of some hydrographic properties of the shelf waters off the west coast of India. Bull. Natl. Inst. Sci. India, No. 38 Part I, 310-318.
- Sharma, G.S., 1978. Upwelling off the south west coast of India. Indian J. Mar. Sci., 7: 209-218.
- Shay, T.J. and M.C. Gregg, 1986. Convectively driven turbulent mixing in the upper ocean. J. Phys. Oceanogr. 16: 1777-1798.
- Shetye, S.R. 1986. A model study of the seasonal cycle of the Arabian Sea surface temperature. J. Mar. Res., 44: 521-542.
- Shukla, J., 1975. Effect of Arabian Sea surface temperature anomaly on Indian summer monsoon. A numerical experiment with the GFDL Model. J. Atmos. Sci., 32: 503-511.
- Shukla, J and M. Misra, 1977. Relationship between SST, wind speed over central Arabian Sea and monsoon rainfall over India. Mon. Weath. Rev., 105: 998-1002.

- Smith, S.D., 1974. Eddy flux measurements over lake Ontario. *Boundary Layer Meteorol.*, 6: 235-255.
- Smith, S.D., 1980. Wind stress and heat flux over the ocean in gale force winds. *J. Phys. Oceanogr.*, 10: 709-726.
- Smith, S.D. and E.G. Banke, 1975. Variations of sea surface drag coefficient with wind speed. *Quart. J. Roy. Meteorol. Soc.*, 101: 665-673.
- Smith, W.L., Herman, L.D., Schreiner, T., Howel, H.B. and P. Menzel, 1981. Radiation budget characteristics of the summer monsoon. *Internatl. Conf. Early Results of FGGE and Large Scale Aspects of its Monsoon Expts.* April 1981. (6) 16 - (6) 26.
- Stewart, R.W., 1975. Atmospheric boundary layer. *WMO bulletin*, 24: 82-86.
- Subrahmanya, I. and S.R.M. Rao, 1984. Some mean meteorological conditions over Bay of Bengal. *Mahasagar*, 17: 189-195.
- Suryanarayana, R. and D.R. Sikka, 1965. Evaporation over the Indian Ocean during 1963. *Proc. Sym. Meteorol. Results of IIOE, Bombay.* (Ed. Pisharoty, P.R.), 68-69.
- *Sverdrup, H.U., 1937. On the evaporation from the oceans. *J. Mar. Res.*, 1: 3-14.
- Sverdrup, H.U., Johnson, M.W. and R.H. Fleming, 1942. *The oceans - their physics, chemistry and biology.* Prentice Hall Inc, Englewood Cliff, N.J., 1087 pp.
- Swallow, J.C., 1980. Indian Ocean Experiment - Introduction. *Science*, 209: 588.
- Swallow, J.C. and J.G. Bruce, 1966. Current measurements off the Somali coast during southwest monsoon of 1964. *Deep Sea Res.*, 13: 861-888.
- Swallow, J.C. and M. Fieux, 1982. Historical evidence of two gyres in the Somali current. *J. Mar. Res.*, 40 (Suppl): 747-755.
- Swallow, J.C., Molinari, R.L., Bruce, J.G., Brown, O.B., and R.H. Evans, 1983. Development of near surface flow pattern and watermass distribution in the Somali Basin in response to southwest monsoon of 1979. *J. Phys. Oceanogr.*, 13: 1398-1415.
- Varadachari, V.V.R., 1961. On the process of upwelling and sinking on the east coast of India. In: *Mahadevan Shastiyabatapurti Vol.*, (Osmania University Press, Hyderabad), 159-162.
- Varkey, M.J., 1980. Power spectra of currents off Bombay. *Indian J. Mar. Sci.*, 9: 278-280.
- Varkey, M.J., Premchand, K. and J.S. Sastry, 1978. Current measurements off Bombay during March 1976. *Mahasagar*, 11: 115-123.

- Varma, K.K., 1988. Annual cycle of heat transport in north Indian Ocean. *Current Science*, 57: 422-424.
- Varma, K.K., and C.K. Gopinathan, 1977. Currents off Bombay during February 1976. *Mahasagar*, 10: 1-8.
- Varma, K.K., Das. V.K. and A.D. Gouveia, 1980. Thermohaline structure and watermasses in the northern Arabian Sea during February-April. *Indian J. Mar. Sci.*, 9: 148-155.
- Varma, K.K. and N.N. Raman, 1987. Turbulent fluxes over east central Arabian Sea during MONEX. *Proc. Indian Acad. Sci. (Earth & Planet Sci.)*, 96: 123-133.
- Venkateswaran, S.V., 1956. On evaporation from Indian Ocean. *Indian J. Meteorol. Geophys.*, 7: 265-284.
- Vijayarajan, P.K. and M.R. Santha Devi, 1987. Fine thermal structure of the mixed layer in February off Beypore. *Proc. Sym. Short-term Variability of Physical Oceanographic Features in Indian Waters. 19-20 Feb. 1987, Cochin*, 73-77.
- Vonder Haar, T.H. and A.H. Oort, 1973. New estimate of annual poleward energy transport by northern hemispheric oceans. *J. Phys. Oceanogr.*, 3: 169-172.
- Warren, B.A., 1966. Medieval Arab references to the seasonally reversing currents of north Indian Ocean. *Deep Sea Res.*, 13: 167-171.
- Warren, B.A., Stommel, H. and J.C. Swallow, 1966. Watermasses and patterns of flow in the Somali Basin during southwest monsoon of 1964. *Deep Sea Res.*, 13: 825-860.
- Washington, W.M. and G.A. Meehl, 1984. Seasonal cycle experiment on climate sensitivity due to a doubling of CO₂ with an atmospheric general circulation model coupled to a simple mixed layer ocean model. *J. Geophys. Res.*, 89 (D6): 9475-9503.
- Weare, B.C., 1979. A statistical study of the relationships between ocean surface temperature and Indian monsoon. *J. Atmos. Sci.*, 36: 2279-2291.
- Weare, B.C., 1983. Interannual variation in net heating at the surface tropical Pacific Ocean. *J. Phys. Oceanogr.*, 13: 873-885.
- Wilson, B.W., 1960. Note on surface wind stress over water at low and high wind speeds. *J. Geophys. Res.*, 65: 3377-3382.
- Wooster, S., Schaefer, M.B. and M.K. Robinson, 1967. Atlas of the Arabian Sea for fishery oceanography. University of California, 37 pp. 140 figures.
- Wu, J., 1969. Wind stress and surface roughness at air-sea interface. *J. Geophys. Res.*, 74: 444-455.

- Wu, J., 1980. Wind stress coefficients over surface near neutral conditions - A revisit. *J. Phys. Oceanogr.*, 10: 727-740.
- *Wunch, C., 1980. Meridional heat flux of north Atlantic Ocean. *Proc. Natl. Acad. Sci.*, 77: 5043-5047.
- Wyrcki, K., 1971. Oceanographic Atlas of International Indian Ocean Expedition. Natl. Sci. Foundation, Washington, D.C. 531 pp.
- Wyrcki, K., 1973. An equatorial jet in the Indian Ocean. *Science*, 181: 261-264.
- Wyrcki, K. and L. Ulrich, 1982. On the accuracy of heat storage computations. *J. Phys. Oceanogr.*, 12: 1411-1416.

* Not referred in original.